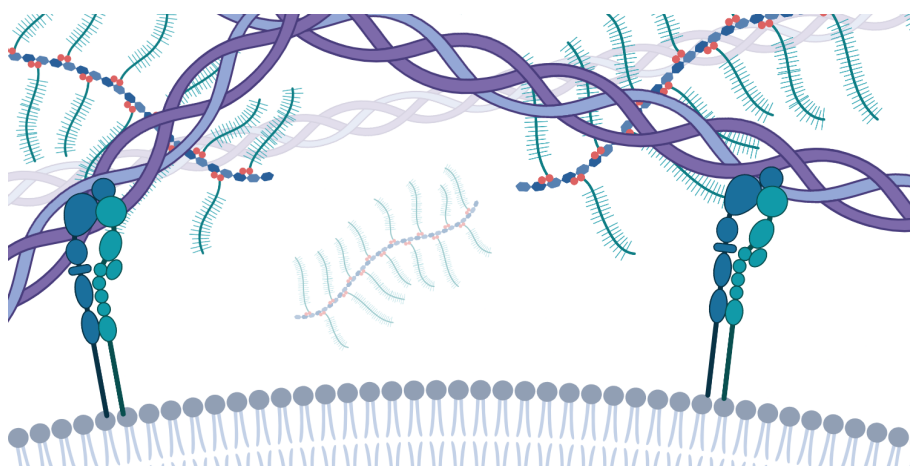


Kim Andre Ulvik

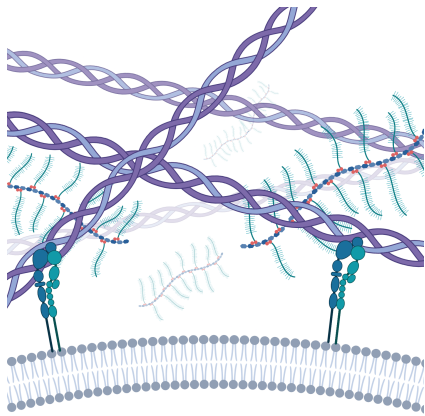
Effekten av ultralyd på transporten av nanopartikler i ekstracellulær matriks

Masteroppgave i Nanoteknologi
Veileder: Catharina de Lange Davies
Medveileder: Caroline Einen
Juli 2021



Kim Andre Ulvik

Effekten av ultralyd på transporten av nanopartikler i ekstracellulær matriks



Masteroppgave i Nanoteknologi
Veileder: Catharina de Lange Davies
Medveileder: Caroline Einen
Juli 2021

Norges teknisk-naturvitenskapelige universitet
Fakultet for naturvitenskap
Institutt for fysikk



Kunnskap for en bedre verden

Preface

It has been a challenging year to study due to the COVID-19 pandemic. During the pandemic, the possibilities of both curricular and extracurricular activities have been limited. At the moment of writing, vaccines are being distributed and society is slowly approaching normality. Thus this master thesis signifies not only the end of my 5th and final year of studies, but also the transition into a new daily life where social activities no longer are shunned.

The thesis was written under the Department of Physics at NTNU, and is part of a collaboration with Centre of Excellence PoreLab, St. Olavs hospital, SINTEF and several international parties. The title of the collaborative project is "Ultrasound-mediated transport of nanoparticles in tissue: Creating a predictive model combining theory, simulations and experiments". It is a direct continuation of my project assignment of fall 2020. I want to thank my supervisor Catharina de Lange Davies for letting me write my thesis on this exciting topic, and for all the support I've gotten through this whole process. I also want to send a thanks to my co-supervisor Caroline Einen for great discussions and assistance with creating some of the experimental setups used in this thesis. I want to thank Astrid Bjørkøy for a great amount of training and guidance in using the available instrumentation at CAM - Center for Advanced Microscopy, and for always having an open door. In addition to this, I want to thank Sylvie Lelu for assistance in procuring equipment, Sigrid Berg for help in using the equipment at Department of Circulation and Medical Imaging, and Rune Hansen for good guidance in understanding some of the parameters of ultrasound therapy. I want to thank all the people of the nanoparticle group at biophysics at NTNU for good advice and feedback. Finally, I want to send a thanks to friends and family for all the support I've gotten.

The figures in this thesis were created with BioRender.com

Trondheim, July 2021

Kim Andre Ulvik



Sammendrag

Kombinasjonen av cellegift med mikroboble og ultralyd har vist potensiale i å forbedre ekstravasasjon av medisiner over blodåreveggen. Derimot er penetrasjon av medisiner gjennom ekstracellulært matriks (ECM) fortsatt en utfordring, og er per nå en av de aspektene ved denne behandlingen som er minst forsket på. I ECM er diffusjon den viktigste transportmekanismen. Hovedbarrierene for diffusjon i ECM er elektrostatiske og steriske interaksjoner med kollagen, og redusert hydraulisk konduktivitet på grunn av glykosaminoklykaner. I dette prosjektet ble en gel laget av 5 mg/mL kollagen, 1 mg/mL hyaluronsyre og 10% kondensert melk brukt som en fantom for å undersøke diffusjonen av to typer PEGylerte polymeriske nanopartikler i et akustisk felt. Partiklene ble levert av SINTEF. Kondensert melk ble valgt som en tilsetning etter å ha optimalisert et akustisk attenuasjons-oppsett, og undersøkt effekten av forskjellige konsentrasjoner av bovint serumalbumin og kondensert melk i agarosegeler. Agarosegeler ble brukt fordi leverandøren ikke klarte å levere kollagen. Målinger av diffusjonskoeffisienten til nanopartiklene i kollagengel-fantomet ble gjort med et selvbygd oppsett. Det var en positiv trend mellom diffusjonskoeffisient og ultralydtrykk og -driftssyklus. Derimot var oppsettet sensitivt for vibrasjoner, og mer arbeid er nødvendig før det gir pålitelige resultater.

Abstract

Combining chemotherapy with microbubbles and ultrasound has shown great promise in improving the extravasation of drugs across the blood vessel wall. However, penetration of the drugs through the extracellular matrix (ECM) remains a challenge, and is so far one of the least researched aspects of this treatment. In the ECM, diffusion is the most important transport mechanism. The main barriers for diffusion in the ECM is believed to be electrostatic and steric interactions with collagen, and a reduced hydraulic conductivity due to glycosaminoglycans. In this project a gel consisting of 5 mg/mL collagen, 1 mg/mL hyaluronic acid and 10% evaporated milk was used as a phantom to investigate diffusion of two types of PEGylated polymeric nanoparticles in an acoustic field. The particles were provided by SINTEF. Evaporated milk was chosen as an additive after optimizing an acoustic measurement setup, and investigating the effect of different concentrations of bovine serum albumin and evaporated milk in agarose gels. Agarose gels were used due to the manufacturer being unable to ship collagen. Measurements of the diffusion coefficient of the nanoparticles in the collagen gel phantom was done with a custom built setup. There was a positive trend between diffusion coefficient and the ultrasound pressure and duty cycle. However, the setup was sensitive to vibrations, and more work is needed before it can be reliably used.

Contents

Preface	iii
Sammendrag	iv
Abstract	v
Contents	vi
1 Introduction	1
2 Theory	3
2.1 Tumours and drug delivery	3
2.2 Enhanced Permeability and Retention effect (EPR)	3
2.3 Nanoparticles as drug carriers	3
2.4 Extracellular Matrix (ECM)	4
2.5 <i>In vitro</i> ECM phantoms	6
2.6 Hydrogels	6
2.7 Brownian motion and Diffusion	8
2.8 Transport in ECM	9
2.9 Ultrasound in diagnostics	9
2.10 Ultrasound in drug delivery	10
2.11 Increasing acoustic attenuation of gels using additives	13
2.12 Experimental techniques	13
2.12.1 Fluorescence and Stokes' shift	13
2.12.2 Confocal Laser Microscopy	14
2.12.3 Second Harmonic Generation (SHG)	15
2.12.4 Particle tracking	16
3 Materials and Methods	17
3.1 Preparation of Collagen and Hyaleric Acid composite gel	17
3.2 Preparation of agarose gels with additives	18
3.3 Imaging the collagen gels	18
3.4 Estimating gel pore size from collagen images	19
3.5 Acoustic attenuation measurements of gels	19
3.6 Measuring temperature dependent diffusion in gels and water	23
3.7 Design of setup for measuring transport properties of nanoparticles under effect of US	24
3.8 Characterization of diffusion-measurement setup	26
3.9 Measuring diffusion of nanoparticles in Collagen gels with US treatment	28
4 Results	29
4.1 Characterization of collagen structure with, and without, 1 mg/mL HA and 10% evaporated milk	29
4.2 Pore size in collagen gels	31
4.3 Optimization of acoustic attenuation setup	34

4.4	Acoustic attenuation of agarose gels with additives	37
4.5	Acoustic attenuation on Collagen with additives	47
4.6	Diffusion of nanoparticles in water	52
4.7	Temperature-dependent diffusion of PACA NPs in collagen gel	52
4.8	Ultrasound beam profile in diffusion setup	53
4.9	Effects of ultrasound on diffusion of nanoparticles in collagen gels	55
5	Discussion	58
5.1	Acoustic attenuation of gels	58
5.1.1	Reliability of acoustic attenuation measurement setup	58
5.1.2	Comparison of additives for improving acoustic attenuation	59
5.1.3	Acoustic attenuation of collagen gels with evaporated milk	60
5.2	Transport of nanoparticles in gels	61
5.2.1	Collagen gels as an experimental ECM phantom for diffusion experiments	61
5.2.2	Important nanoparticle characteristics for diffusion in collagen gels . . .	62
5.2.3	Effect of ultrasound on the transport of nanoparticles in gels	63
5.2.4	Evaluation of the experimental setup used in the transport measurements	64
5.3	Closing remarks	65
6	Conclusion	67
	Bibliography	69
A	CORNING® COLLAGEN I High Concentration (HC), Rat Tail - Certificate of analysis	78
B	Precision Acoustics PA504 Test certificate	82

Chapter 1

Introduction

Cancer is the collective term for several diseases where the body's own cells start dividing abnormally and begin eliciting parasitic behaviour. Since the cancerous cells are similar to the body's own cells, they will not be recognized as harmful by the immune system. Additionally, the cancerous cells usually have a high mutation rate, which further promotes their own growth at the cost of the host's health. This makes any treatment challenging as the cancer will over time adapt to, and become more resistant to most treatments.

If left untreated a cancer diagnosis means certain death, but in the recent years advances have been made, and several treatment options are available. Chemotherapy is the most common, often in conjunction with other treatments such as radiation therapy, surgery, hormone therapy, or others depending on the specific type of cancer. However, these treatments are lacking in efficacy and specificity, and often will target both healthy and cancerous cells. Thus sequential treatments at lower doses are necessary to prevent serious side-effects. Additionally, some forms of cancers are situated in areas with a complicated physiology, increasing the risk of complications for some treatment options. For these reasons, many cancer types still have a poor prognosis, especially if not discovered early [1, 2]. Although the prognosis for those diagnosed with cancer improves every year, this improvement is less pronounced when compared to other diseases. For instance, in 2016 cancer surpassed cardiovascular diseases as the most common cause of death in Norway [3].

To improve the outcome of cancer treatments, more efficient ways of delivering drugs to tumours are needed. Several nanoparticle platforms have been suggested used as drug carriers. Nanoparticles are larger than free drug molecules, and thus experience a lower renal clearance. This leads to a heightened retention in the blood. Additionally, the particles can be functionalized in ways to improve their targeting to tumour sites. This could allow for the delivery of larger doses of drugs, with less side-effects. However, few of the so far proposed nanoparticle platforms have reached clinical applications. There are several possible reasons for this. Firstly, since the nanoparticles are relatively large, they seldom penetrate far into tumour tissue. Secondly, the nanoparticles usually rely on the *enhanced permeability and retention effect*. This is an effect where the endothelial cells aligning the capillary wall show an increased penetration of the nanoparticles as compared to healthy tissue, and experience an increased retention due to lacking lymphatic system [4]. However, a lot of the evidence for this effect is from studies on mice, and in the recent years several studies have stated that this effect might have been overestimated in human tumours [5, 6].

There is a search for novel strategies for improving the delivery of drugs to tumours. One suggested solution is the combined usage of focused ultrasound with gas bubbles and nanoparticles. The gas bubbles display physical phenomena in combination with ultrasound, which

has the potential to increase the nanoparticle penetration over the vasculature wall and into the bulk tissue. This will exclusively happen in the area near the focus of the ultrasound, and thus larger localized drug doses with a deep tissue penetration can potentially be achieved. One variant of this treatment, *Acoustic Cluster Therapy*, has shown a deep penetration of drugs and a complete tumour regression for immunodeficient mice with a xenografted human prostate tumour [7]. These results are promising, but the treatment is not equally efficient for all forms of cancer. Additionally, the full mechanism of the deep tissue penetration is poorly understood. Understanding the effects of the treatment parameters is very important for translating it to clinical applications, and generalize it to more types of cancers [8]. There are currently several clinical trials ongoing which combine chemotherapy with microbubbles and ultrasound [9, 10].

One knowledge gap that requires investigation is how gas-bubbles together with ultrasound creates an interstitial fluid flow. The driving force for this flow is hypothesized to be vibrations in the endothelial wall induced by the treatment [11, 12]. A gas bubble is lodged in the capillary and the pressure differences induced by the ultrasound causes it to expand and retract. During the expansion phase the capillary wall is stretched leading to an increased penetration of nanoparticles through it. In the interstitium, three forces interact: acoustic streaming, pressure gradients and concentration gradients, all of which are caused by the acoustic field. The asymmetry toward a net outward flow is caused by volume conservation and asymmetric boundaries. The aim is to investigate this hypothesis, and eventually arrive at a predictive model of ultrasound-mediated transport of nanoparticles through tissue. This work will be done in collaboration with Centre of Excellence PoreLab, St. Olavs hospital, SINTEF and several international parties [13].

To create this predictive model, a physical model with predictable characteristics is necessary. The physical model will provide experimental data which can be used to test the predictions of the theoretical model. During my project assignment fall 2020, I worked on creating an ultrasound phantom for use in transport experiments, which included characterizing its acoustic, structural, and rheological properties. From that project, a gel containing 5 mg/mL collagen and 1 mg/mL hyaluronic acid was chosen as an appropriate phantom. However, further work was needed as there was some uncertainty in the results, especially with the acoustic attenuation measurements, which did not seem to follow a power-law frequency dependency as they should. This is believed to be due to the low sensitivity of the experimental setup. The setup will thus be optimized, and new measurements will be made. If the attenuation is not high enough, the attenuation of the gel will be improved with the addition of additives. In parallel, a setup for imaging nanoparticle behaviour under the influence of ultrasound will be designed. And through that, attempt to measure the effect of ultrasound on nanoparticle transport in gels. The setup will use a 1 MHz transducer since this is thus far the most relevant transducer in clinical and pre-clinical studies [9, 10, 14–18]. This setup will be characterized and used together with the gel phantom to establish if ultrasound has any noticeable effect on the transport of nanoparticles. Thus, the overall aim of the master thesis is to establish a model for the interstitium to be used to obtain new knowledge on ultrasound-mediated transport of nanoparticles, and to characterize acoustic attenuation in various gel phantoms and measure transport of nanoparticles in collagen gels.

Chapter 2

Theory

2.1 Tumours and drug delivery

One of the most common treatments for cancerous tumours today is chemotherapy, where cytostatic or cytotoxic drugs are introduced with repeated injections at low concentrations. These drugs are designed to inhibit the growth of, and/or kill, the tumour cells, but have a limit in their non-specific targeting due to systemic injection in blood [1]. Cancerous cells are very similar to healthy cells, which proves a challenge since efficient treatment needs to either take advantage of some biological effect restricted to cancer, or needs a specialized method of delivery[2].

2.2 Enhanced Permeability and Retention effect (EPR)

The Enhanced Permeability and Retention effect (EPR) is a phenomenon seen in cancerous tissue. Tumours grow rapidly, and has an up-regulated release of pro-angiogenic factors, leading to disorganized and hastily built vascular network [4, 19]. The capillaries in tumour tissue are often overly fenestrated, leading to a higher permeability and thus retention of the drugs in the tumours. Additionally, due to the rapid growth, tumours often have a poorly developed lymphatic system, which further increases the retention of drugs. However, newer studies suggests that parts, if not most, of the enhanced permeability is due to an increase in transcytotic behaviour in the vasculature's endothelial cells [20, 21].

A lot of the evidence for the EPR effect comes from research on mice. For mice the pore sizes in the capillary wall can be two to three orders of magnitude larger in tumours compared to healthy tissue. However, murine tumours grow more rapidly than human tumours relative to the hosts size, has a higher rate of metabolism, and the host has a significantly shorter lifespan. This, combined with the limited success in taking advantage of this effect in clinical applications, has incited some doubt on whether mice are a good model for predicting response to some cancer treatments [5, 22, 23].

2.3 Nanoparticles as drug carriers

As a way to improve cancer treatment, nanoparticles are studied heavily due to their promise as a means for specific targeting and enhanced retention in blood, drawing more utilization of the EPR effect than free drug molecules [24]. Nanoparticles are particles which exhibit nano-scale phenomena. This is typically true for particles with a size below around 200 nm. These particles

are on a biologically relevant size scale and have a big surface-to-volume ratio. Nanoparticles can be made of several different materials, but the most investigated in a biological context are metal oxides, metals, lipids and polymers. Other characteristics which are of importance in a biological context are the zeta-potential, which is a measure of the surface charge of a particle, and the dispersity, which is a measure of how uniform the size distribution of the particles is. For polymeric nanoparticles, dispersity is often given as a Poly-Dispersity Index (PDI), where a lower number means a more uniform size distribution.

The nanoparticles can be functionalized in different ways to take more advantage of the small dissimilarities between cancerous and healthy tissue. Some typical particle functionalizations are for instance through drug loading, implementation of drug release mechanisms, surface modifications to inhibit immune responses, or attachment of targeting ligands [25].

The efficacy of nanoparticles as drug carrier has been shown with great success in laboratories. However, there has been limited success in translating this to clinical situations [23]. One noteworthy nanoparticle platform in use clinically today is Doxil[®], which are PEGylated liposomes loaded with the cytostatic doxorubicin. They utilize passive targeting through the EPR effect, and show superior targeting efficacy compared to free doxorubicin. [26].

PEGylation

PEGylation denotes the process of attaching polyethylene glycol (PEG) on the surface of a nanoparticle. The general structure of PEG is a long chain of polyether with hydroxyl groups at each end, which can be attached to the nanoparticle both covalently and non-covalently. The PEG coating will increase the hydrodynamic radius of the particle which prevents renal clearance, and thus increases circulation time. Additionally, the PEG molecules lowers the zeta-potential, and provides steric hindrance, which shields the underlying nanoparticle from recognition by the immune system. Both by preventing the attachment of antibodies, as well as preventing the recognition by immune cells. Studies have shown that the circulation time of nanoparticles can be increased from only a few minutes or a couple of hours at most, to several hours or even days [27]. This allows the particle to take more advantage of the EPR effect, as the increased retention time in blood increases the likelihood of particle accumulation at the tumour site.

However, the PEG coating has also been shown to prohibit the uptake of the nanoparticles into the tumour cells. This leads to varying results in studies, where some show that PEGylation leads to an overall increase in uptake, while others show no effect on the uptake, or even a reduction [28].

2.4 Extracellular Matrix (ECM)

The extracellular matrix (ECM) is the medium in the interstitium between cells, and forms a scaffolding in which they are attached. It is dominantly produced by fibroblasts in connective tissue, chondrocytes in cartilage, and osteoblasts in bone. The ECM is heterogenous within tissue, and depending on tissue type it can be either anisotropic or isotropic. [29].

The ECM contains two classes of macromolecules: fibrous proteins and proteoglycans. The fibrous proteins include collagens, laminin, elastin and fibronectin, and they imbue the matrix with its tensile properties, such as strength and elasticity [29]. Collagen is the most abundant of the fibrous proteins, and exists in many variants with different abundances in different tissue types, whereas type I is the most common. It is a protein with sequential hydrophobic,

positively charged and negatively charged regions. Three such proteins get together in a tri-helical structure to form a fibrill, and the fibrills combine together to form large fibers. These fibers function as a scaffolding for other ECM constituents to bind to, and is thought to be the main inhibitor of the transport of larger particles through the matrix. [30].

The other group of macromolecules are the proteoglycans which are Glycosaminoglycan (GAG) molecules covalently attached to a protein backbone. GAG is a polysaccharide comprised of repeating units of disaccharides. The GAG is negatively charged and usually adapts an extended configuration which imposes a high viscosity and compressive resistance to the matrix. The proteoglycans have a wide variety of functions depending on bodily context. However, they generally play an importance in hydrating and buffering the ECM, and in intercellular signal transduction. Additionally, The charge and the steric occlusion imposed by the extended conformation acts as another mechanism to inhibit transport in the ECM, especially for small or negatively charged particles. [29].

One notable exception of the proteoglycan group is Hyaleronic acid (HA) which is a GAG that does not covalently attach to proteins, but creates complexes with other proteoglycans through linker proteins. It is also the largest polysaccharide produced by human cells, with molecular weights of 100,000 - 10,000,000 Da. HA also has a high turnover in the tissue, and while 30% is expected to be metabolised locally, the rest is removed through lymphatic routes [31]. Since it has superior water-binding properties relative to its molecular weight it is believed to be a major contributor in maintaining water homeostasis, and one of the contributors to a fluid flow in the cell interstitium [32, 33].

An illustration of the ECM can be seen in figure 2.1.

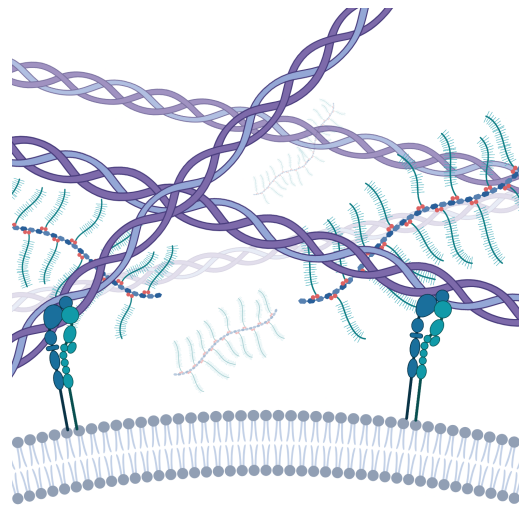


Figure 2.1: Simple illustration of the ECM close to a cell. The collagen (purple) is the tri-helical structure connected to the integrin proteins on the cells surface, and GAG's (green, branched) are dispersed between the fibers. (Other ECM constituents not shown)

ECM in tumours

Due to space-inhibited growth the tumours are usually more dense, with a more tightly packed ECM. This, in addition to other factors such as the EPR effect, and an underdeveloped lymphatic system, leads to increased interstitial fluid pressure (IFP) and thus a heightened resistance against drugs [34, 35]. Additionally, collagen and HA in tumours vary in amount and structure between different types, which is one of the reasons leading to varying response to treatment

to the same drug [36]. The relative amounts of HA and Collagen in different tumour ECMs can be seen in table 2.1, and some data for GAG and collagen content in healthy tissue can be seen in table 2.2. Furthermore, HA is an important indicator of cancer severity. An over-expression of HA has been linked to a poor prognosis for people with many different forms of cancers. Additionally, the HA found in cancers is generally of lower molecular weight as compared to healthy tissue [37, 38].

Table 2.1: Concentration of hyaleronic acid and collagen in different tumour ECM grown in mouse dormal chambers. Adapted from [39], based on data from [36]

Tumour name	Tumour type	Collagen [mg/mL]	HA [mg/mL]
MCaIV	Mammary carcinoma	9.0 ± 2.5	0.80 ± 0.15
LS174T	Human colon adenocarcinoma	9.0 ± 2.5	0.55 ± 0.10
U87	Human glioblastoma	44.5 ± 21	0.55 ± 0.15
HSTS26T	Human soft tissue sarcoma	29 ± 5.5	0.80 ± 0.10

Table 2.2: Concentration of GAGs and collagen in different human tissues, relative to interstitium weight. Adapted from [33]

Tissue	Collagen [mg/g]	GAG [mg/g]
Vitreous body	8	0.5
Myocardium	14	1.2
Skeletal muscle	50-100	2.5 - 7.5
Dermis	300 - 400	1.2 - 5.5
Sclera	240	4.8
Subcutaneous tissue	112	1.0 - 3.5

2.5 *In vitro* ECM phantoms

Doing studies on phantoms, which acts analogues to real ECM can be beneficial in several ways. Phantoms are compared to animal studies; often cheaper, require less ethical considerations, more reproducible, and can be tailored to highlight the exact properties under investigation. Noteworthy phantoms which can mimic ECM include different gels which may or may not contain ECM-constituents and cells, ECM from mono-layered cell-cultures, and spheroids which are small aggregations of cells dispersed in solution. In the latter cases, with cell-grown ECM, there is a trade-off in higher accuracy against less control of the ECM constitution and simplicity [40, 41].

2.6 Hydrogels

Hydrogels are made of long hydrophilic polymers, with water as dispersion medium. These polymer chains cross-link to form a large porous network, and the water helps stabilize a 3D geometry. Hydrogels have the advantage in that a large amount of control can be exerted on its constitution and fabrication parameters. The exact constitution of each gel is usually adapted to the exact properties which it will be used to measure, and can include both biological and synthetic polymers, as well as different additives. Hydrogels have been extensively used, with

success, in different medical sciences to emulate tissue [42–44]. Additionally, the ECM is a gel and as such a synthetic hydrogel made of ECM constituents can be a good approximation [45].

Collagen hydrogel formation

Collagen reconstitution and experimental conditions such as pH, temperature and ionic strength has been studied in great detail. The collagen monomers, which exist as triple helices, cluster together and form aggregates of 5-17 helices. These assemble into fibrils, which might bundle into fibers consisting of two or more fibrils. The process is driven by an increase in entropy in the solvent. The collagen is usually stabilized by both covalent and non-covalent cross-linking between the fibers, but *in vitro* the stabilization is mainly due to entanglement of the fibers, making it a physiochemical gel [46].

The gelling process is consistent with a nucleation and growth mechanism. During the nucleation phase most of the fibers are formed and their thickness is determined. Generally a higher concentration, increased pH, lowered ionic strength and lower gelling temperature leads to more nucleation cores and thus more, but thinner fibers. After the nucleation phase a growth phase is initiated in which the fibers grow in length, intersect, and form complex networks. This process continues until the collagen is used up in the solution. The amount of nucleation cores and collagen concentration is thus the determining factors in the length of the fibers achieved [47–49].

Collagen-HA-composite hydrogel

A collagen-HA gel is expected to be a better phantom for investigating transport in ECM than pure collagen gels. This is due to being one of the most abundant molecules in the ECM, and including it in the gel is expected to lead to a more tissue-similar response to the ultrasound.

HA in collagen gels has not yet been widely studied because it is believed to have less of an impact on the microstructure of collagen gels than other proteoglycans [50, 51]. However, it has been shown that collagen fiber formation kinetics and fiber thickness is affected to some extent by the addition of HA. Gels with HA display shorter, thinner and more numerous fibers. This can be explained by HA having an inhibitory effect on the formation of collagen fibers. [52].

Agarose gel

Agarose is a polysaccharide consisting of repeating units of D-galactose and 3,6-anhydro-L-galactopyranose. Agarose usually comes as a white powder which can be dissolved in water near the boiling point. When the agarose solution cools, the agarose forms helical fibers which again form a porous 3D network. The pores in this network typically have a diameter of 50-200 nm depending on the agarose concentration.

The network is stabilized by hydrogen bonds, and the gel can thus be re-melted. Agarose exhibits thermal hysteresis, so the melting temperature is significantly different from the gelling temperature. Agarose comes in different types based on the extraction source and the degree of methylation. Depending on the specific type, the gelling temperature typically lie between 30-50°C, while the melting temperature lie between 85-95°C.

Agarose has seen wide adoption in research for use as molecular sieves for protein separation, gel electrophoresis[53], and scaffoldings for 3D cell cultures[54]. It has also seen some usage as a tissue substituting phantom for ultrasound experiments [55, 56].

2.7 Brownian motion and Diffusion

Brownian motion is the random movements seen for particles suspended in a fluid. The movement of the particles arise because of anisotropic momentum transfer from the surrounding fluid molecules. Due to the apparent randomness in how individual molecules move in the fluid, this also translates to an apparent random motion of the suspended particles. An illustration of this effect can be seen in figure 2.2.

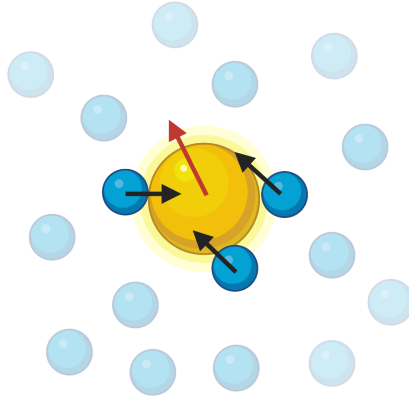


Figure 2.2: An illustration on how the random motion of fluid molecules (blue) can impart a force, and a transfer of momentum, to a suspended particle (yellow).

For an ensemble of particles, the random motion gives rise to a tendency for the particles to spread out and become homogeneously dispersed in the fluid. This effect is called diffusion, and explains at which rate an ensemble of particles move from an area of high concentration to an area of low concentration. Diffusion is modelled mathematically through the *diffusion equation*,

$$\frac{\partial \phi(\mathbf{r}, t)}{\partial t} = D \nabla^2 \phi(\mathbf{r}, t), \quad (2.1)$$

where ϕ is the particle concentration at a given position and time, and D is the diffusion coefficient.

For non-interacting nanoparticles diffusing through a homogeneous liquid, the diffusion coefficient can be estimated through the *Stokes-Einstein relation*,

$$D = \frac{k_B T}{6\pi\eta r_H}, \quad (2.2)$$

where k_B is the *Boltzmann constant*, T is the temperature, η is the viscosity of the medium, and r_H is the hydrodynamic radius of the particle [57]. The viscosity is usually also to a large extent dependent on the temperature, and this needs to be taken into account when using this relation. The viscosity of water at a selection of different temperatures is included in Table 2.3.

Table 2.3: The viscosity of water at different temperatures. Taken from [58]

Temperature [$^{\circ}\text{C}$]	Viscosity [$\mu\text{Pa s}$]
20	1002
25	889
30	796
35	718
40	652

2.8 Transport in ECM

Transport of particles and molecules in the ECM is mediated by two main phenomena: convection and diffusion. The equation governing this for nanoparticles is

$$\frac{\partial \phi(\mathbf{r}, \mathbf{t})}{\partial t} + \mathbf{v} \nabla \phi(\mathbf{r}, \mathbf{t}) = D \nabla^2 \phi(\mathbf{r}, \mathbf{t}) + R, \quad (2.3)$$

which is an extension of equation 2.1 which also takes into account the convection flow velocity, \mathbf{v} , of the fluids through the second term on the left-hand side, as well as a constant term, R , on the right-hand side which captures the behaviour of removal of particles through adhesion to the matrix constituents, degradation of particles or uptake into cells.

For cancer tissue the IFP is usually homogenous in the core, so the convection flow velocity is usually negligible except at the periphery. In addition to this, the IFP is high near the tumour boundary. This leads to a diminished, or in some cases reversed, pressure gradient from the capillaries and into the tissue. With the extinction of the influence of IFP, diffusion becomes the most important mechanism for particle transport through cancerous ECM. [22].

While diffusion is the most important transport mechanism in the ECM, it is severely hampered by the GAG and collagen content of the matrix. GAG content has been shown to be inversely correlated with the hydraulic conductivity of the tissue[32]. Furthermore, the diffusion coefficient is inversely correlated with the collagen content. However, the full transport limiting effects of GAG and collagen likely arises from an interplay between the two, where collagen acts as a scaffolding for the GAG to bind to, and thus strengthen its negative impact on the hydraulic conductivity [33, 36].

Due to the hampered diffusion, it alone is not a strong enough mechanism to provide efficient drug delivery to tumours. There is a need to increase the transport through some other means. Using high intensity ultrasound is a proposed method to achieve this. Ultrasound exhibits mechanical effects which potentially can be utilized in a drug-delivery system, and it has additional benefits such as being non-invasive, and its usage is to some extent already established in the health sector.

2.9 Ultrasound in diagnostics

Ultrasound (US) is any sound wave that has a frequency which is greater than the capabilities of human hearing. This is generally true for any sound with a frequency above 20 kHz. Sound waves are pressure waves in some medium with areas of low and high density which travel in some direction. US has been widely employed for diagnostic imaging due to being non-invasive, soft tissue displaying little acoustic absorbance, and the capability of ultrasound

to reflect off interfaces between tissue types which can be caught by a receiver. It has widespread application, and is for instance commonly used to image fetuses during pregnancy or to discover kidney and gall stones, but can also be used to measure the elasticity of different tissues and the flow of blood in the vascular system [59, 60].

Contrast agents can be used to expand upon the capabilities of ultrasound imaging. This has successfully been employed to image for instance soft tissues and vasculature. To make a good contrast agent, an interface between materials with different acoustic impedance is important, and for that reason gas-filled microbubbles are the preferred choice. The microbubbles will show a big reflectance to the US waves and can therefore easily be imaged. [61]

Ultrasound waves are governed by the wave-equation,

$$\frac{\partial^2 \mathbf{u}}{\partial t^2} = C^2 \nabla^2 \mathbf{u}, \quad (2.4)$$

where u is the spatial distribution of the wave, t is time, and C the speed of sound in the medium.

2.10 Ultrasound in drug delivery

US has not only shown promise for its diagnostic modalities, but also as a means for enhancing therapeutics. It's being actively utilized to treat kidney stones by shattering them with high intensity waves[62], and has also been shown to increase bone regeneration. Likely through the activation of mechanosensitive ion channels [63]. In addition to this, a novel therapeutic application is being investigated. The microbubbles traditionally used as contrast agents display several interesting effects besides being reflective in an acoustic field. The bubbles will absorb or redirect some of the energy in the acoustic field, and can begin to compress and expand, and or impart momentum to the surrounding medium. These effects can be utilized as part of a drug delivery system to possibly overcome the poor diffusion and convection seen in most tissues. There are several studies which are looking into utilizing ultrasound for better delivery to for instance both tumours, and through the blood-brain barrier [64, 65].

Several parameters of the US are important in which effects microbubbles and tissue display during treatment. The most important are the frequency, the pulse repetition frequency, the pulse length and the mechanical index (MI). [66] The pulse repetition frequency is how often a pulse is sent, the pulse length is the duration of the pulse and MI is a parameter defined by the peak negative pressure of the wave and its frequency. It was initially used to predict the occurrence of cavitation, but has found use as a general prediction tool in ultrasound related effects of microbubbles in tissue[67]. MI is defined as

$$MI = \frac{P_{neg}}{\sqrt{f}}, \quad (2.5)$$

where P_{neg} is the peak negative pressure of the US wave, and f is the frequency. A brief summary of some of these parameters can be seen in figure 2.3.

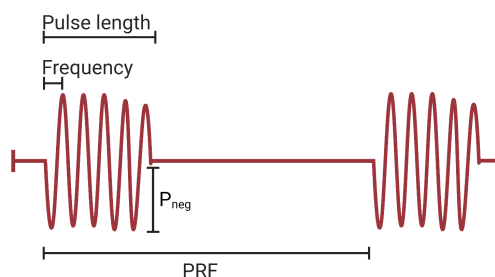


Figure 2.3: Illustration of some of the most important ultrasound parameters. The pulse repetition frequency (PRF), pulse length and frequency are shown.

Hyperthermia

Deposition of energy from the acoustic field from the US induces a localized heating of the tissue. In the context of drug delivery this has been utilized with some success together with nanoparticles which are functionalized with thermosensitive drug-release mechanisms. For instance thermosensitive liposomes loaded with doxorubicin, under the tradename ThermoDox[®], has gone through phase 1 trials. In that study, 7 of 10 patients had a more than a doubling of intratumoural doxorubicin with the exposure of ultrasound, as compared to without [68, 69].

However, in methods which rely on the mechanical effects of the ultrasound, hyperthermia is generally an unwanted effect. This is due to the necrotic effect that thermal ablation can have on cells. In a mechanical context where pressure and frequency are fixed, hyperthermia can be mitigated by a reduction of the pulse repetition frequency or pulse length.

Cavitation

High intensity US, which has a high MI, can induce cavitation in microbubbles if the frequency is close to the resonant frequency of the bubble. These bubbles will oscillate with the acoustic field, and at lower pressures the oscillation can be with a stable amplitude. When the cavitation is close to a surface, such as a capillary wall, the bubble oscillation can induce microstreaming, which is a net flow of the surrounding medium. [70, 71]. Additionally, the capillary wall can begin to oscillate with the same frequency as the ultrasound [11, 12].

If the MI is sufficiently high, and the frequency is at the resonance frequency of the bubble, the oscillations can have an increasing amplitude over time. Eventually, if the amplitude gets great enough, the bubble will implode violently, causing supersonic shockwaves. This latter effect is termed inertial cavitation, and can cause high localized heating[72], rupture nearby cells[66], and induce the formation of reactive free radicals[73]. There is an active search to utilize this mechanism in drug delivery [74]. Figure 2.4 illustrate how cavitation in microbubbles in principle could help with drug delivery.

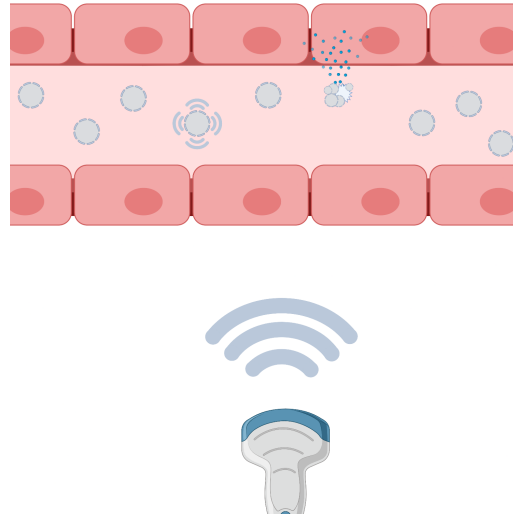


Figure 2.4: Illustration of the cavitation effect when MBs are exposed to an acoustic field. They start to oscillate, implode and release their drug payload to the surrounding tissue.

Acoustic Radiation Force (ARF)

Acoustic Radiation Force (ARF) is a non-linear effect seen with intense US treatment, leading to a transfer of momentum from the acoustic field to the medium. The general requirement is that there is a gradient in acoustic energy through attenuation mechanisms. ARF is proportional to the absorption coefficient of the medium, and the rate of energy applied [75]. If the ARF is high enough, it is capable of inducing local displacements in tissue. The degree of this displacement is dependent on the Young's modulus [76]. In fluids, ARF can lead to acoustic streaming, a net movement along the acoustic field which is capable of transporting particles [75, 77].

ARF's relevancy in drug delivery hasn't been extensively investigated. However, one study utilized ARF-forces to improve the targeting efficacy of lipid nanoparticles with targeting ligands in an *in vitro* capillary model[78]. However, an earlier study which looked at the influence of ARF of displacements of nanoparticles in a collagen gel found that the effect was negligible. It is believed that the lack of displacement is due to the low attenuation of the collagen gels [79].

Acoustic attenuation

Acoustic attenuation is a measure of how much energy is lost from a sound wave through different mechanisms when it propagates through some medium. The mechanism by which this energy is lost include the ones listed in the previous sub-sections as well as others, but can be broadly separated into the following categories: scattering, reflection and absorption. The acoustic intensity, I , at a point z in a medium relative to the starting intensity, I_0 is governed by this relation:

$$I = I_0 e^{-\alpha z}, \quad (2.6)$$

where α is the acoustic attenuation coefficient. The attenuation coefficient shows a frequency dependence by this relationship:

$$\alpha(f) = \alpha_0 f^c, \quad (2.7)$$

where α_0 is the attenuation constant derived from material properties, and c is some exponent denoting that the attenuation has some power-law scaling with frequency. c has a value of 2 for water, but typically lies in the range of 1 to 1.6 in soft tissue [80]. The attenuation coefficient for different tissues can be seen in table 2.4. Additionally, the expected acoustic attenuation of gels similar to the ones used in this report, as found from literature, is listed in table 2.5.

Table 2.4: List of density and attenuation coefficient for some tissue types. Adapted from [80].

Material	Density [mg/mL]	Attenuation [dB/cm/MHz]
Blood	1060	0.2
Bone, Cortical	1975	6.9
Brain	1040	0.6
Breast	1020	0.75
Fat	950	0.48
Soft tissue (average)	1043	0.54

Table 2.5: The acoustic attenuation measured for agarose and collagen gels similar to the ones used in this report. The data for the agarose gels is adapted from [81], and the data for the collagen gel is calculated from the power law fit, $0.024f^{1.5}$ (equation 2.7), provided by [82]

Gel	α_{1MHz}	α_{3MHz}	$\alpha_{3.5MHz}$	α_{5MHz}
	$dB\ cm^{-1}$			
2% Agarose	0.18 ± 0.14	0.23 ± 0.19	-	0.26 ± 0.14
5.5% Agarose	0.33 ± 0.22	0.39 ± 0.18	-	0.80 ± 0.30
4 mg/mL Collagen	0.02	-	0.16	0.27

2.11 Increasing acoustic attenuation of gels using additives

There has previously been some success in using evaporated milk as an additive to agar and gelatin gels to increase their acoustic attenuation. The attenuation in the evaporated milk was found to be 0.8 dB/cm/MHz, which exceeds the values in soft tissue (Table 2.4). Replacing some of the water content in collagen-HA gels with evaporated milk could be a way to increase the attenuation [83, 84].

Bovine Serum Albumin (BSA) is another additive which has seen some usage in ultrasound phantoms. Though it is mostly used as a dosimetry test, as the BSA will become opaque when denatured. It does however increase the acoustic attenuation of a polyacrylamide gel significantly. The acoustic attenuation at 1 MHz of a 40% polyacrylamide gel With 9% BSA was measured to be 0.18 db/cm, while a similar gel with 3% BSA was measured to 0.08 db/cm [85].

2.12 Experimental techniques

2.12.1 Fluorescence and Stokes' shift

Fluorescence is the process in which a molecule is put in an excited state by a photon, relaxes to a slightly lower energy state, and emits a photon of a lower energy than the initial absorbed

photon. This disparity between the emission and absorption spectra of the molecule is termed the Stokes' shift, and can be utilized to detect certain marker molecules by using band-pass filters which only allow the emitted light through. The benefit of this is that unmarked parts of the sample will not be visible, and it is possible to resolve even single molecules. Fluorescent molecules of different types are often attached to nanoparticles to be able to detect them beyond the resolution limit of the microscope.

2.12.2 Confocal Laser Microscopy

Confocal microscopes, in contrast to traditional widefield microscopes, utilize lasers and a pinhole to image a sample. By positioning the pinhole in the conjugate aperture plane it limits the focal depth and leads to a more precise depth focus. Also, the laser has a very constrained xy-distribution, and an image is obtained by scanning it over the sample. This minimizes the contribution from out of focus planes above and below the focal plane. In effect this leads to an image with less background noise.

Confocal Reflective Microscopy (CRM) is a technique sometimes used on a confocal microscope which utilizes the inherent reflectance of materials and boundaries, and thus does not need any staining procedures for contrast. However, this comes at the cost of not being able to image features aligned vertically at some cutoff angle [86]. An illustration of the working principle behind confocal microscopy can be seen in figure 2.5, and an illustration of the cutoff-effect, when looking at collagen gels, can be seen in figure 2.6.

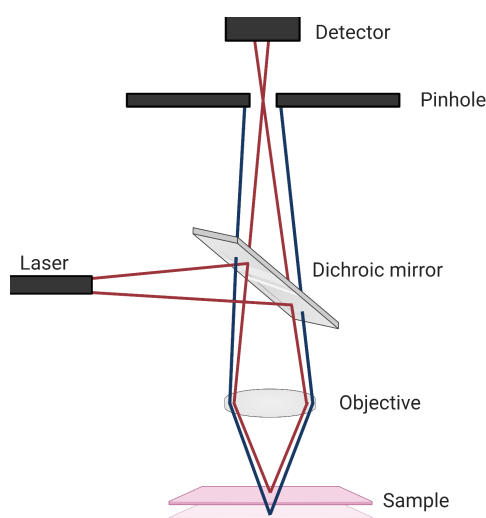


Figure 2.5: Illustration of the working principle behind a confocal microscope. The laser light is reflected off a dichroic mirror and hits the sample. The light reflected off the sample passes through the objective and a pinhole positioned in the aperture plane before hitting the detector. The pinhole blocks the rays emitted from outside the focal plane.

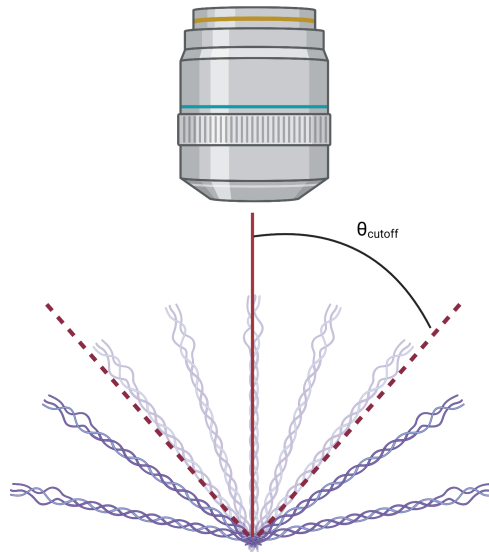


Figure 2.6: An illustration of the cutoff-effect perceived when doing confocal reflectance microscopy or second harmonic microscopy. Fibers aligned at an angle below the cutoff angle will not be visible in the images. Based on figure from [87].

2.12.3 Second Harmonic Generation (SHG)

Second Harmonic Generation (SHG) is a two-photon process in which two photons of equal wavelength interact with a sample, are combined, and released as one photon with twice the energy/frequency. SHG requires a material with a non-linear susceptibility that experiences induced dipole moments. Collagen fibers is one such material, and SHG can be used to image the fiber structure, analogous to CRM. The added benefit by using SHG over CRM is that the SHG signal will predominantly measure collagen fibers in tissue, while CRM will give an output for most material over a certain size. [88, 89] SHG has similar issues as CRM when imaging fibers aligned vertically above some critical angle [87].

Pore size in isotropic random networks imaged by SHG and CRM

Collagen gels have been shown to closely resemble ideal isotropic random networks [90]. The pore sizes of such networks can be estimated through the *nearest object distance* (NOD), which is the distance to the nearest network fiber at any given point in the matrix. The NODs in such a network are distributed through the Rayleigh distribution:

$$p(r_{nod}) = \frac{r_{nod}}{\left(\sqrt{\frac{2}{\pi}} r_{mean}\right)^2} \exp\left(-\frac{r_{nod}^2}{2\left(\sqrt{\frac{2}{\pi}} r_{mean}\right)^2}\right), \quad (2.8)$$

where r_{nod} is a particular NOD, $p(r_{nod})$ is the probability of observing that particular NOD, and r_{mean} is the mean NOD.

To estimate the mean NOD of a network, voxels (3D analogue of a pixel) can be randomly distributed in a skeletonized 3D representation of the network, and the NOD for each of the voxels can be measured. Since the NOD distribution will closely resemble the Rayleigh distribution, the mean NOD can be extracted through a curve fit. However, due to using CRM and SHG to image the collagen microstructures, fibers oriented at a polar angle less than the cutoff

angle will be invisible on the images. Thus, the measured r_{mean} will be directionally biased, and give the appearance of an anisotropic network [87].

Since the fibers in CRM and SHG images have differing brightness dependent on their orientation in relation to the objective, calculating the second moment (variation around the mean) of the voxel intensities will normally show a uniform distribution in the azimuthal direction, and a sine distribution in the polar direction. The cutoff angle can be determined from the difference between the integrals of the idealized sine distribution and the second-moment polar distribution, and be used to unbiased the measured NOD through the relation

$$r_{mean,unbiased} = r_{mean,biasd} \sqrt{\cos \theta_{cutoff}}. \quad (2.9)$$

This value can be converted to give similar results as the more widely established Covering Radius Transform (CRT) by multiplication with a constant:

$$r_{crt} = 1.82r_{mean}. \quad (2.10)$$

The CRT is more widely used in literature, and is normally found by estimating the the largest spheres that are possible to fit into the pores of a skeletonized network.

2.12.4 Particle tracking

To get an estimate of the diffusion coefficient of a particle in some medium, a widely used technique is individual particle tracking. By imaging the system at multiple, constantly separated, time points, and measuring the displacement of each particles in that time, it is possible through statistical means to extract a diffusion coefficient.

The diffusion coefficient, D_i , of an individual particle can be calculated through its relation to the particle's mean square displacement (MSD) in two dimensions,

$$\langle \mathbf{r}_i^2 \rangle = 4D_i t, \quad (2.11)$$

where $\langle \mathbf{r}_i^2 \rangle$ is the mean of all the measured, and squared, displacements for a particle, within a given time t .

The diffusion coefficient for the ensemble of particles can then be estimated by either taking the mean of all the individual particles' diffusion coefficients, or by a linear curve fit of the mean square displacements plotted over several time separations.

Chapter 3

Materials and Methods

3.1 Preparation of Collagen and Hyaleric Acid composite gel

A HA stock solution was made by dissolving 4.24 mg sodium hyaluronan (2.0-2.2 MDa from recombinant *Streptococcus Equi*, Sigma Aldrich) per 1 mL 4X Phosphate Buffered Saline (PBS, Sigma Aldrich) at 4 °C, which would result in a 1 mg/mL concentration of HA when the solution is diluted to 1X. The dissolving took place in a large eppendorf on a shaker-board at 4 °C over-night. Before preparing the solution, pipette tips and eppendorfs were cooled on ice for at least 30 minutes. The finished stock solution was stored in a fridge at 4 °C for a maximum of one week.

As with the HA stock solution, all required tools and chemicals were cooled on ice for at least 30 minutes before preparing the gels. The required tools which were chilled includes sample holders, eppendorfs, pipette-tips, pH-electrode (SenTix[®] Mic-B), de-ionized water (DI-water), NaOH, and evaporated milk. Additionally, an effort was made to minimize the handling time when material had to be taken off the ice during the following procedures.

Depending on the exact collagen (COLLAGEN TYPE I High Concentration 8-12 mg/mL, CORNING[®]) concentration in the batch used, the exact volumes of chemicals added were adapted, so the gels reached a target concentration of 5 mg/mL collagen. The preparation started by pipetting out HA stock solution to an eppendorf so it would reach a concentration of 1X in the final gel, this corresponds to $\frac{1X}{4X} = 25\%$ of the total volume. The HA solution was diluted with DI-water such that the solution would dilute the collagen to its target concentration when combined with it, subtracted for other ingredients not yet accounted for. 1M NaOH was added to the HA solution at volume of 16 μ L per mL of target volume, since by experience it is roughly the amount necessary to reach a target pH of 7.4 ± 0.2 in the gels. In the cases where evaporated milk was used in the gels, most of the DI-water was replaced, so the final gel had a concentration of 10% evaporated milk (Tørsleffs[®], unsweetened) by volume. The solution was then thoroughly mixed with a pipette tip. This step was done carefully to avoid formation of gas bubbles.

To complete the preparation of the gel, the required volume of collagen was reverse-pipetted into the HA-solution, and it was mixed with a pipette-tip. To verify that the pH was acceptable, at least three measurements were done with the pH-probe, and if necessary 1M NaOH or 1M HCl was added to adjust it. The added volume from any adjustments (0-2 μ L/mL) was deemed to have a negligible effect on the final concentration of the other constituents in the gel.

In the cases where nanoparticles were included in the gels, the nanoparticles were added to the gel solution in a fume hood to their desired concentration. This was typically 60 μ g/mL

, which corresponds to a volume increase of 0.77-2.31 $\mu\text{L}/\text{mL}$. Two types of polymeric nanoparticles were used. They were both made from the same monomer and were fluorescence labeled, but had different PEGylation and size. They are referenced by their batch-name from the manufacturer as TT-28 and ENP-135. Their characteristics are shown in table 3.1.

The finished gel solution was reverse-pipetted into the desired sample holders depending on further processing, and incubated for an hour at 37 °C. A timer was started at the moment of mixing the collagen with the HA solution, and the time it took from then until the gels were in the oven was in the range of 15-30 minutes. The gels were either used immediately or stored in a fridge at 4 °C for a maximum of 24 hours.

Table 3.1: A list of relevant characteristics of the two types of nanoparticles used in the experiments.

Characteristic	TT-28	ENP-135
Manufacturer	SINTEF	SINTEF
Batch name	TT-28	ENP-135
Material	Poly(Ethylbutyl Cyanoacrylate)	Poly(Ethylbutyl Cyanoacrylate)
Hydrodynamic diameter	172 nm	94 nm
Poly-Dispersity Index	0.11	0.18
PEGylation	Kolliphor & Pluronic	Jeffamin & Brij
Zeta potential	-1.5 mV	-
Fluorescence label	NR668	NR668
Stock concentration	78 mg/mL	26 mg/mL
Stock solution pH	~ 3	~ 3

3.2 Preparation of agarose gels with additives

Due to obstructed deliveries of collagen, some experiments were done with agarose gels as substitutes. The gels were made by first measuring out the required amount of agarose powder (Agarose, BioReagent, for molecular biology, low EEO, Sigma-Aldrich). Agarose gels were made in concentrations of 2% (20 mg/mL) and 5% (50 mg/mL). The powder was then mixed with DI-water, and dissolution took place in a water bath kept right below boiling temperature, and under constant stirring using a magnetic stir bar. The gels were ready when the liquid had become clear, and there were no visible gas bubbles.

Several types of additives were included in the gels. In those cases, the DI-water content was reduced and replaced with appropriate amounts of the additive. The used additives were evaporated milk and Bovine Serum Albumin (Bovine Serum Albumin, lyophilized powder, BioReagent, suitable for cell culture, Sigma-Aldrich) (BSA). In the case of BSA, it was first dissolved in water, such that the target concentrations of both BSA and Agarose could be reached when combined at appropriate proportions. The dissolution took place in glass flask with a magnetic stir bar, and the finished BSA solutions were stored in the fridge at 4 °C.

3.3 Imaging the collagen gels

A Leica TCS SP8 Confocal Microscope was used with a 25x water immersion objective (HCX IRApo, NA = 1.95) to image the microstructure of the gels. The microscope is equipped with

a Coherent® TiSp-laser Chameleon Vision-S multiphoton-laser (MP) which uses an electro-optical modulator (EOM) for intensity control. The MP laser is used together with a hybrid detector (HyD) for SHG imaging. CRM was done with a white-light laser (WLL) at the 410 nm spectral line, using photomultiplier tube (PMT) detectors. The gels were prepared by pipetting 200 μL gel solution into WillCo® Glass-bottom dishes covered by a glass cover-slip, and placed on the microscope sample stage. Brightfield microscopy was used to focus near the bottom of the sample by finding the well-edges. CRM was used to precisely locate to bottom cover glass to micrometer precision. This can be done due to the high reflectance of the glass which gives a clear indication. The focus was then moved 20 μm into the sample to minimize boundary effects. Z-stacks (a series of images at different focal position, but same xy-position) were taken with both CRM and SHG at three different positions in each gel with an area of 116.45x116.54 μm^2 distributed over an image size of 512x512 px^2 in the xy-plane. Each stack contains 46 images with a z-resolution of 0.23 μm , thus imaging the gel in the depth range of 20.00-30.57 μm . The optical section was kept at 1.0 μm for all images. The WLL and MP laser were not in the same focal position and thus the MP laser's focal point had to be manually shifted 2.84 μm into the sample relative to the WLL to image the same layer.

3.4 Estimating gel pore size from collagen images

Image stacks of gels were opened in ImageJ, and each image in the stack was stored as an individual bitmap-file, without any meta-data such as the Look-Up Table (LUT). A script was written in python which automated the process of thresholding, skeletonizing, and NOD-measurements on the collagen gel images. The script made several calls to binaries which were compiled from the source code provided by Krauss et al. [91]. For each image stack, the binaries returned a histogram of NODs, and equation 2.8 was curve-fitted to the histogram to give a mean NOD. The final pore size estimate was calculated as the mean of all NOD measurements, with equal weights on each sample. The NOD measurement was then transformed to a CRT equivalent value by equation 2.10.

The cutoff-angle was similarly estimated by calls to compiled binaries from source code provided by Krauss et al., and by taking the mean between all measurements. The measured cutoff angle was then used to unbias the measured pore size with equation 2.9.

3.5 Acoustic attenuation measurements of gels

The acoustic attenuation, α , through the gels were measured as the loss of power in decibels, as compared to a reference:

$$\alpha = \frac{1}{d}(20 \log_{10} \mathbf{S}_{ref} - 20 \log_{10} \mathbf{S}), \quad (3.1)$$

where S is the frequency-domain signal received through a media, S_{ref} is the frequency-domain reference signal received, and d is the length the sound travelled through the material. The frequency-domain signals, \mathbf{S} and \mathbf{S}_{ref} , were calculated by taking the absolute value of the fast fourier transform of the raw signal. This results in a vector containing the signal intensity at different frequency bins. The frequency bins correspond to the time step sampled divided by the total amount of samples in that time. It follows from this that α is also a vector that contains the attenuation at the same frequency bins. Due to the broad bandwidth of the transmitted signal arising from the short pulse length, a measurement of the attenuated signal is also

possible some distance away from the center frequency. However, the signal-to-noise ratio rapidly decreases further away from the center frequency.

Experimental setup for attenuation measurements

The same setup as used in A. Finnøys's master's thesis [92], which had previously been adapted for measurements of gels, were used. The measurement setup works by emitting an ultrasound beam which travels through the sample positioned 70 mm away from the transducer, gets reflected off a 25 mm thick acrylic slab positioned 27 mm behind the sample, and goes back through the sample before hitting the transducer. The transducer is wired with a t-junction to a LeCroy Wavesurfer 44Xs oscilloscope and an Agilent 33500B Series waveform generator. This ensures that the oscilloscope is able to measure both the signal from the generator and the reflected signal from the transducer. Attaching the waveform generator to the trigger on the oscilloscope ensures that the reflected signal shows up as a peak with a constant time delay relative to the initiating signal (Tbase). Three transducers optimized for the frequencies 1 MHz, 3.5 MHz and 5 MHz were used. Characteristics of the transducers can be seen in table 3.2, and an image of the setup can be seen in figure 3.1.

Table 3.2: The three different ultrasound transducers used, and some of their important characteristics.

Type	Optimal frequency	Aperture size	Focused	Focus distance
	MHz	mm		mm
Ultran WS-1P85	1	32	Yes	85
Panametrics V381	3.5	19	Yes	70
Panametrics V309	5	13	No	70

To prepare the experimental setup, the ultrasound transducer was attached (using an adapter if necessary) to the chamber. Then, the chamber was filled to above the transducer with room-temperature degassed de-ionized water, which was degassed by bringing the water to the boiling point and letting it cool. The water was poured in slowly to prevent the absorption of air. The waveform generator and the oscilloscope was configured according to table 3.3. The considerations going into these parameters included having a short pulse length to ensure a high bandwidth of the emitted signal, as high as allowed voltage to increase the signal-to-noise ratio, and a high degree of averaging to further reduce the impact of noise. After turning it on, several peaks could be seen on the oscilloscope corresponding to the primary signal, reflections of the sample stage, reflections from the acrylic back-slab and other secondary reflections. The oscilloscope was focused on the reflection from the slab, as this will be a signal that has traversed the sample exactly twice.

A MATLAB[93] script was used to communicate with the oscilloscope and store the raw signal data as *.mat*-files.

Table 3.3: List of configuration for the waveform generator and oscilloscope for the three transducers used. The Tbase is approximate, as there might be some slight variation in the delay before the arrival of the reflection from the acrylic slab.

Parameter	Ultran WS-1P85	Panametrics V381	Panametrics V309
Waveform generator			
Waveform	Sine	Sine	Sine
Driving frequency, MHz	1	3.5	5
Amplitude, Vpp	10	10	10
Burst period, ms	10	10	10
Oscilloscope			
DC Coupling, Ω	50	50	50
Averaging, sweeps	200	200	200
Max samples, kS	500	500	500
Sampling rate, $GS\ s^{-1}$	2.5	2.5	2.5
Amplitude per division, mV	2	5	10
Time per division, ns	1000	200	200
Time delay (Tbase), μs	~ 139	~ 137	~ 134

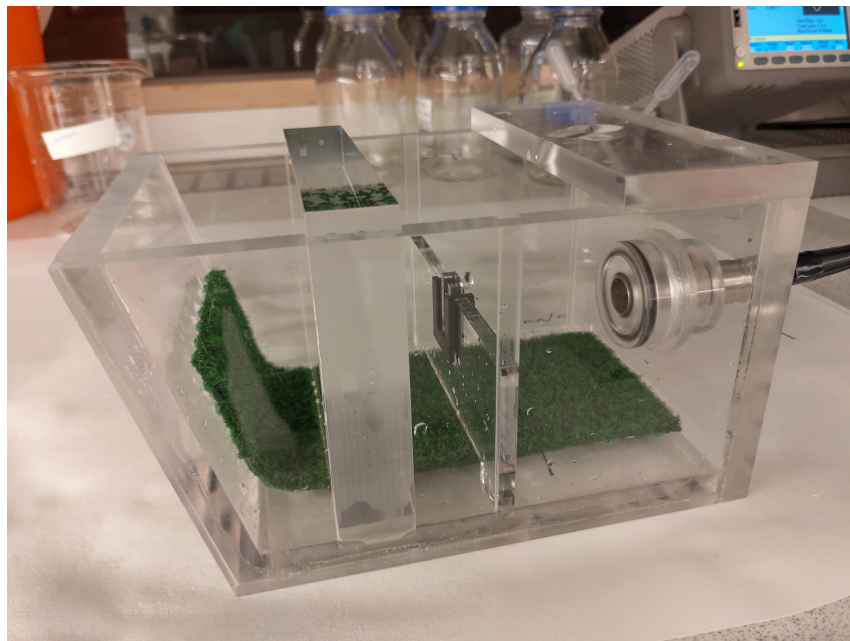


Figure 3.1: The setup used for the attenuation measurements. The ultrasound is emitted from the transducer on the right, passes through the sample in the middle, and is reflected off the back acrylic wall on the left. The ultrasound then returns the same way it came, back through the sample and is reabsorbed by the transducer. This reabsorption creates an electric signal which is detected on the oscilloscope. Note that the setup shown here is with the old, small, sample holder

Optimizing the attenuation measurement setup

Previous measurements done on gels with this setup had shown conflicting results. To ensure reliable results, a full re-design of the sample holder was merited. The previous sample stage was not large enough to accommodate the beam profile of all the transducers. So a sample holder with larger dimensions was designed. The new sample holder was designed for a volume of 3.125 mL, and the exact dimensions can be seen in figure 3.2.

Furthermore, it was discovered that the mylar sheet which was previously glued to the faces of the sample holder had a relatively large attenuation compared to the gels. Therefore, it was replaced with plastic wrap (Toppits[®]). Instead of using glue, double-sided tape (0.1 mm thick) was used and the plastic wrap was taped under tension on a table before adhesion to the sample holder. This ensured a smooth surface, mitigating the risk of an uneven thickness of the gel. Additionally, when gels were introduced to the sample holders, a piece of mylar was cohesed to the surface of the plastic wrap with a drop of water, to prevent the plastic wrap from deforming before and during the cross-linking. Before measurements, the mylar was removed, and the surface of the plastic wrap gently wiped clean with a tissue.

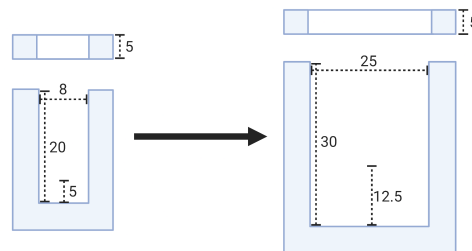


Figure 3.2: Schematic of the old (left) and the new (right) sample holder used in the attenuation measurements. All dimensions are given in mm, and the holder is shown from the top (top) and the front (bottom). The focus area of the ultrasound transducers were 5 mm from the bottom.

Attenuation measurements of collagen and agarose gels

To ensure that the reference signal is from the same sample holder as the gel, the full measurement procedure was repeated twice. Once for the empty sample holder, and once for the same sample holder filled with gel. To fill the sample holders, 3.125 mL gel solution was reverse-pipetted into them. The gels were covered with parafilm to prevent solvent escape, and incubated in an oven at 37°C for an hour.

Three measurements with no sample holder in the stage were done before and after the measurements of both the empty sample holders and the ones containing gels. In other words, reference measurements were done with only water in the ultrasound path. This allows for the calculation of the attenuation through equation 3.1 independently for the empty sample holder and the sample holder containing the gel. To get the attenuation of the gel itself, the attenuation of the empty sample holder was subtracted from the attenuation of the sample holder containing gel.

To do the measurements, the sample stage was taken out of the chamber and the sample holder was slid into it. The sample stage was slid back into the instrument and a pasteur pipette was used to remove entrapped air in the sample holder, as well as remove any air bubbles adhered to the surfaces inside the chamber. Between each measurement the sample stage was removed from the chamber and put back in. Before taking the next measurement,

the memory of the oscilloscope was cleared, and given enough time to record at least 200 new ultrasound pulses. To switch to the other transducers, the chamber was first emptied of water, and new degassed water was poured in.

The data files created by the MATLAB script were opened in Python[94], and a Fourier transform was done on each of the measurements. All the measurements for the same transducer have equal frequency bins, so the mean was taken first between measurements from the same gel solution, then between all gels of the same type. The attenuation was calculated according to equation 3.1. The error was calculated as standard deviation between samples. The results were plotted using the Matplotlib[95] library in Python. The frequencies plotted were limited to the distance around the center frequency before signal noise started to visibly dominate the result.

3.6 Measuring temperature dependent diffusion in gels and water

Collagen samples with HA and evaporated milk were prepared according to section 3.1. Gels with both types of nanoparticles were used. The gels were prepared by pipetting out 200 μL gel solution in WillCo[®] Wells, and covered with a glass cover slip. The nanoparticle-water solutions were prepared with an equal concentration of 60 $\mu\text{g}/\text{mL}$, by simply diluting the stock solution in DI water.

The samples were put on a Zeiss LSM-800 up-right AiryScan confocal microscope with a 40x water immersion objective (NA 1.2, C-Apochromat, WD 0.28). A Pecon[®] heating insert slotted in the microscope stand was used for temperature adjustment. The WillCo[®] wells were filled with small amounts of water to allow for better heat conductivity from the heating insert to the sample, as well as to act as a thermal mass to stabilize the temperature. The temperature had to be over-adjusted on the regulator due to thermal losses through the objective, and a digital thermometer was used to control the temperature before, between and after measurements. It was confirmed that the temperature was within $\pm 0.5^\circ\text{C}$ of the target temperature before starting each measurement. Three different temperatures were investigated: 25°C, 30°C and 35°C.

For the nanoparticles in water measurements, the experimental settings were optimized for frame rate with a trade-off against image quality, and time series data was collected with a zoom-ratio of 4x, corresponding to a 39.97x39.97 μm^2 area of the sample, distributed over a resolution of 128x128 px^2 , at the lowest pixel dwell time possible. The achieved frame-rate was 26.3 frames per second.

The nanoparticles in gel measurements were optimized for position and image quality, and a larger 1024x1024 px^2 resolution was used, at the cost of a lower frame-rate. The pixel dwell time was adjusted such that a frame-rate of two frames per second was achieved. Additionally, some measurements with the same settings as for the free-diffusing particles were used to verify that no fast-moving particles were missed.

For each sample, three videos were extracted. The videos were opened in ImageJ, and particle tracking was done using the TrackMate plugin [96]. The built-in Laplacian-of-Gaussian detector was used to detect the particles, and the expected particle size and threshold was adjusted by hand to best fit the data, while avoiding false positives. The detected points were filtered by the built-in contrast gradient filter to remove any agglomerations, and residual false positives (due to diffraction artifacts). The particle tracking was done using the built-in Linear Assignment Problem tracker. To get accurate results, it is important to choose a good linking distance, which is the maximum distance a particle can move between two frames. For the nanoparticles in water measurements, this was chosen from a normal distribution,

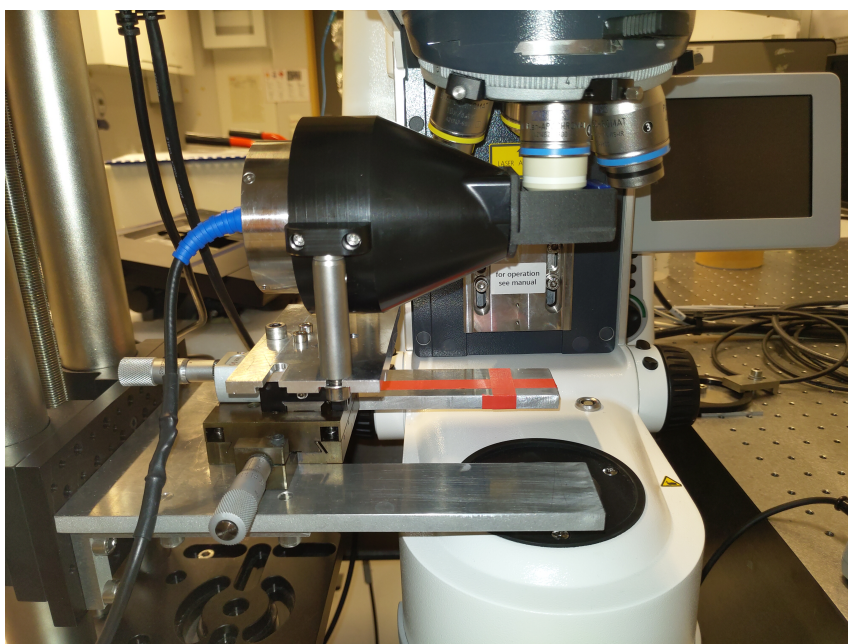
with the MSD as variance. The point where the distribution gave less than a 1% chance of a given displacement was used as the linking distance. The MSD used for this was calculated from the diffusion coefficient predicted through the Stoke-Einstein equation (equation 2.2) for the highest temperature used in the measurements. No frame gap-closing was applied, which means that no attempts were made to correlate particles which disappeared for some frames, but reappeared later. However, in the nanoparticles in gel measurements the linking distance used was found by experimentation, and visual inspection. Additionally, a frame gap-closing was allowed for up to two frames where the particle was missing.

The found particle tracks were saved as csv-files and opened in python for analysis. All tracks shorter than 5 frames were discarded to reduce influence of edge effects, and a diffusion coefficient was calculated for each particle by calculating the mean square displacement, and using its relation to the diffusion coefficient through equation 2.11. The mean was then taken of all the diffusion coefficients, of all the individual particles, to find the coefficient of the ensemble associated with the csv-file. The final estimated diffusion coefficient was found by taking the mean, and standard deviation, between the diffusion coefficient found for each individual measurement (csv-files) on a sample.

3.7 Design of setup for measuring transport properties of nanoparticles under effect of US

A custom setup was designed for measuring the transport of nanoparticles in gels under the influence of US. The setup was manufactured by the mechanical workshop at NV-faculty based on drawings. Several design considerations were taken into account. There was a desire to make the measurements clinically relevant, and a 1 MHz transducer (PA504, Precision Acoustics LTD) was thus used. Since the expected increase in transport relative to diffusion was expected to be in the same direction as the US waves, placing the objective orthogonal to the US was a wanted property. To achieve this, and still position the sample in the center of the ultrasound beam, the sample holder was raised so that it covered half the beam. Also, the setup was designed with a dipping objective in mind. This is necessary due to the sample having to be submerged in water. Acoustically absorbing material was used to mitigate the risk of standing waves between the transducer and the blocked off part of the sample holder. Additionally, the same material was used for the same purpose on the back wall behind the sample. A slot with the same dimensions as a 18x18x0.17 mm glass cover slip was cut out in the sample holder. This ensures precise positioning of the sample, that the sample can with relative ease be swapped out, and that the acoustic reflections because of the glass cover-slip are minimized. Additionally, the sample holder can be disconnected from the transducer cone, so alterations on the setup in the future are possible.

Other considerations which were of importance were the ability to some extent control the position of the objective relative to the sample in all three axes, and having a stable mounting of the setup on the microscope table. The transport measurement setup was thus installed on a metal plate which was connected to two orthogonally connected single-axis translation stages. This gave a freedom of movement in the xy-plane. Movement in the z-axis was implemented by installing the setup on a microscope stage which allowed for manual focusing. The microscope stage was mounted on the same optics table which the microscope was on. The final consideration was that larger volumes of gels are costly to produce, and this setup has a minimal gel usage. The full setup can be viewed in detail in figure 3.3.



(a) The ultrasound transport measurement setup installed on a Leica LSM700 confocal microscope. The setup is installed on two single-axis translation stages which allow xy-positioning of the sample relative to the microscope, and a microscope stage which permits manual focusing in the z-direction. The setup consists of a water-filled cone for the transducer which shrinks in width as the ultrasound gets more focused, and a sample holder which can be seen with a dipping objective submerged in it.



(b) Close-up of the sample holder, with a gel sample on a glass cover-slip installed. The sample is fastened with water-resisting tape to prevent it from moving around during measurements. The sample holder can easily be removed by loosening three white screws, and a plastic film separates it from the transducer cone which is filled with degassed water. As can be seen, half the ultrasound beam is blocked off, and acoustically absorbing material (blue) is used to prevent standing-waves. When measuring, the setup will be raised to submerge the objective, and filled with water.

Figure 3.3

3.8 Characterization of diffusion-measurement setup

The sample holder of the ultrasound setup had a complicated geometry, which makes direct measurement of the ultrasound field difficult. This is because there is not enough room to fit a hydrophone. A separate adapter was thus made, which blocks half the opening of the ultrasound cone with absorbing material in the same way as the real sample holder. However, it does not contain the other features such a slot for the sample or a back-wall. This adapter allows the measurement of the relation between input voltage and peak pressure at different locations behind the opening, but does not account for any influence imparted by the back-wall, the sample, or the objective being present.

The setup was characterized at Department of Circulation and Medical Imaging (ISB) at NTNU. The measurements were done in an Onda AIMS III scanning tank with an Onda HGL-0200 hydrophone connected to an Onda AH-2010-100 pre-amp and a PicoScope 5244A oscilloscope connected to a computer.

The ultrasound setup was submerged in the tank with the beam direction facing downwards, and the hydrophone directed towards the beam opening on the transport measurement setup. An image of the characterization setup can be seen in figure 3.4. The hydrophone position was calibrated by doing a xy-plane scan and finding the position with highest intensity. This was set as the zero-point in the xy-plane. To find the focus distance, a similar scan was done in the z-direction to find the highest intensity point. This position was defined to be the focus length, and defined to be 73.5 mm away from the transducer, as specified by the transducer manufacturers specification (appendix B).

At the focus length, in the center of the beam xy-plane, the input voltage to the power amplifier connected to the transducer was gradually increased in 20 mV increments. At each input voltage, the peak negative, and the peak positive pressures were measured and plotted. The voltage was increased until a peak negative pressure of 1 MPa was achieved. Similar measurements were done at 80 mm distance from the transducer, as a mistake was done in the design of the transport measurement setup, where the distance from the transducer to the center of the sample was measured from the frame of the transducer, instead of the center of the diaphragm. This puts the sample in the far-field of the ultrasound beam.

In addition to measuring the relation between peak pressure and voltage, 2D scans of the beam profile were also performed. The scans were done in 0.1 mm increments over a $2.5 \times 2.5 \text{ mm}^2$ area, with the ultrasound focus in the center. Scans were done at a distance of 73.5 mm and 80 mm away from the transducer.

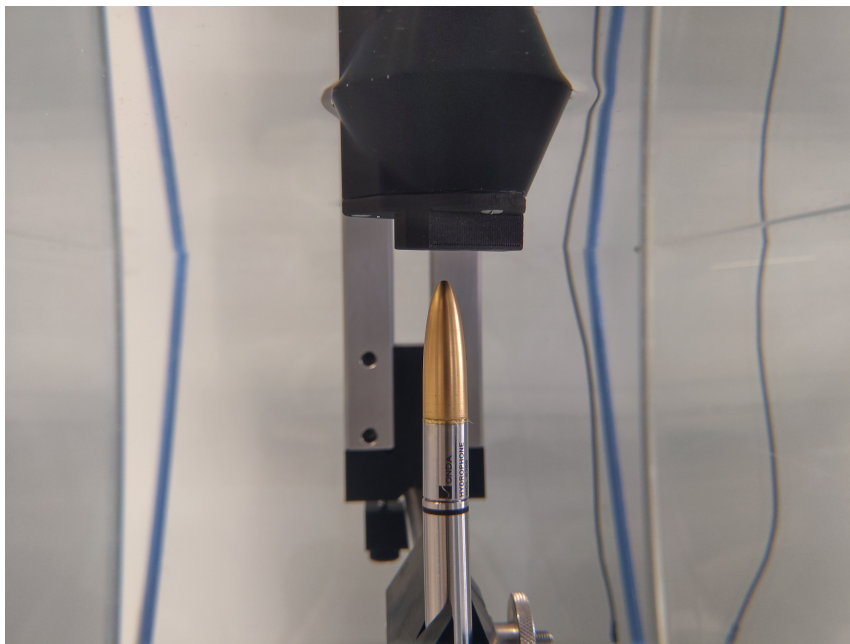


Figure 3.4: The ultrasound transport measurement setup with a custom adapter made for characterization. The setup is submerged in water, and the hydrophone is pointed towards the opening of the transducer.

3.9 Measuring diffusion of nanoparticles in Collagen gels with US treatment

Collagen gel samples with HA, evaporated milk and nanoparticles were prepared according to section 3.1, and a $200\mu\text{L}$ droplet was pipetted onto $18\times 18\text{ mm}^2$ glass cover slips. The cover slip was placed inside small glass-bottom dishes during cross-linking and storage, to minimize solvent evaporation and risk of physical damage to the gels.

To do measurements on the gels, the glass cover slips were placed in the sample socket of the ultrasound transport measurement setup. The setup was assembled under a Zeiss LSM700 confocal microscope, with a 40x water dipping objective (NA 1.0, Plan Achromat, WD 3.5). Each corner of the cover slip containing the sample was taped to the setup with water-resistant tape. This prevented the sample from moving around during measurements. When the sample was secured, the setup was raised so the objective was near the sample. The setup was then filled with water until a small meniscus formed. Positioning of the focus parallel to the ultrasound field was done by letting the objective rest against the edge of the setup, while positioning in the orthogonal direction was done by measurements with a ruler. Height positioning was done by turning on the microscope, adjusting the pinhole to its maximum size, and slowly moving the sample upward until the fluorescent signal from the nanoparticles were found. The pinhole was then reduced to one airy unit, and the focus was moved a little bit further into the sample to avoid measurement of surface-specific effects.

Three measurements were performed on each sample, as well as an equal amount of control measurements in the same positions. The first measurement was taken in the center of the sample, the second shifted 0.50 mm to the left orthogonal to the ultrasound field, and the third 0.50 mm to the right. Focus in the z-direction was adjusted as necessary after shifting the position of the sample. The setup was given approximately 5 minutes of rest between measurements, to allow for cooling of the transducer and sample. 5 minutes was deemed sufficient since it was stated as the required time to cool the transducer in the test certificate (appendix B).

The results from the characterization of the ultrasound setup (figure 4.19b) was used to find the correct input voltage to achieve a peak negative pressure of either 1 MPa or 2 MPa at the center of the sample slide. For the 2 MPa measurements, the input voltage was linearly extrapolated. An Agilent 33500B Series waveform generator was configured for 1 second bursts with 1,000, 10,000, or 100,000 cycles in that time. Respectively, this corresponds to a duty cycle of 0.1%, 1%, and 10%. Thus a total of 6 different modes of ultrasound exposure were performed.

Two datasets of 3 measurements each were collected, with slightly different imaging parameters. In both datasets, the measurements were done as a 2 minutes time series over a $40\times 40\mu\text{m}^2$ large region. However, in the first dataset the imaged region was distributed over $256\times 256\text{ px}^2$, with approximately 6 frames per second, while in the second dataset the resolution was increased to $1024\times 1024\text{ px}^2$, and a framerate of 2 frames per second. The increased spatial resolution was done because the temporal resolution was more than sufficient, and more precision in position was desirable. Additionally, in the second dataset the third measurement was done as a 15 minute time series. Except for in the controls, ultrasound was applied for the full duration of the measurements. A Shapiro-Wilks test was done on the pre- and during-US measurements to determine if the results are normally distributed using a p-value of 0.05, and a Welch's t-test was used to establish if any of the results were statistically significant.

Chapter 4

Results

4.1 Characterization of collagen structure with, and without, 1 mg/mL HA and 10% evaporated milk

Collagen gels with and without additives were imaged with CRM and SHG microscopy. Some variation was discovered in some of the gels within one of the batches. Where there was one sample with visibly thin and long fibers, one with shorter and thicker fibers, and one which was somewhere in between those two extremes. Images of the gels are included in figure 4.1.

In the gels which included evaporated milk the collagen structure was not clearly visible in the CRM images. This is due to other reflective constituents. The gel is filled with small nodular lumps, and some collagen fibers can barely be discerned around them. The SHG image reveals a more dense and clustered collagen network compared to the gels without milk. CRM and SHG images of a gel containing both hyaluronic acid and evaporated milk is included in figure 4.2.

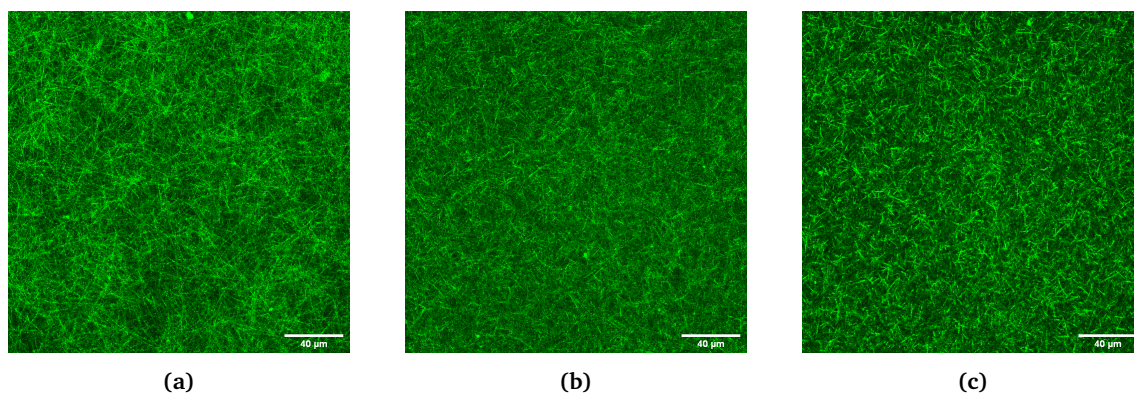


Figure 4.1: Three CRM images showing poor reproducibility within a single batch of collagen gels. Each of the samples appeared homogeneous throughout. The sample in 4.1a shows distinctively thinner and longer fibers, while 4.1c shows shorter and thicker fibers. The sample in 4.1b displays features which lie somewhere between the samples 4.1a and 4.1c. The brightness in the images has been artificially enhanced.

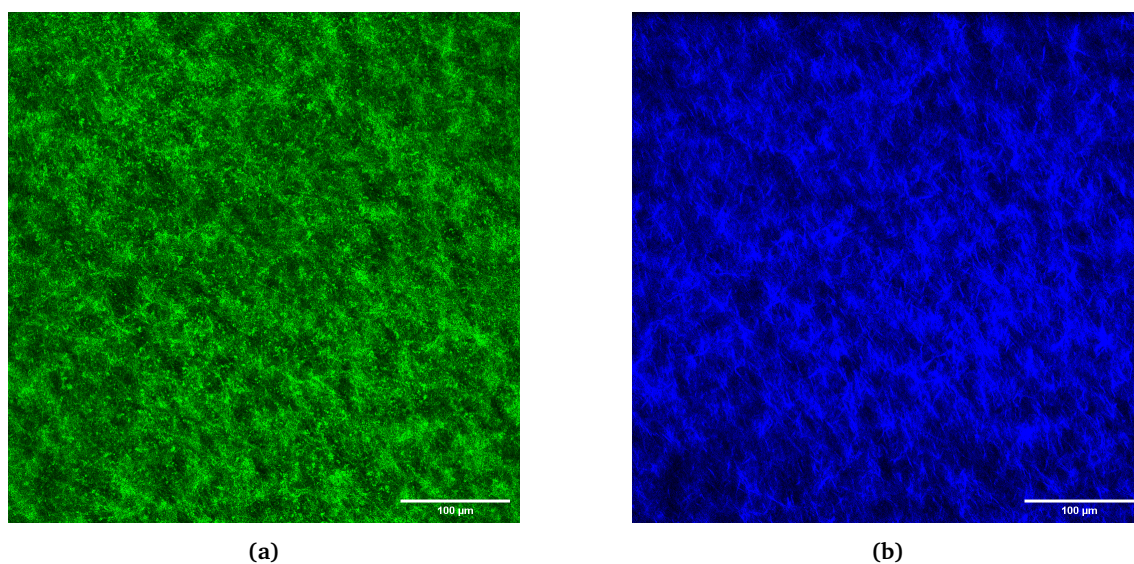


Figure 4.2: A CRM (a) and a SHG (b) image of a collagen gel with HA and evaporated milk. In the CRM image small nodules, which are believed to be fat, can be seen among the fibers. On the SHG image only collagen fibers can be seen.

4.2 Pore size in collagen gels

The CRM NOD measurements were generally in good agreement with the Rayleigh distribution, and resulted in good curve fits. Typical curve fits can be seen in figures 4.3a and 4.3b. The SHG measurements showed a poor fit, where the distribution had a shoulder to the right of the main peak, as can be seen in figure 4.3c. This signifies a systemic bias, and the thresholded and skeletonized network can not be said to be an isotropic random network. The SHG images were thus excluded from the rest of the analysis.

The mean NOD value was found from curve-fitting against the Rayleigh distribution for many different gels, as seen in figure 4.5b, together with the polar cutoff angle as found from figure 4.4 and equation 2.9. From this, a pore size including standard deviation was estimated to $1.75 \pm 0.23 \mu m$ for the gels without HA, and $1.81 \pm 0.15 \mu m$ for the gels with HA. However, the pore size measured for the gel with HA only reflects the pores in the collagen matrix, and does not take into account the other constituents. There is a considerable standard deviation in the result. However, even the lower pore size estimate is many times larger than any of the nanoparticles used in the experiments.

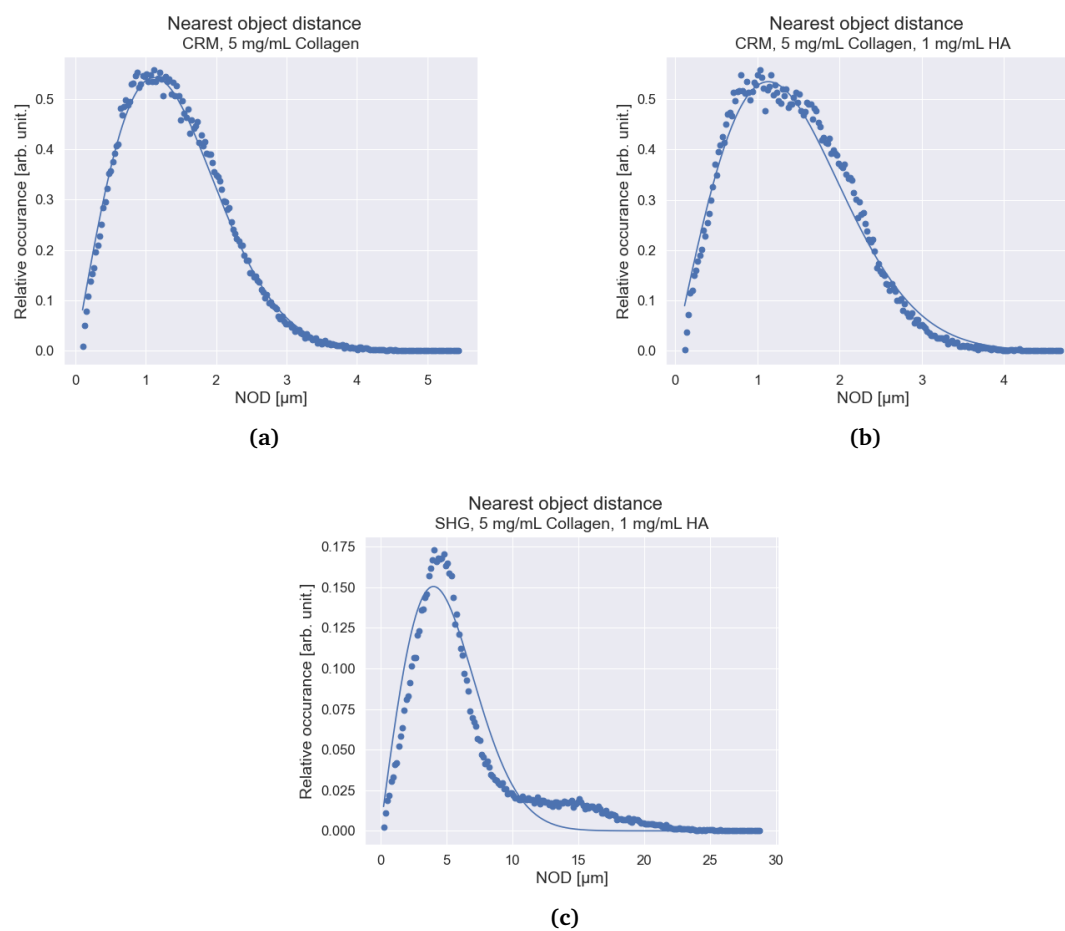


Figure 4.3: Typical raw data from NOD-measurements, and curve fits against the Rayleigh distribution for CRM images on a 5 mg/mL collagen gel (a), CRM images on a 5 mg/mL collagen gel with 1 mg/mL HA (b), and SHG images of a 5 mg/mL collagen gel with 1 mg/mL HA (c).

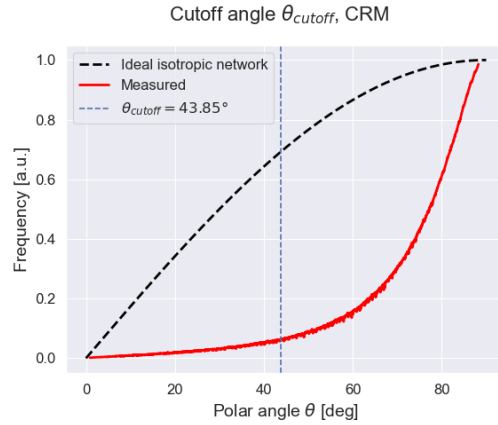


Figure 4.4: The measured polar angles for CRM image-stacks of 5 mg/mL collagen gels, compared to the theoretical distribution for an ideal isotropic network. The vertical line represents the cutoff-angle, and is positioned such that the area under the idealized curve on the right side of the line, matches the area between the two curves.

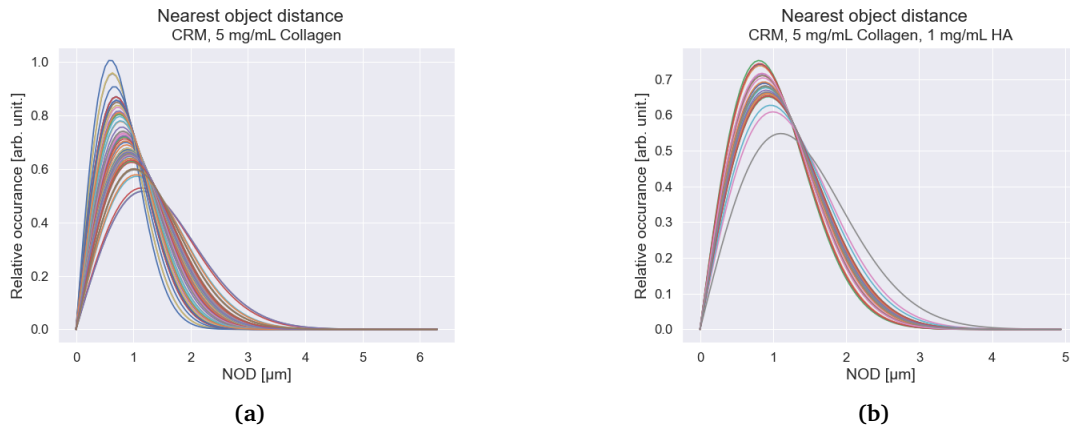


Figure 4.5: Curve fits of the mean nearest object distances measured on 10 samples with 3 CRM image stacks on each for 5 mg/mL collagen gels with no additives (a), and 5 samples with 4 CRM image stacks on each for collagen gels with 1 mg/mL HA (b). The pore size was calculated from the mean of all the curve fits.

4.3 Optimization of acoustic attenuation setup

The effects of the improvements on the acoustic attenuation measurement setup included a replacement of the mylar on the sample holders with plastic wrap, creating larger sample holders, and alterations to the protocol which enabled the use of the same sample holder as reference to the gel measurements. The replacement of the mylar sheet resulted in a decrease of the inherent acoustic attenuation from approximately 0.45 to 0.05 dB at 1 MHz, and from 8 to 0.35 dB at 5 MHz. The full measured spectrums can be seen in figure 4.6. On the same figure, in the lower right quadrant, it can also be seen that there is some variation between individual sample holders, highlighting the need for using the same sample holder for reference and gel measurements.

The up-scaling of the sample holder showed a reduction of inherent attenuation in the sample holders for the 1 MHz transducer, from a level of around 1.6 dB to a negligible amount (technically less than 0, but this is physically impossible and implies other sources of noise are more important). However, the attenuation with the 5 MHz transducer was similar between the two sample holders. The measured spectrums can be seen in figure 4.7. There is considerable variation between frequencies in the plots for the small sample stage, likely arising from a combination of the result being based on a single measurement and spectral leakage. In the large sample stage measurements there is also some variation between frequencies. This gives an indication that the sensitivity limit seems to be somewhere around $\pm 0.07 dB$ near the center frequency, and any difference below that can arise from artifacts from the Fourier transform or other sources of noise.

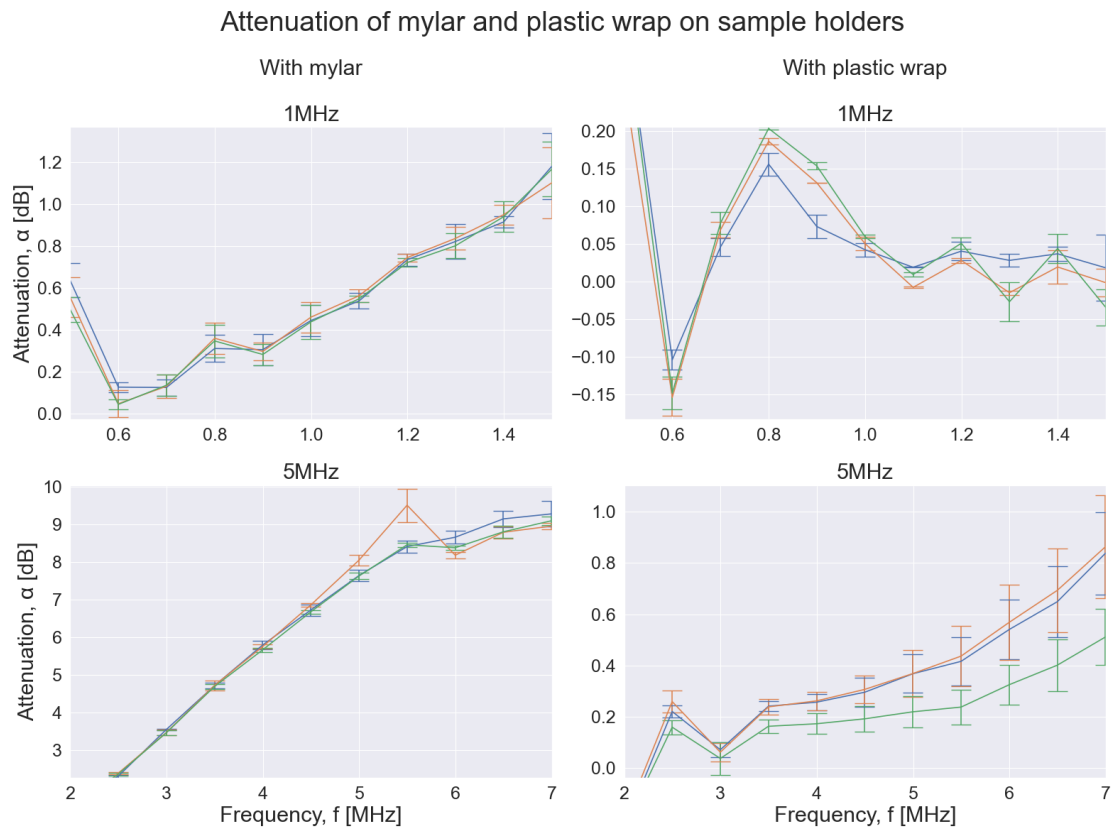


Figure 4.6: Comparison of using either mylar sheet or plastic wrap on the attenuation sample holders. The signal passes through either a layer of mylar or plastic wrap a total of four times, two times for each of the two sides of the sample holders. The results are shown for the 1 MHz and the 5 MHz transducer, and the mylar sheet (left) attenuates the signal by a total of approximately 0.45 dB at 1 MHz, and 8 dB at 5 MHz. The plastic wrap (right) attenuates the signal by approximately 0.05 dB at 1 MHz and 0.4 dB at 5 MHz. 5 measurements were done on three different sample holders of each type. The plots are on different y-axes to better visualize the variations seen between neighbouring frequencies.

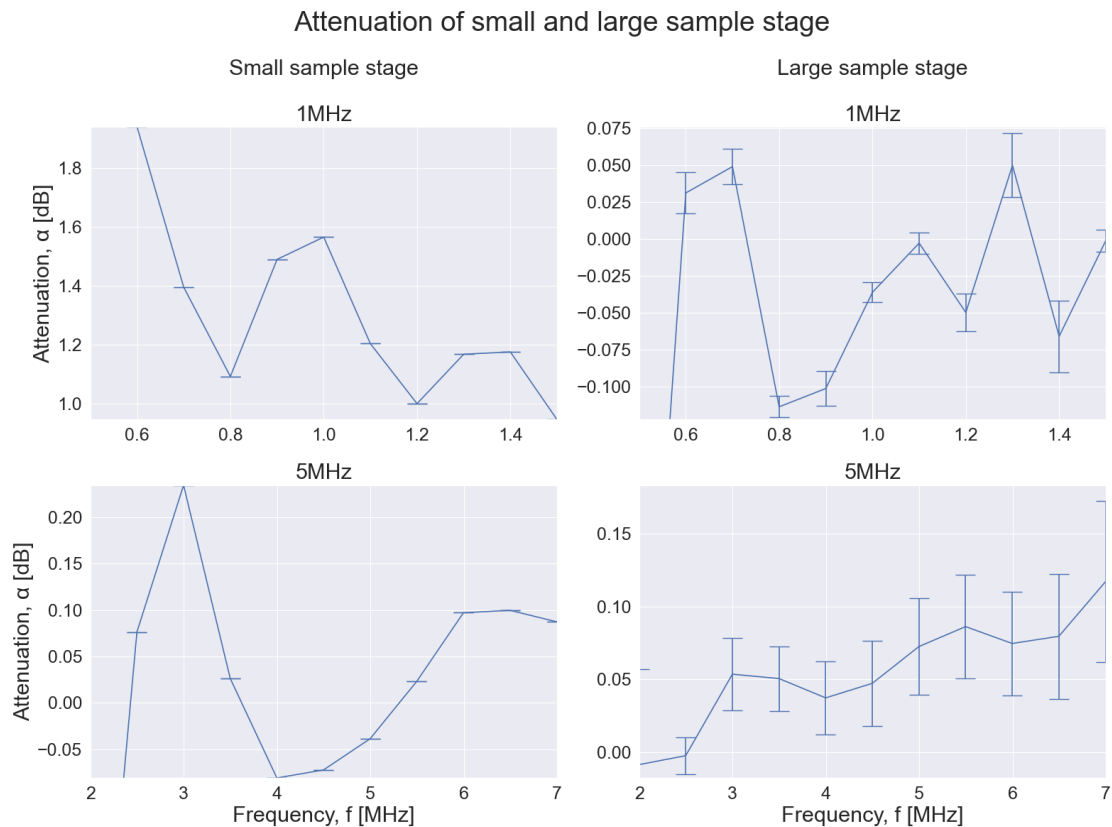


Figure 4.7: Comparison of the sample stage for the small and the large sample holders with the 1 MHz and the 5 MHz transducer. The small sample stage attenuates the acoustic signal by approximately 1.6 dB at the center frequency of the 1 MHz transducer, and less than 0 dB at the center frequency for the 5 MHz transducer. The large sample stage attenuates less than 0 dB for the center frequency for the 1 MHz transducer, and between approximately 0.05 and 0.1 dB for the center frequency of the 5 MHz transducer. The results from the small sample stage are based on 1 measurement, while the results for the large sample stage are based on 3 measurements. The plots are on different y-axes to better visualize the variations seen between neighbouring frequencies. They likely arise due to noise caused by spectral leakage.

4.4 Acoustic attenuation of agarose gels with additives

The results from the acoustic attenuation measurements on 2% and 5% agarose gels with different additives are shown in figures 4.8-4.15. The addition of either BSA or evaporated milk clearly increases the acoustic attenuation of the gels. This effect is most noticeable with the 3.5 MHz and the 5 MHz transducer, but a similar trend is seen at 1 MHz. The addition of milk has a slightly higher effect on the attenuation, as opposed to BSA at similar concentration.

For all the gels the attenuation increases with frequency, which is consistent with equation 3.1. Additionally, the results for the different transducers align within a standard deviation at overlapping frequencies for the other transducers. Furthermore, the data for the 2% agarose gel is consistent (within a standard deviation) with the data from table 2.5, while the data for the 5% agarose gel is consistent at 3.5 and 5 MHz, but not at 1 MHz. The measured attenuation at that frequency is significantly lower than reported in table 2.5.

The 3.5 MHz measurements on the 5% agarose gels with 10% or 20% milk show two distinct populations of measurements. Both populations have a similar slope with frequency. The population with the highest measured attenuation (orange and blue lines in the 3.5 MHz plots in figures 4.14 and 4.15) aligns well with the attenuation of the overlapping frequency bins in the 1 MHz and 5 MHz measurements. The population with lower attenuation does not align with the attenuation at overlapping frequency bins in the other plots, and falls below 0 for frequencies below around 2 MHz. Considering this, and the fact that this was only noticeable on the results from a single transducer, it is interpreted as a measurement error during the reference measurements.

The acoustic attenuation at the center frequency of the transducers is summarized in table 4.1 for 2% agarose gels, and 4.2 for 5% agarose gels.

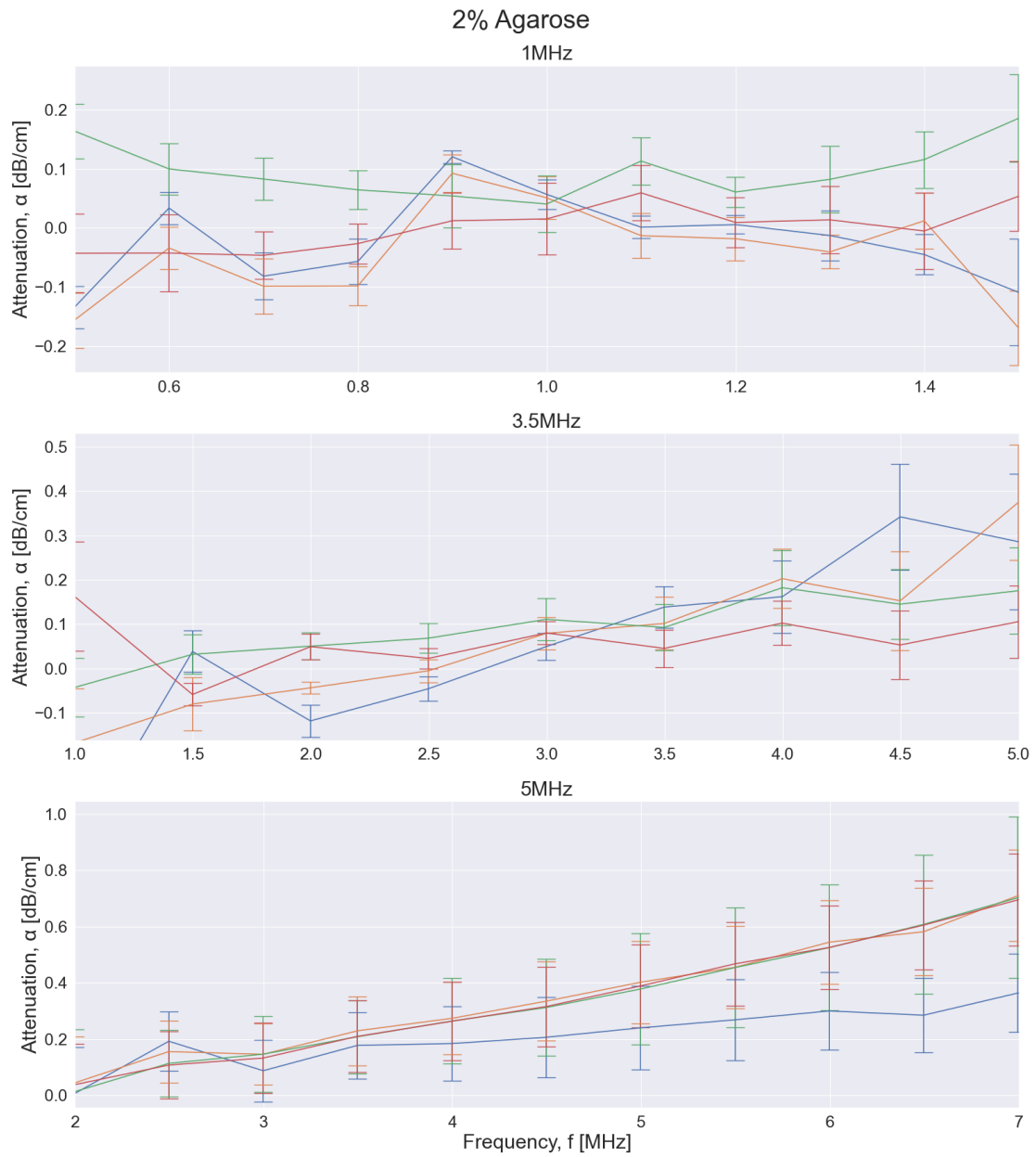


Figure 4.8: Acoustic attenuation of 4 samples from 2 batches of 2% agarose gels. Independent plots for the three different transducers used in the experiments are shown.

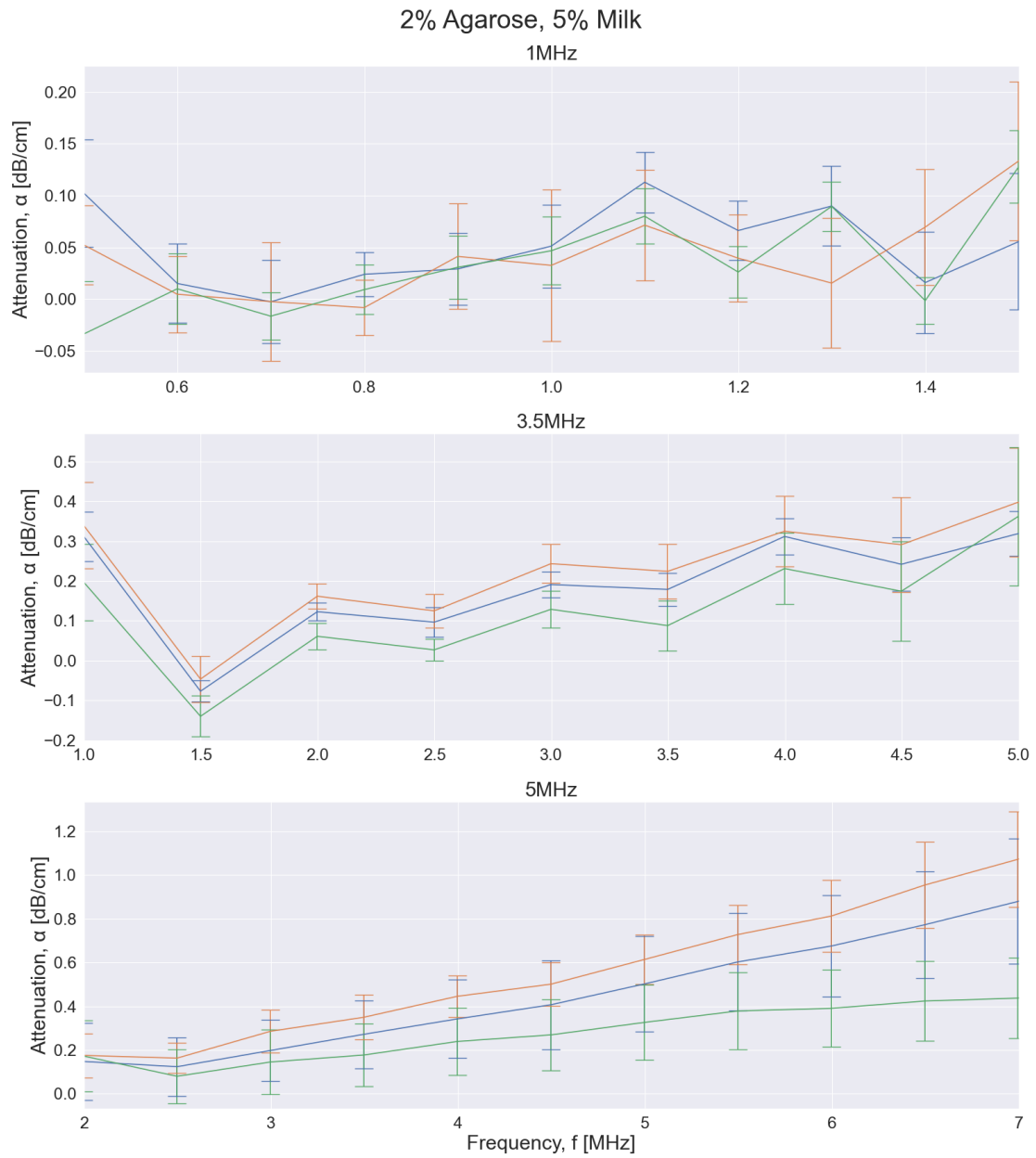


Figure 4.9: Acoustic attenuation of 3 samples from 2 batches of 2% agarose gels containing 5% evaporated milk. Independent plots for the three different transducers used in the experiments are shown.

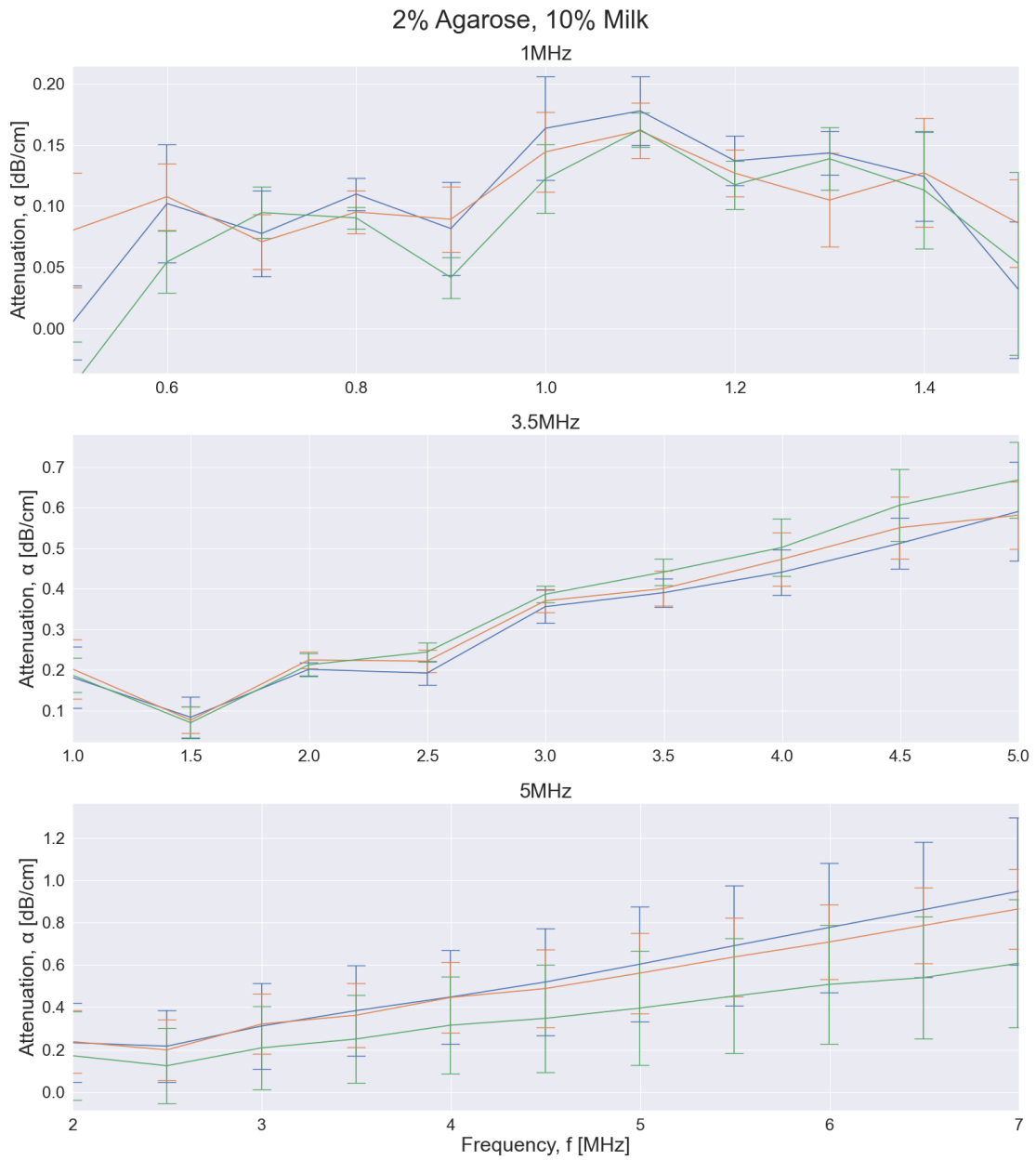


Figure 4.10: Acoustic attenuation of 3 samples from 2 batches of 2% agarose gels containing 10% evaporated milk. Independent plots for the three different transducers used in the experiments are shown.

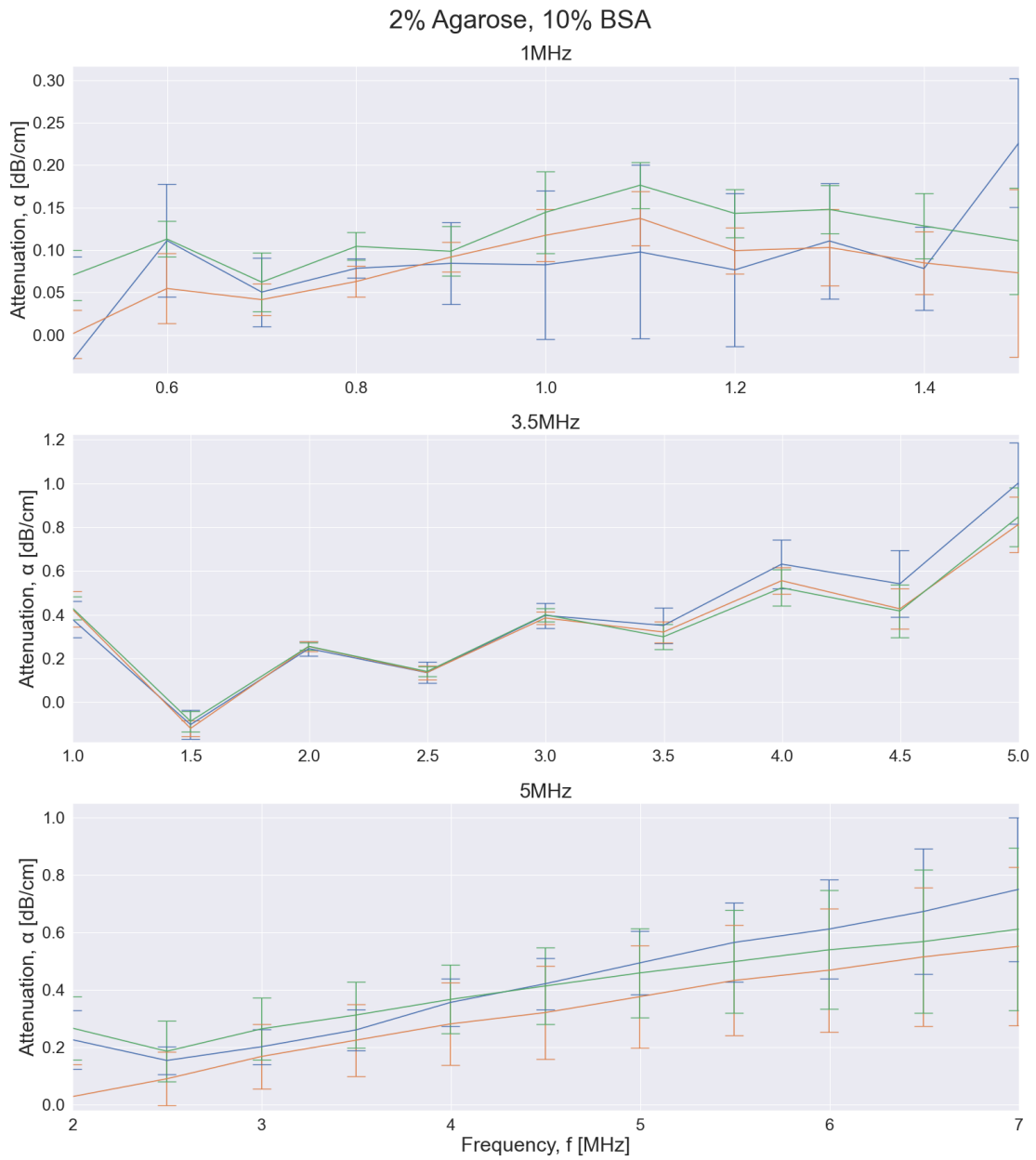


Figure 4.11: Acoustic attenuation of 3 samples from 2 batches of 2% agarose gels containing 10% bovine serum albumin. Independent plots for the three different transducers used in the experiments are shown.

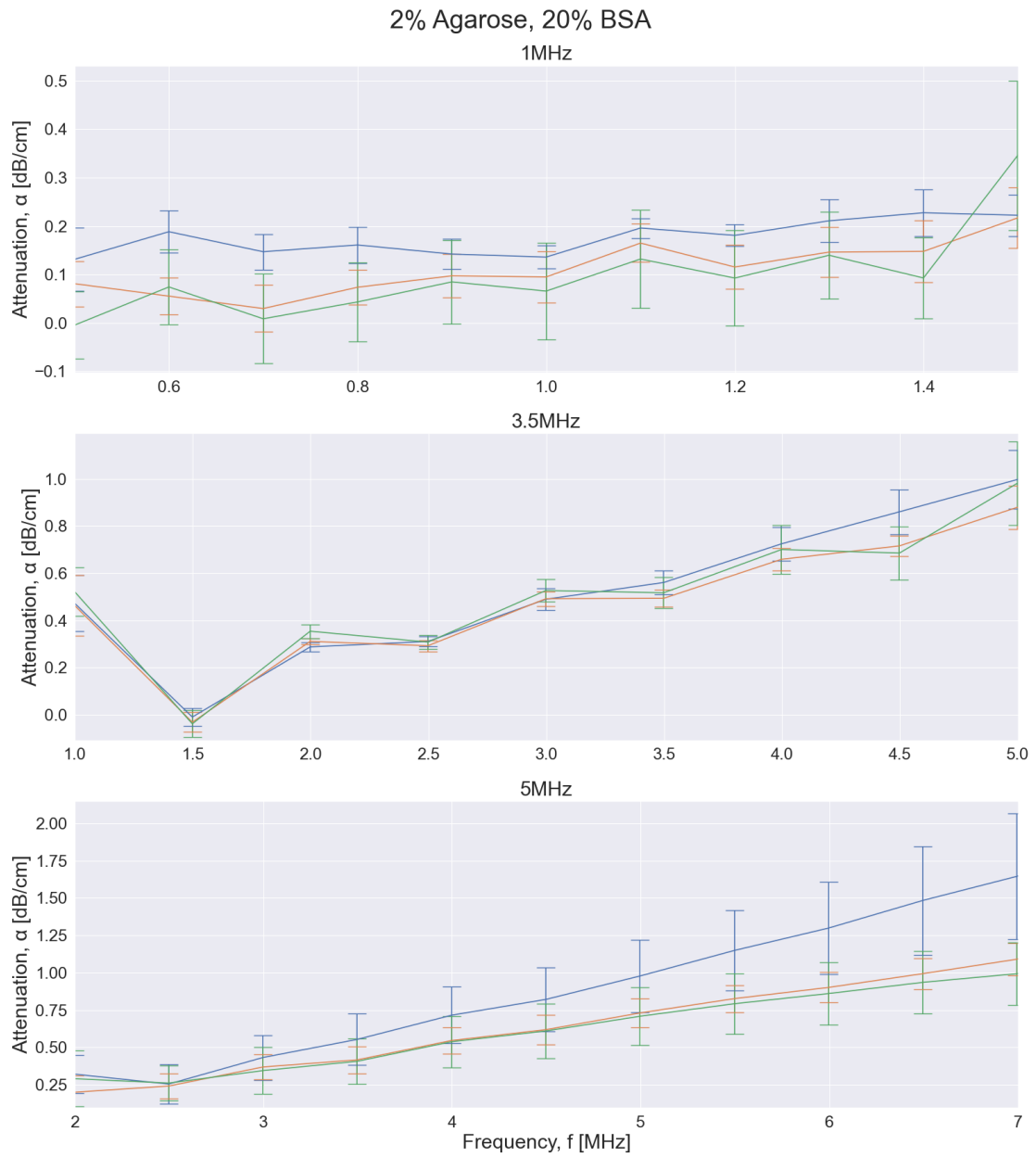


Figure 4.12: Acoustic attenuation of 3 samples from 2 batches of 2% agarose gels containing 20% bovine serum albumin. Independent plots for the three different transducers used in the experiments are shown.

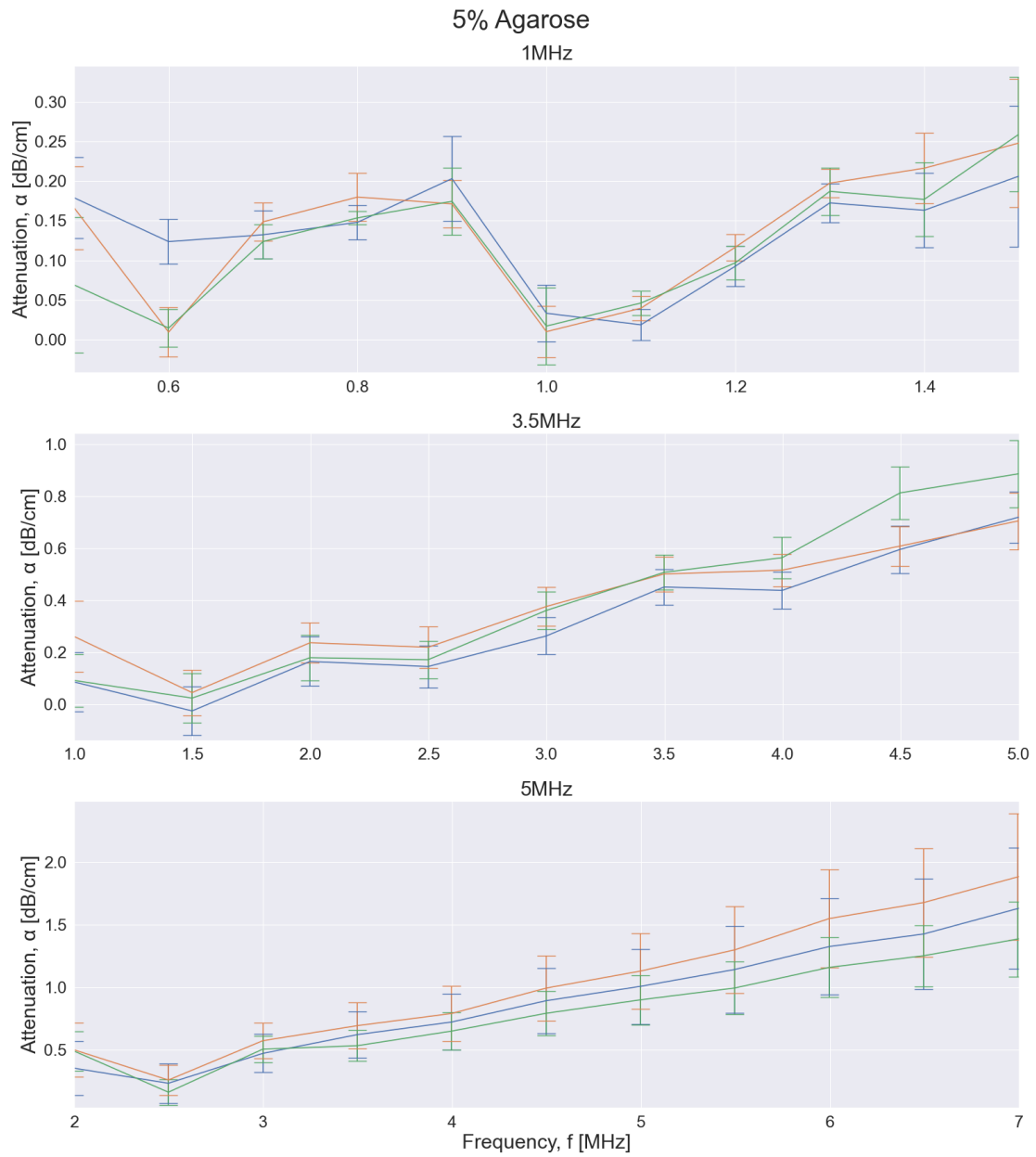


Figure 4.13: Acoustic attenuation of 3 samples from 2 batches of 5% agarose gels. Independent plots for the three different transducers used in the experiments are shown.

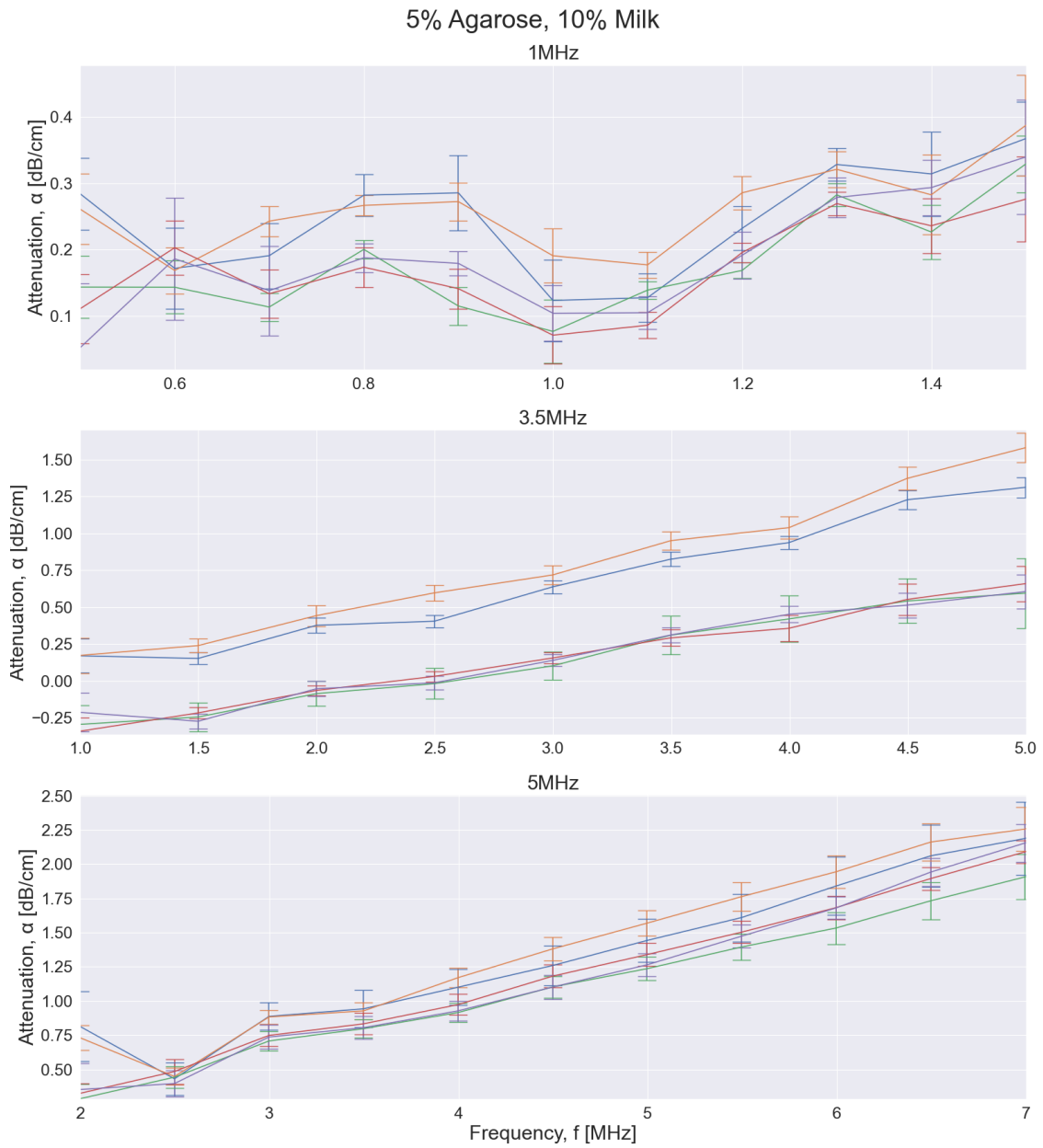


Figure 4.14: Acoustic attenuation of 5 samples from 2 batches of 5% agarose gels containing 10% evaporated milk. Independent plots for the three different transducers used in the experiments are shown.

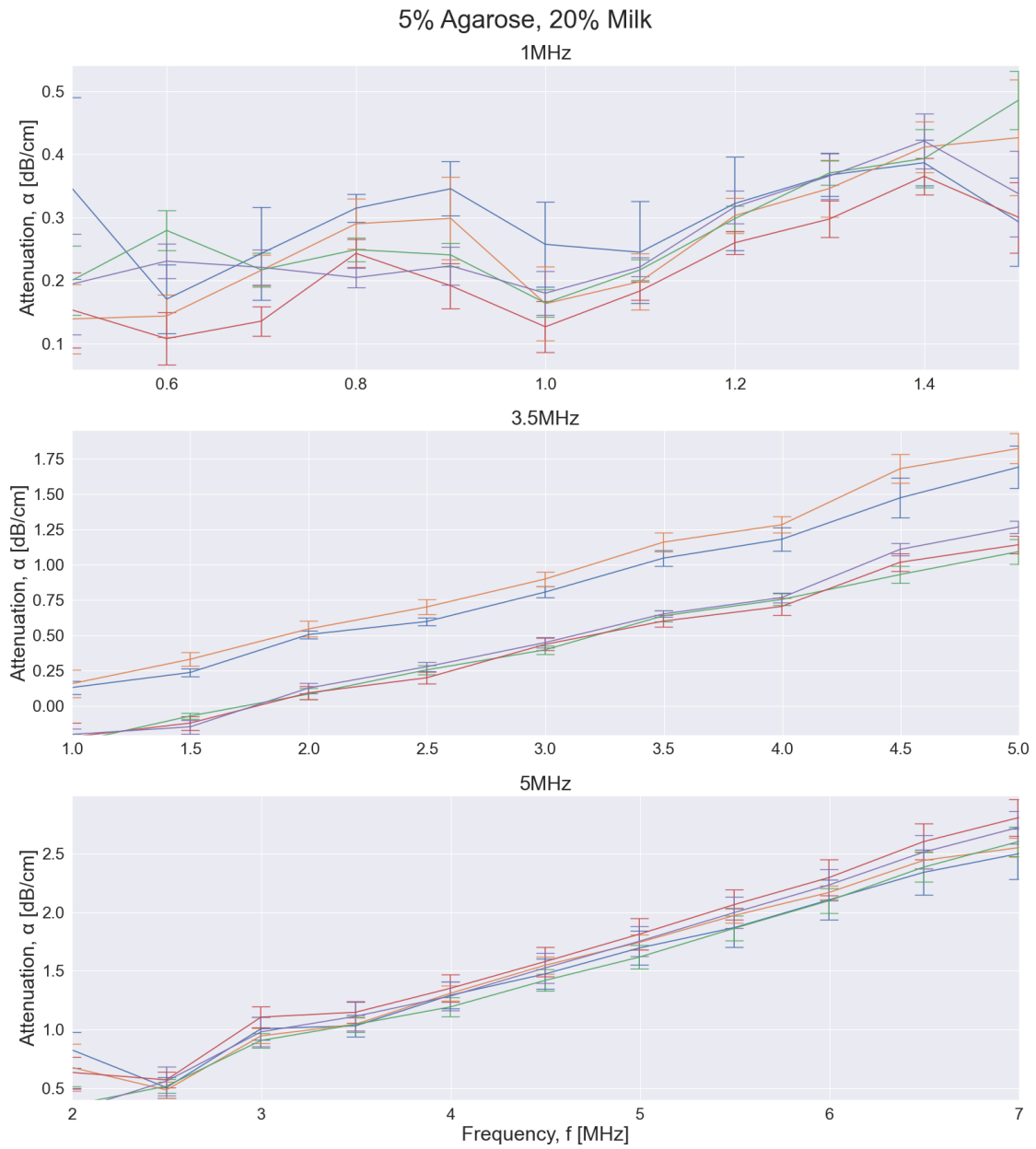


Figure 4.15: Acoustic attenuation of 5 samples from 2 batches of 5% agarose gels containing 20% evaporated milk. Independent plots for the three different transducers used in the experiments are shown.

Table 4.1: The results of attenuation measurements on 2% agarose gels with different additives. The attenuation at the center frequency is shown. Each of the measurements were done over $n = 3$ samples unless otherwise stated.

Sample	$\alpha_{1\text{MHz}}$	$\alpha_{3.5\text{MHz}}$	$\alpha_{5\text{MHz}}$
	dB cm^{-1}		
2% Agarose ($n = 4$)	0.04 ± 0.02	0.10 ± 0.03	0.35 ± 0.07
+ 10% BSA	0.11 ± 0.03	0.32 ± 0.02	0.44 ± 0.05
+ 20% BSA	0.10 ± 0.03	0.52 ± 0.03	0.81 ± 0.12
+ 5% milk	0.04 ± 0.008	0.16 ± 0.06	0.48 ± 0.12
+ 10% milk	0.14 ± 0.02	0.41 ± 0.02	0.52 ± 0.09

Table 4.2: The results of attenuation measurements on 5% agarose gels with different concentrations of evaporated milk. The attenuation at the center frequency is shown. Each of the measurements were done over $n = 5$ samples unless otherwise stated.

Sample	$\alpha_{1\text{MHz}}$	$\alpha_{3.5\text{MHz}}$	$\alpha_{5\text{MHz}}$
	dB cm^{-1}		
5% Agarose ($n = 3$)	0.02 ± 0.01	0.49 ± 0.03	1.01 ± 0.09
+ 10% milk	0.11 ± 0.04	0.54 ± 0.29	1.37 ± 0.12
+ 20% milk	0.18 ± 0.04	0.82 ± 0.24	1.73 ± 0.07

4.5 Acoustic attenuation on Collagen with additives

The results from the acoustic attenuation measurements on collagen gels with additives are shown in figures 4.16-4.18.

All the samples had a very low attenuation at 1 MHz, which in the case of the 5 mg/mL collagen gel, with and without HA, even gave a negative result. For the 5 mg/mL gel with HA and evaporated milk the results were positive, but still significantly different to what is expected of soft tissue, which is on average 0.54 db/cm/MHz (from table 2.4). Besides this, the attenuation has an increase with frequency, which is consistent with equation 3.1. Additionally, the overlapping frequencies for the different transducers seem to overlap. This is most noticeable for the gel with HA and evaporated milk. For the pure collagen gel and the collagen gel with only HA, the standard deviation is high relative to the measured signal, thus the margins for considering the frequencies as overlapping are quite lenient.

The acoustic attenuation at the center frequency of the transducers is summarized in table 4.3.

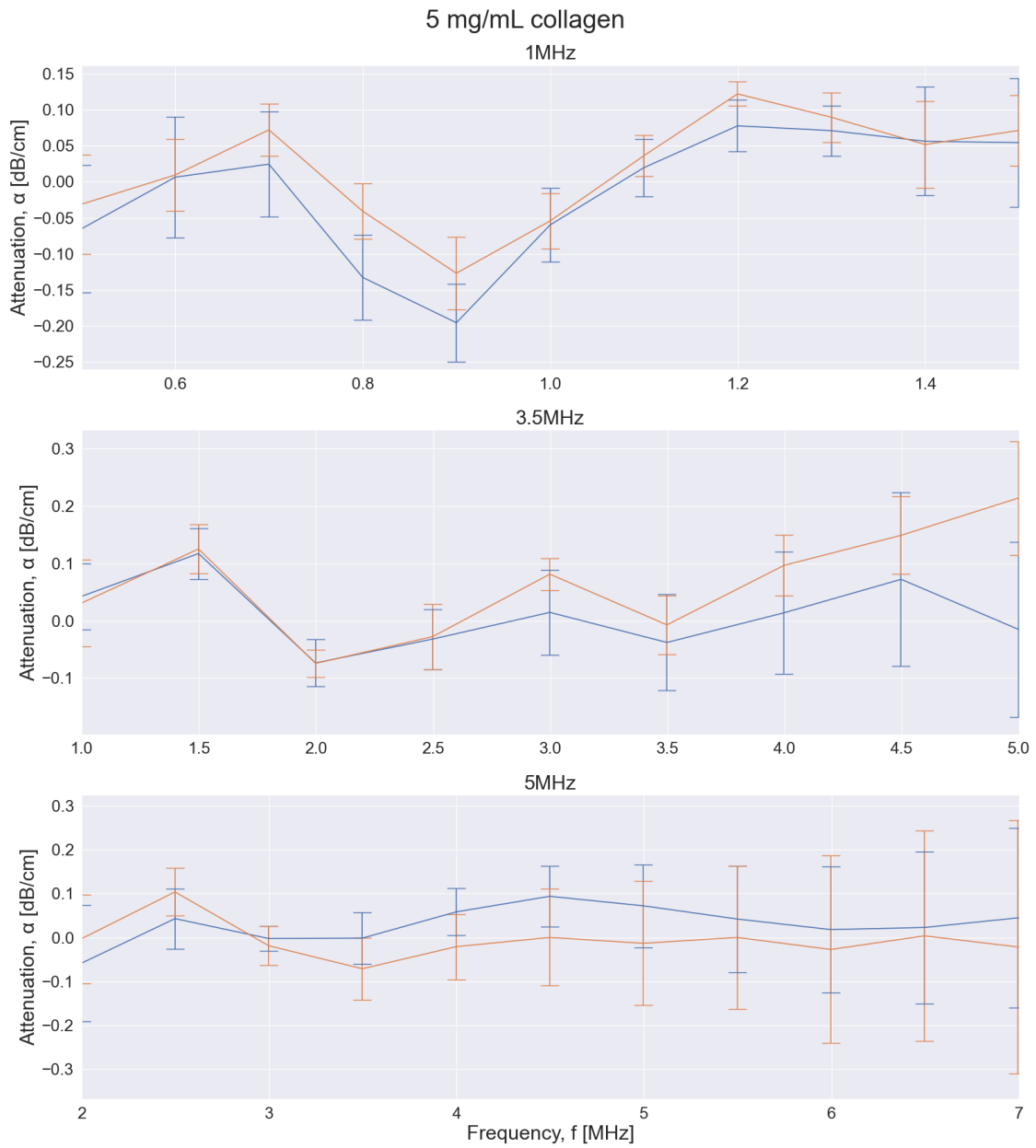


Figure 4.16: Acoustic attenuation of 2 samples from 1 batch of 5 mg/mL collagen gels. Independent plots for the three different transducers used in the experiments are shown.

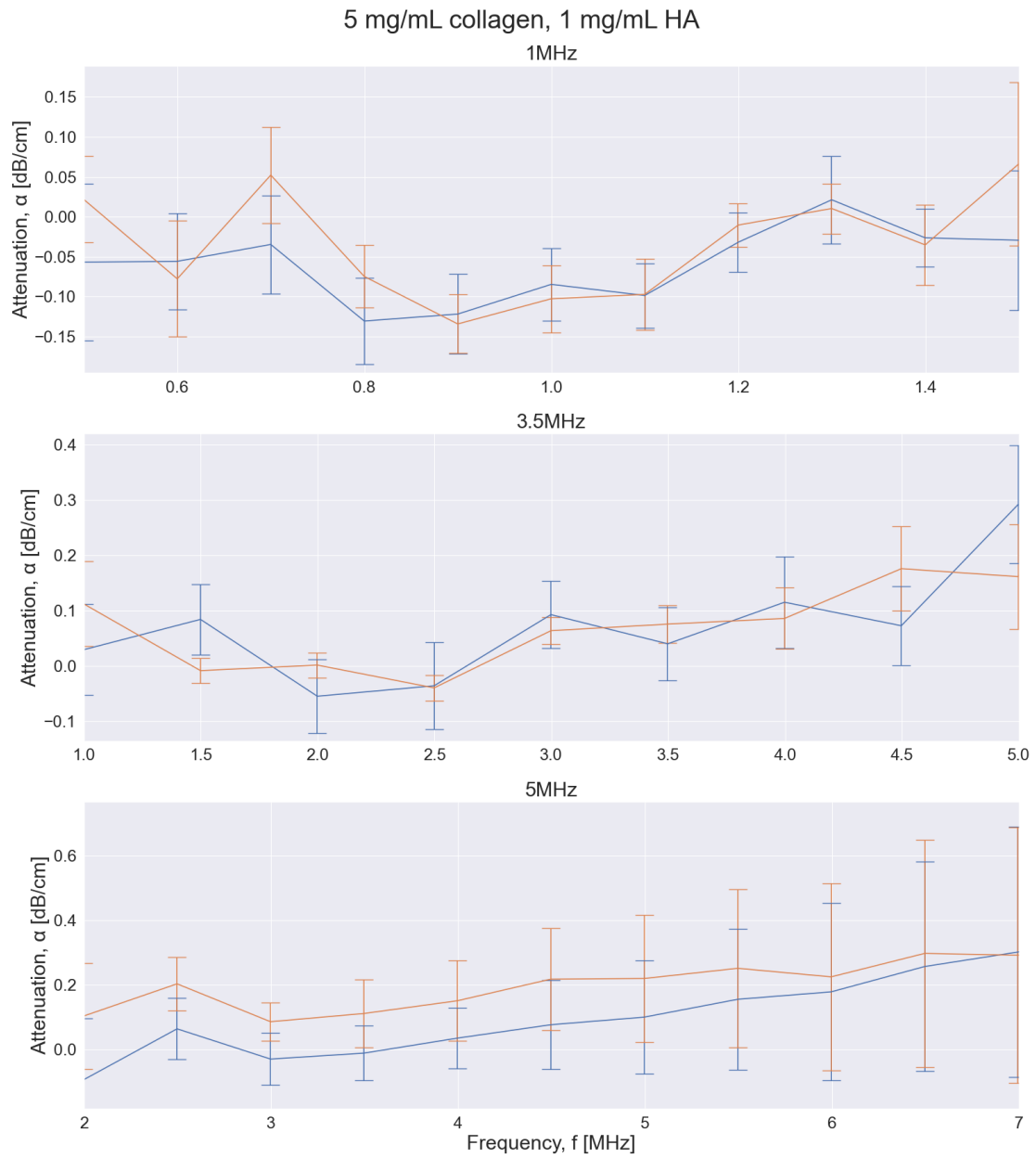


Figure 4.17: Acoustic attenuation of 2 samples from 1 batch of 5 mg/mL collagen gels containing 1 mg/mL hyaluronic acid. Independent plots for the three different transducers used in the experiments are shown.

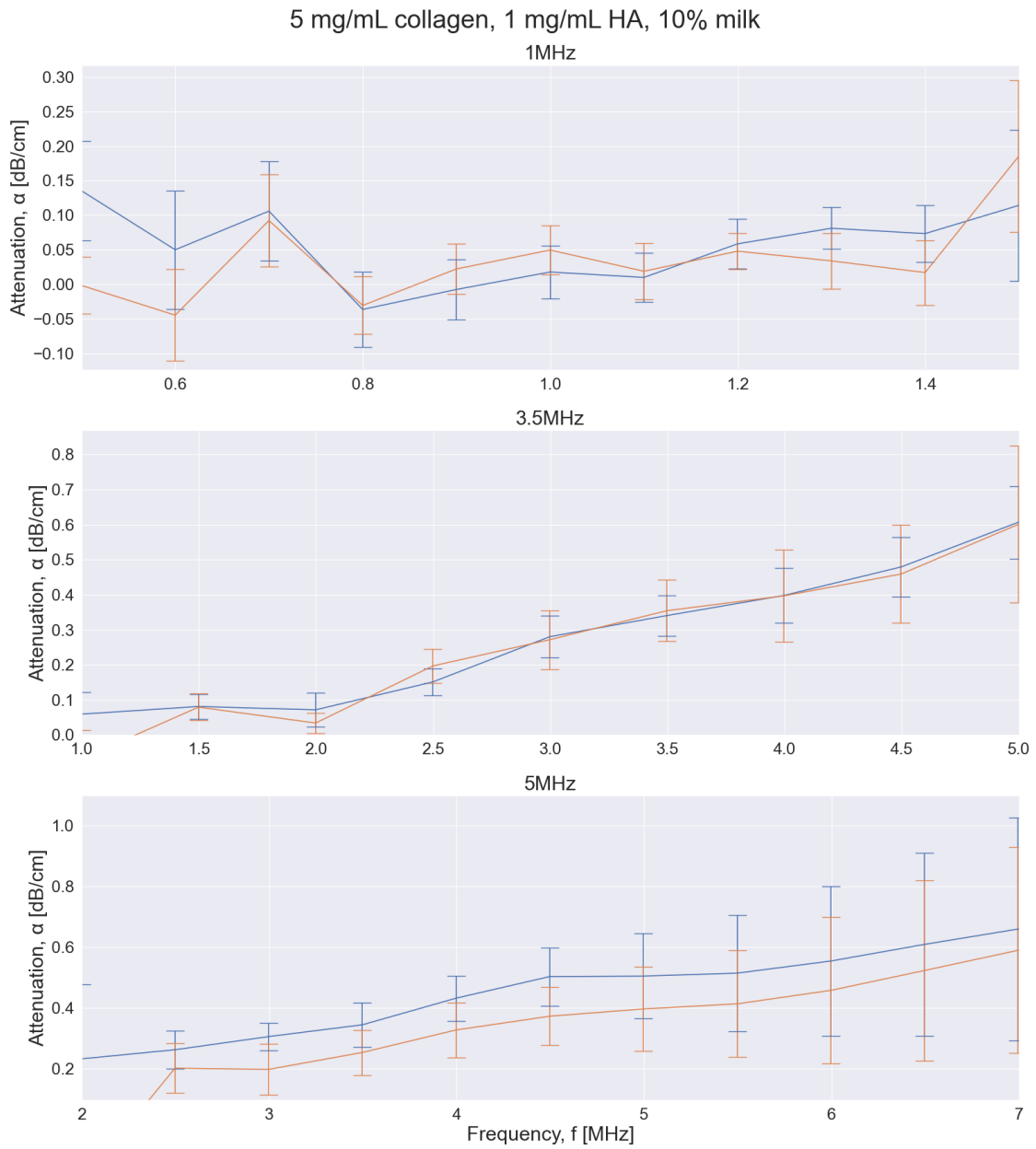


Figure 4.18: Acoustic attenuation of 2 samples from 1 batch of 5 mg/mL collagen gels containing 1 mg/mL hyaluronic acid and 10% milk. Independent plots for the three different transducers used in the experiments are shown.

Table 4.3: The results of attenuation measurements on 5 mg/mL collagen gels with, and without, 1 mg/mL hyaleric acid and 10 % evaporated milk. The attenuation at the center frequency is shown. Each of the measurements were done over $n = 2$ samples. A negative attenuation is physically impossible, and in those cases values have to be taken as qualitatively "very low" instead of quantitatively.

Sample	$\alpha_{1\text{MHz}}$	$\alpha_{3.5\text{MHz}}$	$\alpha_{5\text{MHz}}$
	dB cm^{-1}		
5 mg/mL Collagen	-0.05 ± 0.003	-0.02 ± 0.02	0.03 ± 0.04
+ HA	-0.09 ± 0.009	0.06 ± 0.02	0.16 ± 0.06
+ HA and milk	0.03 ± 0.02	0.35 ± 0.007	0.45 ± 0.05

4.6 Diffusion of nanoparticles in water

The particle tracking of the TT-28 and ENP-135 in water at different temperatures, resulted in measured diffusion coefficients similar to the predictions of the Stoke-Einstein equation. The results are summarized in table 4.4.

Table 4.4: Measurements of the diffusion coefficient in water for both types of nanoparticles, at different temperatures, are shown together with a prediction from the Stoke-Einstein relation (equation 2.2), using data from table 2.3 for the viscosity. Three measurements on a single sample were done for each data point.

Temperature	TT-28		ENP-135	
	Predicted	Measured	Predicted	Measured
	$\mu\text{m}^2\text{s}^{-1}$			
25°C	2.86	2.85 ± 0.02	5.23	5.72 ± 0.08
30°C	3.24	3.06 ± 0.03	5.94	5.90 ± 0.18
35°C	3.66	3.69 ± 0.006	6.69	6.74 ± 0.23

4.7 Temperature-dependent diffusion of PACA NPs in collagen gel

The particle tracking of the TT-28 and ENP-135 nanoparticles in collagen gels with HA and evaporated milk resulted in a measured diffusion coefficient in the order of magnitude of $10^{-4}\mu\text{m}^2\text{s}^{-1}$ for both particles. This is a diffusion coefficient around 10 times lower compared to earlier work done by Løvmo et al. [79], for gels with a collagen concentration of 2.5 mg/mL. However, it was not possible to separate the particles into separate diffusion groups as done by Løvmo et al.

For both the particles there is a slight increase in diffusion coefficient with temperature. The only exception to this is the 25°C measurement of the ENP-135 particles, which is higher than for higher temperatures. This measurement also has a fairly large standard deviation which might account for this discrepancy.

The diffusion coefficient of the TT-28 particles is roughly half of the measured diffusion coefficient for the ENP-135 particles, which is consistent with the results from section 4.6.

The results are summarized in table 4.5.

Table 4.5: Measurements of the diffusion coefficient in collagen gels with HA and evaporated milk. The results are based on three measurements on two samples, and the error is given as standard deviation between individual measurements.

Temperature	TT-28	ENP-135
	$10^{-4}\mu\text{m}^2\text{s}^{-1}$	
25°C	8.0 ± 0.8	23.6 ± 2.8
30°C	9.2 ± 1.6	20.5 ± 0.6
35°C	9.5 ± 1.2	22.1 ± 1.7

4.8 Ultrasound beam profile in diffusion setup

The peak pressure of the ultrasound beam in the diffusion setup, which was measured by a hydrophone in the water tank, is shown for two different distances from the transducer in figures 4.19a and 4.19b. There is an apparent linear relationship between the input voltage to the power amplifier, and the measured peak pressures of the ultrasound beam. This is only true for low input voltages, and the true relationship is a slowly increasing exponential as can be seen in the transducer's test certificate (Acoustic Power vs Frequency for PA504, appendix B).

The obstruction of half the ultrasound beam gave the beam profile an irregular shape. The cutoff-line where the beam was blocked is clearly visible in the surface and contour plots in figures 4.19c-f. The beam also has an extra pressure peak outside this region, where ideally there would be no ultrasound due to the absorbing material. This implies that the absorbing material either failed to absorb all the acoustic energy, or that the ultrasound diffracted over the edge. However, this secondary peak had a low pressure intensity of -9 dB in reference to the main peak.

Measurements were taken at two distances away from the transducer. At the focus area 73.5 mm away from the transducer, and at the center of where the slide with the sample would be 80.0 mm away from the transducer. The latter measurement was needed due to a mistake in the design of the set-up. Comparing the measurements from the ultrasound focus area and the center of the slide, an input voltage of 190 mV is necessary to reach a peak negative pressure of 1 MPa in the focus area, while 320 mV is needed to reach the same pressure in the center of the slide. The contour and surface plots in figures 4.19c-f highlights this, as the focus area plots have a much sharper peak where the pressure rapidly decreases from the center. In the center of the slide plots, the pressure is more spread out and decreases more slowly out from the center. However, in both cases the first contour line of -3 dB pressure decrease is approximately 0.5 mm wide.

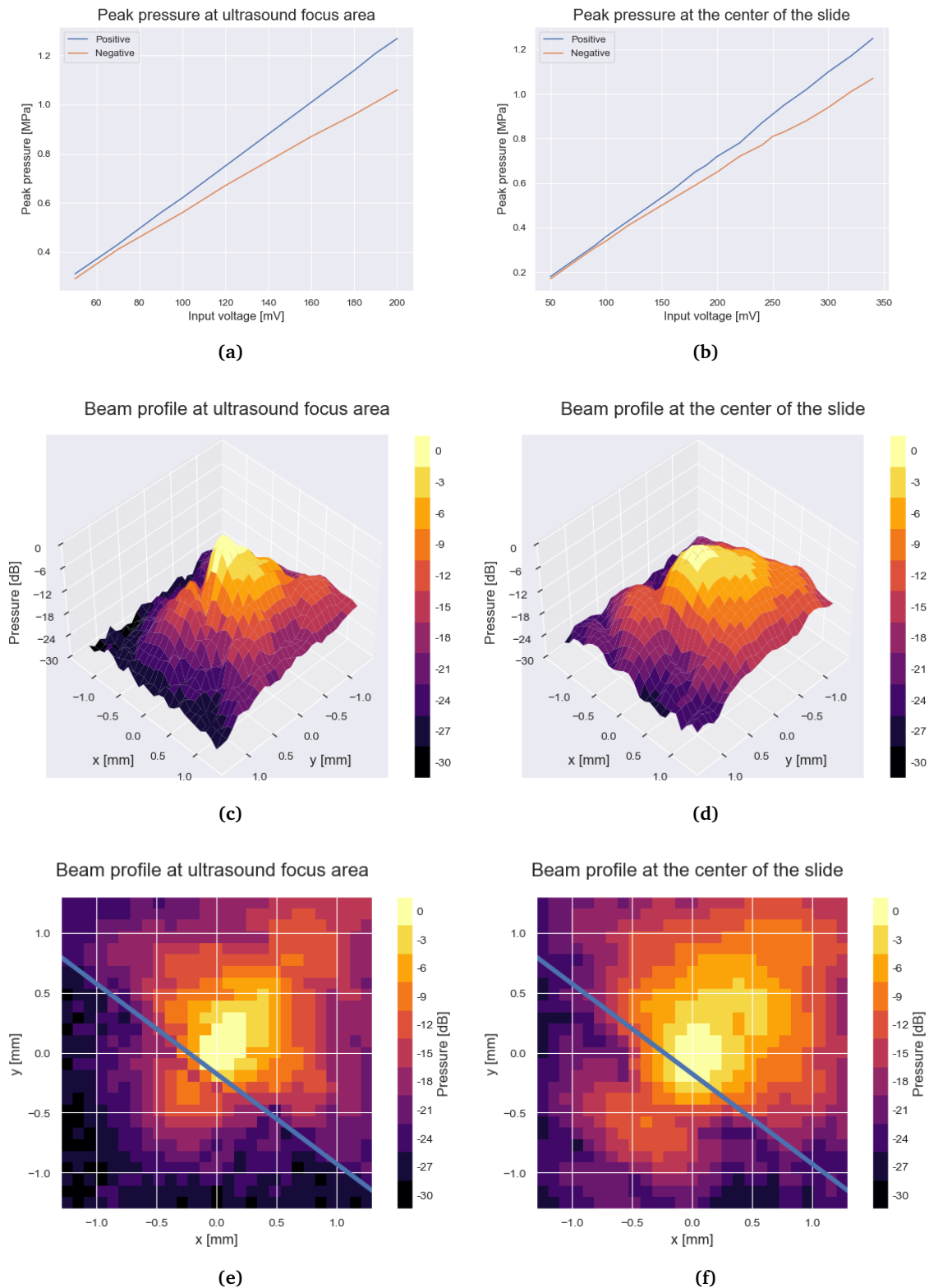


Figure 4.19: Characterization of the ultrasound transport measurement setup at two different distances, 73.5 and 80.0 mm away from the transducer diaphragm. This represents the focus area of the transducer, and the center of the sample slide which is in the far-field of the ultrasound beam. Figures a and b show the relationship between input voltage to the power amplifier and peak positive and negative pressure. Figures c and d show 3D surface plots of the ultrasound pressure related to position, and figures e and d show the same information as filled contour plots. The area to the bottom left of the blue line in plot e and d is where the beam from the ultrasound transducer is blocked off.

4.9 Effects of ultrasound on diffusion of nanoparticles in collagen gels

The results of the measurements of the diffusion coefficient for 5 mg/mL collagen gels with HA and evaporated milk are shown for 1 MPa peak negative pressure in figure 4.20, and for 2 MPa peak negative pressure in figure 4.21. The difference between the US and control measurements at varying number of cycles are generally positive, and similar between the TT-28 and ENP-135 particles. Additionally, there is a positive trend of increasing difference between the measurements pre- and during- US with increasing number of cycles. Only one of the results are statistically significant, for the TT-28 nanoparticles at 2 MPa and 100k cycles. With a p-value less than 0.01.

For most of the 2 MPa measurements, and the 1 MPa 100k cycles measurement on the ENP-135 nanoparticles, there is a fairly large spread in the measured diffusion coefficient on both the pre- and during- ultrasound measurements, which converge when looking at the difference between the two.

A Shapiro-Wilks normality test was done on the difference on the pre- and during US treatment measurements. The null hypothesis (that the data is normally distributed) was rejected in four instances with a p-value less than 0.05. Three times in the pre-US measurements: for the TT-28 nanoparticle at 1 MPa and 1K cycles, and at 2 MPa 1k cycles. Also for the ENP-135 nanoparticle at 2 MPa and 100k cycles. Additionally, the null hypothesis was rejected once in the during-US measurements for the TT-28 nanoparticle at 1 MPa and 10k cycles.

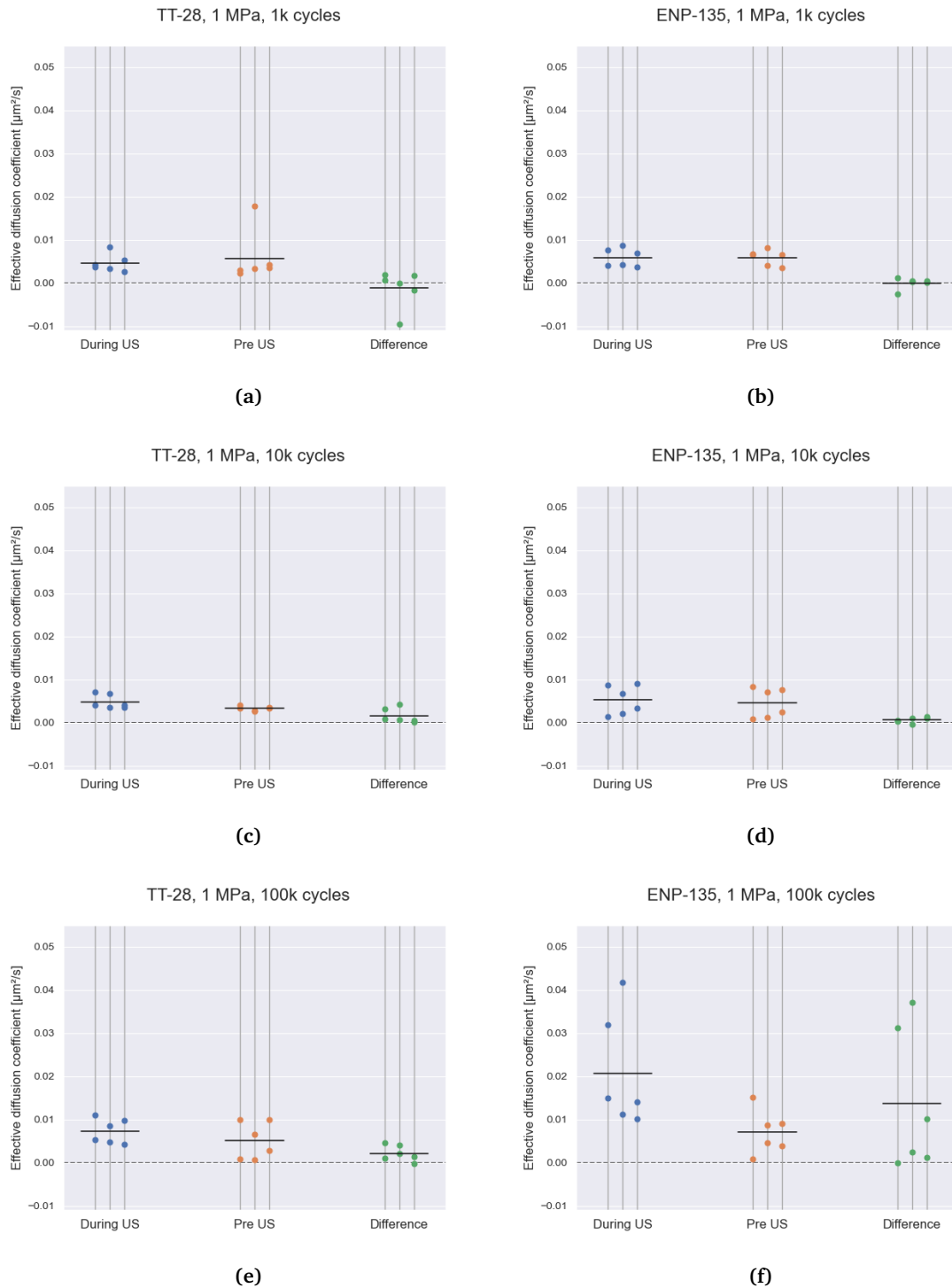


Figure 4.20: The measured effective diffusion coefficient at 1 MPa peak negative pressure, and at varying duty cycles. Results pre- and during ultrasound exposure for each measurement location are shown, as well as the difference between them. The three vertical tracks within one group represents from left-to-right the first, second, and third ultrasound treatment of each sample. The black line represents the mean of all 6 measurements in that group.

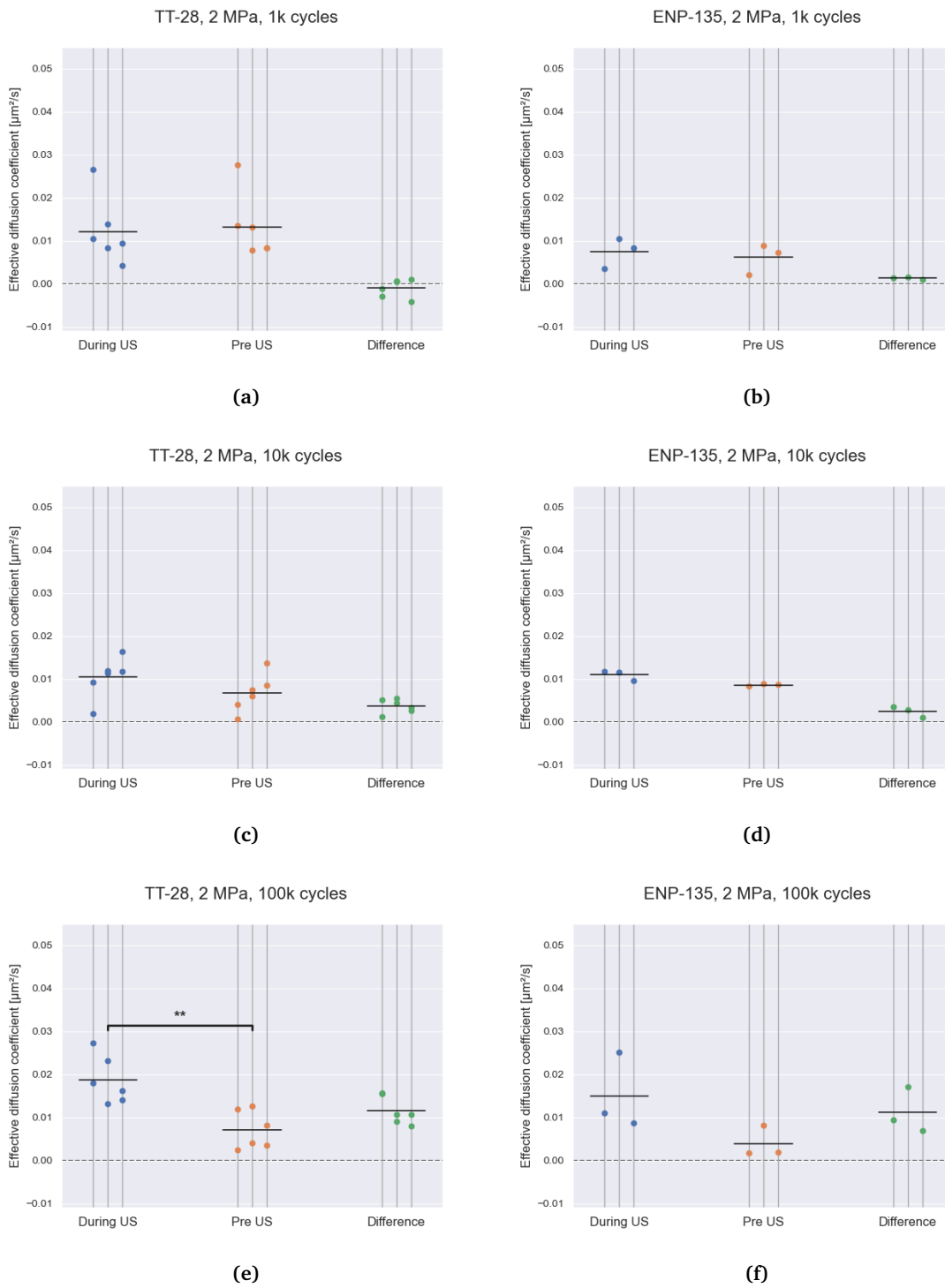


Figure 4.21: The measured effective diffusion coefficient at 2 MPa peak negative pressure, and at varying duty cycles. Additionally, the difference between the pre- and during US measurements are shown. The three vertical tracks within one group represents from left-to-right the first, second, and third ultrasound treatment of each sample. The black line represents the mean of all measurements in that group (6 for TT-28 and 3 for ENP-135). Statistical significance is shown with an asterisk. (** $p < 0.01$).

Chapter 5

Discussion

The overall aim of the master thesis was to study the effect of ultrasound on the transport of nanoparticles in collagen gels with hyaluronic acid and evaporated milk. This was investigated at different ultrasound parameters, and with two different nanoparticles in a custom built setup. Evaporated milk was included in the gels to increase their acoustic attenuation, and thus increase the likelihood of seeing an effect with ultrasound. Before studying diffusion of nanoparticles, the collagen gels needed to be characterized and the experimental setups for attenuation and diffusion measurements needed to be established. The producer of collagen could not ship collagen before end of April, thus agarose gels were used to establish and test the experimental setup and measure the attenuation when additives were included in the gels.

5.1 Acoustic attenuation of gels

Parts of my project thesis involved measuring the acoustic attenuation of collagen gels at varying concentrations. The results from those measurements revealed that the setup was not sensitive enough to resolve the attenuation reliably. During the master the setup was optimized, and said optimizations were evaluated. With a more sensitive setup the acoustic attenuation of different additives in agarose gels were investigated. An additive was chosen and used in a collagen gel with hyaluronic acid to increase its attenuation. In the following subsections the reliability of the acoustic attenuation measurement setup, the different additives, and the resulting collagen gel, is discussed.

5.1.1 Reliability of acoustic attenuation measurement setup

The experimental setup for measuring acoustic attenuation used during my project assignment of fall 2020 gave unreliable results, and did not fit the expected power law relation between frequency and attenuation. Some results even showed a decrease in attenuation with frequency. The setup utilizes looks at the backscattered signal from a reflector behind the sample, and the same transducer acts as both the transmitter and the receiver of the signal. Another option for measuring the attenuation, which seems to be more common, is to look at the transmitted signal directly. Instead of reflecting the signal back to the transducer, a hydrophone or a separate transducer is placed behind the sample to act as a receiver [97–100].

The reason for the unreliable results was expected to be due to high noise levels induced by the high inherent attenuation of the components of the experimental setup. To increase the signal-to-noise ratio, several optimizations of the experimental setup was done during the master. Firstly, the replacement from mylar to plastic wrap on the sample holders had a great

effect on the inherent attenuation of the sample holders. The attenuation was measured to be an order of magnitude greater at all frequencies for the holders with mylar compared to the ones with plastic wrap. Secondly, the up-scaling of the sample holder ensured that more of the signal from the 1 MHz transducer passed through the sample. Although this only affected one transducer, it was still important since the 1 MHz signal was the least attenuated among the ones tested, and would thus be the most influenced by any noise. Finally, the measurement protocol was altered to use the same sample holder as the gel would be prepared in for the reference measurements. This is of significance since there still is some variation in attenuation between individual sample holders.

The downsides to all these optimizations are that the larger sample holder requires more gel solution, the plastic wrap is flexible and introduces some uncertainty in the gel thickness, and the use of the same sample holders in both the reference and sample measurements require the usage of around twice the amount of time since it has to be done in two sessions.

The result of these optimizations is that all the gel measurements follow the frequency power-law, with an increased attenuation at higher frequencies, and all measurements on agarose gels are in accordance with similar measurements found in literature, although the standard deviations of the measurements in that study are relatively high [81]. Furthermore, the 1 MHz measurements still seemed to be dominantly influenced by noise, especially for the lowest attenuating gels. For collagen gels with and without HA, the 1 MHz measurements showed a negative attenuation which should not be physically possible. This means that the attenuation of the gels were lower than the sensitivity of the setup, and the value has to be taken more qualitatively than quantitatively.

The alternating pattern seen in most of the attenuation plots, where neighbouring frequency bins are alternating between a high and a low value, is likely due to spectral leakage and scalloping. It should be noted that the spectral leakage is very low compared to the measured signals. However, it becomes very apparent due to the low attenuation of the gels, which is the difference between measurements on a sample and a reference. Spectral leakage arises because the fourier transform has an assumption of a periodic signal. If the sampling window does not align perfectly with the measured signal, there will be some leakage from neighbouring frequencies. Scalloping arises because the fast fourier transform is a discrete version of the fourier transform, and when the reciprocal of the number of samples does not perfectly align with the frequencies of the observed signal, they will leak out to nearby frequency bins[101]. Losses due to spectral leakage and scalloping can be modulated by applying different windowing functions to the FFT. Since no windowing was explicitly done on the attenuation data, a rectangular window was implied. This window works well with broadband signals since it has high sensitivity and high resolution of the frequency components. However, this comes at a cost of a poorer dynamic range [102].

5.1.2 Comparison of additives for improving acoustic attenuation

Two different additives were included in agarose gels; bovine serum albumin (BSA), and evaporated milk. Both improved the acoustic attenuation of agarose gels to a similar degree, with evaporated milk increasing it slightly higher at the same concentration. The attenuation of both the 2% and 5% agarose gels are, as mentioned in the previous section, within a standard deviation of literature values found for 2% and 5.5% agarose gels (table 2.5)[81]. However, the standard deviation is fairly large in the found literature values, and comparable to the values themselves.

The attenuation of 0.8 dB/cm/MHz found for evaporated milk from literature corresponds well with the increase of attenuation seen in the gels. It should be noted that the authors of

that study saw an attenuation variation of 6% depending on the date they bought the evaporated milk[83]. With 10% evaporated milk included in 2% and 5% agarose gels the measured attenuation increased by respectively 0.10 and 0.09 dB/cm at 1 MHz. Similarly the attenuation of the 5% agarose gel increased by 0.16 dB/cm with the inclusion of 20% evaporated milk. This is indicative of a linear increase in the attenuation by addition of evaporated milk.

BSA increased the attenuation by less than what was expected from a study on an acrylamide gel. In that gel an increase from 3% to 9% BSA increased the attenuation at 1 MHz of the gel from 0.08 dB/cm to 0.18 dB/cm [85]. In agarose gels with 10% BSA concentration an attenuation of 0.11 dB/cm was measured at 1 MHz. This is around half the effect the BSA had in acrylamide. Since agarose gels need to be at an elevated temperature before gelling, it is possible that some of the BSA denatured and that affected the results. However, it seems likely that BSA simply has less of an effect when included in the agarose gels.

In the 3.5 MHz measurements of the 5% agarose gels with evaporated milk, two distinct populations of gels are seen (figure 4.14 and 4.15). Both populations follow a similar slope of increase with frequency, but the slopes are offset from each other into an upper and a lower population. The lower population's attenuation goes below zero at around 2 MHz, and the attenuation does not correspond with measurements at any of the overlapping frequency bins using the other transducers. The upper population's attenuation correspond well (within a standard deviation) with the measurements of the other transducers at the overlapping frequency bins. This gives justification for trusting the measurements from the upper population, and neglecting the lower. Additionally, this separation into two populations is only seen for the 3.5 MHz measurements, and the measurements with the 10% and 20% evaporated milk were done in the same session, making it likely that it was the measurements themselves, and not the gels which were biased. There are several experimental conditions which could bias the measurements. The two most likely explanations are either gas bubbles forming in the water and thus increasing the measured attenuation of the sample holders. Or alternatively, there was a different temperature in the water when the sample holders were measured, compared to when the gels were measured[103].

Notably, the acoustic attenuation at 1 MHz is increased when 10% BSA, 20% BSA or 10% evaporated milk is added to the 2% agarose gels. However, no significant difference was observed at 1 MHz for the 5% milk compared to not including additives. Also, no difference was observed at 1 MHz between including 10% compared to 20% BSA. As discussed in section 5.1.1, this is due to the attenuation being very low, and the setup is likely not sensitive enough to measure it accurately.

5.1.3 Acoustic attenuation of collagen gels with evaporated milk

Adding evaporated milk to 5 mg/mL collagen gels with 1 mg/mL HA did increase the acoustic attenuation. However, the attenuation is still not in the same order of magnitude as the soft tissue average which is 0.54 (from table 2.4). In fact the collagen gels without evaporated milk are in the noise range of the 1 MHz transducer. This is valid for both the gel with and without HA. Additionally, the HA only gives marginal improvements to the attenuation at higher frequencies. This gives an indication that HA should be included for its effects on the transport of particles through the matrix, and not for attenuation. The low attenuation in the gels has an adverse effect on the acoustic radiation force, and will thus limit what can be expected to be observed in the transport measurements. This is because ARF is proportional to the absorption coefficient in the medium, and absorption is one of the several attenuation mechanisms [75, 79].

The measured attenuation for the 5 mg/mL gel is significantly lower than what would be expected, based on the estimated values found from literature for a 4 mg/mL collagen gel (table 2.5)[82]. This is true for all the measured frequencies. A possible explanation for this is that the samples were inhomogenous, and the concentration of collagen and other constituents were low in the focus area. Larger volumes of gel were used in the attenuation measurements than in any of the other experiments. The larger volumes makes mixing of the gel constituents a greater challenge. A larger sample size could have revealed if this was the case, as both the measured samples came from the same batch. Additionally, making only one sample per batch could have resolved most of the issues the larger volumes introduced. The reason the sample size is small is due to time constraints, the large volumes of collagen consumed per sample, and the limited supply of collagen. The characteristics of the gel preparation, and importantly the mixing of the gels, will be further elaborated upon in section 5.2.1.

Even if the attenuation was similar to the estimated values, it would be significantly lower than for the agarose gels. This is mainly due to the large concentration difference between the collagen and agarose gels. A 2% agarose gel has a concentration of 20 mg/mL, which is 4 times the collagen concentration used. The reason a higher concentration collagen was not used was due to the challenges in either harvesting it from rat tails ourselves, or concentrating the commercially bought solution. Both would be large undertakings in themselves. Increasing the concentration of collagen could be achieved through ultra-centrifugation followed by spectroscopy to measure the achieved concentration [104]. During my project assignment of fall 2020, an unsuccessful attempt to double the collagen concentration through filter-centrifugation was performed. Some of the reasons it failed then was because of the high viscosity of the solution which made it difficult to handle, and the rapid cross-linking which occurred shortly after mixing with PBS.

5.2 Transport of nanoparticles in gels

A custom setup for measuring diffusion of nanoparticles in gels during ultrasound treatment was created. In the following sections, collagen gels as a phantom for measuring transport properties will be evaluated. Also, results from the measurements on the collagen gels will be discussed, as well as a discussion about the performance of the setup.

5.2.1 Collagen gels as an experimental ECM phantom for diffusion experiments

In principle a collagen gel with HA should be an excellent ECM phantom. Collagen and HA are the most abundant molecules of their respective type (fibrous proteins and GAG) in real ECM. Using these materials should make for a more representative model of the transport of macromolecules through real tissue. Earlier studies have shown that the electrostatic interactions between the particles and the positively charged regions of the collagen fibers is of a greater importance than the structural and steric effects [104–106]. However, certain properties of the collagen gel makes it more challenging to control experimentally than other phantoms, such as agarose gels. These variations are apparent as a variation between samples in both the pore size measurements, and the diffusion experiments, both with and without US. In the latter case the variation is in some cases significant even within the same sample.

The collagen gels are cross-linked by a pH-driven process, which is strongly affected by temperature. The cross-linking process begins as soon as the pH is adjusted near a physiological range, but is significantly faster at higher temperatures. This temperature dependency has been shown to have large effect on the final structure of the gels, as earlier studies have shown that

cross-linking at a lower temperature leads to thinner, but more abundant fibers. Because of this, the variation in time taken to produce the gels can have a significant impact on the final microstructure of the gel [47–49, 107]. Care was taken to minimize the time off ice while preparing the gels, and a timer was used to attempt to control the preparation time. However, the time varied by up to 15 minutes depending on the time pH-adjustments and introduction of NPs took.

In the cases where large intra-batch and intra-sample variations were observed, it is believed to be due to poor mixing. The mixing of the collagen with the HA solution had to be performed carefully to prevent the formation of gas bubbles in the gels, which would have a significant impact on the experiments involving ultrasound. This was a challenge due to the high viscosity of both solutions, the low temperature which increases the solubility of gases in the solution, and the time constraints mentioned in the previous paragraph.

Currently there is a high risk that gels will be significantly different depending on the person that prepares them. Therefore, for future experiments it is suggested that the gels are prepared in an environmentally controlled room at 4°C. Secondly, mixing can be performed with the syringe-coupler method. This is a common technique used for mixing bioinks used in tissue engineering, and involves coupling two syringes together with a Luer-lock coupler, and passing the solutions back and forth around 30 times. This will help with a thorough mixing, while preventing gas bubbles [108]. Finally, every step after pH neutralization should be performed at set time points.

5.2.2 Important nanoparticle characteristics for diffusion in collagen gels

The measured diffusion coefficient in gels for the ENP-135 particles are more than twice as great as the coefficient for TT-28 at all temperatures measured. This is as expected due to two properties in the particles, the difference in size, and the difference in PEGylation. The most dominant of these properties is the size difference. However, the PEGylation difference is also expected to increase the measured diffusion coefficient for the ENP-135 nanoparticles. An earlier study which looked at the difference between the PEG combinations Kolliphor&Pluronic and Jeffamine&Brij found that Kolliphor&Pluronic should give the particle a slightly higher diffusion coefficient in collagen gels [109].

In contrast to an earlier study, it was not possible to separate the measured particles into groups of fast and slow diffusing particles. However, all the measurements were in the order of $10^{-3} - 10^{-4} \mu m^2 s^{-1}$, which is in accordance with slow diffusing particles in that study for particles of a similar size, albeit from a different monomer, with different PEGylation and in a lower concentration collagen gel. The reason for the slow diffusion is stipulated to be due to electrostatic interactions between the particles and the collagen network [79]. The lack of particles diffusing in the pores of the network might be for several reasons. Firstly, that study used a higher concentration of particles, and the binding sites on the collagen gel might have been saturated, leaving particles to diffuse freely in the pores. Secondly, it was noted that there was a high degree of accumulation of particles on the surface of the gel. It is feasible, that all the fast moving particles got expelled from the gel during the cross-linking process, or shortly after. Finally, there is a chance that the nanoparticles used in these experiments simply had a stronger preference to adhering to collagen fibers. While the latter might be true, the complete lack of any fast-diffusing particles in that case suggests that the equilibrium condition is only fulfilled when all particles are interacting strongly with the fibers.

Meanwhile, the pore size is not believed to be the reason for the lack of fast diffusing particles, since it was measured with a radius of approximately $1.8 \mu m$, which is several times larger than both the particles used in the experiments. This pore size is slightly larger compared

to results found in other studies, which have reported a theoretically predicted size of $1.3\mu\text{m}$ for a 5 mg/mL collagen gel [90], or a measured size of $1.2\mu\text{m}$ for a 10 mg/mL gel [104]. There is also the possibility of there being smaller fibers/fibrils within the pores which are too small to be imaged reliably with the microscope, or captured by the pore-size estimation technique.

The other constituents of the gel, besides collagen, are not believed to be the main reason only slow diffusing particles were observed. Similar behaviour was also seen for collagen gels without any HA or evaporated milk present. HA is however expected to have an effect on the diffusion, as HA concentration has been negatively correlated to the hydraulic conductivity in gels. This is a determining factor of the diffusion of nanoparticles through the pores in the network. The hydraulic conductivity is less influenced by the amount of collagen [32].

5.2.3 Effect of ultrasound on the transport of nanoparticles in gels

There is a trend of increasing measured diffusion coefficient with increased duty cycle. However, only the results for the TT-28 nanoparticles at 100k cycles shows a statistically significant increase. For the other results, the increase in the measured diffusion coefficient is similar, but the variances between the measurements are large. Additionally, the Shapiro-Wilks test revealed that with a p-value of 0.05 four of the measurement groups were not normally distributed. The lack of normality is likely caused by bimodal data due to differences in the two samples per measurement group, and due to the small sample size. Other effects could also contribute to deviation from normality, but more data is needed to establish if that is the case.

Due to the low attenuation measured for the gels (as elaborated upon in section 5.1.3), very little, if any, of the increase can be attributed to mechanical effects on the gel or the nanoparticles. The hypothesis of any influence from the ARF is through convective flows induced by microstreaming. A relatively high attenuation is necessary for that to be the case. Additionally, the highest duty cycle used is 10%. This amounts to an accumulated treatment dose of $10\% * 120 \text{ seconds} = 12 \text{ seconds}$ for the 2 minute treatments, and $10\% * 300 \text{ seconds} = 90 \text{ seconds}$ for the 15 minute treatments. The duty cycle was kept low for reasons which will be elaborated upon in section 5.2.4, in addition to the potential temperature increase that a high duty cycle would contribute to.

The variance between the measurements likely arises from a multitude of sources. Firstly, there are variations in the measurements caused by the setup itself. These will be discussed more extensively in section 5.2.4. Secondly, there is variation originating from the gels. There are some differences between samples. This can be seen for most measurements at 1 MPa, but it is most noticeable for the 1 MPa, 10k cycles measurements for the ENP-135 nanoparticles (figure 4.20d). The data in those measurement groups was visibly bimodal, and one sample had a higher diffusion coefficient in all three vertical tracks both pre- and during- US. However, taking the difference between the pre- and during- measurements converges the result from those two samples. Additionally, some variation can be attributed to inhomogeneous samples. This would be visible as variation which doesn't follow any pattern between the three vertical tracks in the pre-US measurements. However, it is difficult to quantify the contribution this has on the variation without eliminating other sources. The reason there is considerable variation originating from the gels was discussed more extensively in section 5.2.1.

Other sources of variation relates to either temperature or non-transient effects of the ultrasound on the gel. Variation due to temperature would most likely emerge as an increase between the first, second and third measurements on the same sample. Between each measurement there was a pause of 5 minutes to allow the sample and transducer to cool off. In most cases this seems to be sufficient, as either the setup had reached room temperature, or other sources of noise dominated the results. However, in some of the samples an increasing

trend between the three measurements on a sample were seen. This is most noticeable for the measurements on the TT-28 nanoparticles with 1 MPa and 1k cycles (figure 4.20a), and with 2 MPa and 10k cycles (figure 4.21c). However, it is unclear whether this trend of increasing diffusion coefficient between measurements is due to temperature increase. There was an intent to measure the temperature change in the gels during the US treatment using a fibre-optic sensor, and correlate it to the measurements of the diffusion of nanoparticles in the gel at defined temperatures (section 4.7). However, the sensor wasn't functioning properly and could not be used.

Non-transient effects in the gels could also give a similar pattern of increased measured diffusion coefficient between the first, second and third measurement on the same sample. Earlier *in vivo* studies have looked at the possibility of high intensity ultrasound having lasting effects on the ECM. These studies found an increased accumulation and penetration of nanoparticles in the ECM up to 24 hours after the treatment [110–112]. However, the ultrasound pressures used in these studies are significantly higher than the pressures used in this thesis. If this effect is indeed present in the gels, it is expected to be much smaller than any influence from temperature or inhomogeneities in the gels.

In the 1 MPa, 100k cycles, ENP-135 measurements (figure 4.20f) the first and the second measurements on one of the samples deviates from the mean more than what would be expected from looking at any of the other measurements. A re-examination of those specific data points revealed that the whole sample oscillates visibly with the ultrasound. This effect is not seen with the other samples. It is likely that the high measured diffusion coefficient is due to instabilities in the set-up, or that the whole gel moved during the treatment.

5.2.4 Evaluation of the experimental setup used in the transport measurements

The experimental setup could be used for estimating a diffusion coefficient of nanoparticles under the influence of ultrasound. In most cases, both TT-28 and ENP-135 nanoparticles gave similar results. However, the measured diffusion coefficients are in most of the cases around 5 times larger than was measured during the gel temperature measurements^{4.7}. There are certain aspects of the setup which need further work, and if improved could extend the operational limits of the of the setup.

There was a leak between the sample holder and the transducer cone. Between these two parts there is a plastic film, and the transducer cone is sealed against it with an O-ring and does not leak. However, the sample holder does not have an O-ring. The leak caused droplets to form on the underside of the setup which eventually fell. When these droplets fell they caused vibrations which were visible by eye in the data. Additionally, the loss of water reduced the torque/leverage on the setup, which gradually shifted the focus deeper into the sample. There was an attempt to mitigate this by using a water resistant tape on the joint between the transducer cone and sample stage. This worked to some extent, but did not completely resolve the issue. This made it infeasible to perform longer duration measurements which extended beyond 15 minutes. It is suggested that a new sample holder which also includes an O-ring is created.

There was also some noise related to the ultrasound. Especially at the 2 MPa measurements at higher duty cycles distortions in the images were observed. These are likely due to movements in either the objective or the sample. The distortions themselves would likely not affect the results to a large extent, as the particles were smeared out, and not recognizable spheroids in those frames. The gap-closing (the number of frames a particle can disappear and still be considered the same particle) compensates for this effect. However, it is likely that the ultrasound induced vibrations in the setup which extended beyond the visible distortions and

thus biased the measurements. If feasible, a microscope which supports external synchronization of its acquisition can be used to eliminate the visible distortions completely. Alternatively, a microscope with a faster scan speed can be used, and the frames where there are distortions can be discarded. Another improvement which can be made is to stabilize the setup by mounting it directly on the microscope instead of the optics table. The setup was very sensitive to motion. By simply touching the optics table, there was visible distortions in the collected data. Collecting data at varying (both high and low) frame-rates can help in identifying if vibrations are a factor in the observed diffusion coefficients. If the data was unbiased by any vibrations, the diffusion coefficient would be the same for all frame-rates.

Judging by the low attenuation of the gels, 1 MHz ultrasound is not optimal for detecting the effect of ARF on nanoparticle transport in ECM. Adapters should be made to fit transducers of higher frequencies in the setup. The gels would attenuate the higher frequency ultrasound by a significantly larger amount, thus increasing the likelihood of observing any effect on the diffusion of nanoparticles.

There is a significant risk of standing waves in the setup. The ultrasound ideally gets absorbed by the absorbing material in the back wall of the sample holder. However, if not all of the ultrasound gets absorbed, but reflects back at the transducer, there would be formation of standing waves. When characterizing the setup, a hydrophone in a water tank was used, but the hydrophone didn't fit inside the sample holder due to complicated angles in the setup. Thus the beam profile was only measured with a replacement adapter which only accounted for the blocking of half the ultrasound beam. There was an intent to use a fibre-optic cable to measure the ultrasound beam profile with the gel and objective present in the actual sample holder. However, the fibre-optic sensor wasn't functioning properly, and could not be used. As soon as the equipment is functioning, these measurements should be done. If standing waves is an issue, it can be mitigated by angling the back wall of the next iteration of sample holder 45° to reflect the waves upwards instead of straight back. The same fibre-optic system for ultrasound measurements was also intended for temperature measurements. A small hole should be drilled in the back wall so the fiber can be inserted, as the fiber ideally should be aimed straight at the transducer. The fibers are very fragile, and would likely break if they were bent into position.

5.3 Closing remarks

Creating the setup for measurement of diffusion in gels is a good first step in establishing if ultrasound has an effect on the transport of nanoparticles in gels. However, there were certain weaknesses in the experimental setup which needs to be addressed before it can give reliable results. Several of these issues were related to the stability. Diffusion measurement through mean square displacement is not ideal in such conditions. After the stability is improved as suggested in section 5.2.4, using *fluorescence recovery after photobleaching* (FRAP) could be a better technique as it estimates the diffusion coefficient from the time it takes the nanoparticles to completely spread through a region. It has previously been successfully applied on PEGylated nanoparticles in a collagen gel. However, FRAP is a slower technique, and each measurement took around 35 minutes [113].

Another addition to the experimental setup which will be useful is embedded pressure tubing in front of, and behind the sample. This would enable the measurement and estimation of the dynamic pressure caused by the ultrasound. Additionally, a dynamic pressure can be applied to emulate the conditions of a high IFP in the periphery of tumour tissue. Both of these would be helpful in validating the computer simulations which Centre of Excellence PoreLab

is currently working on.

Furthermore, 1 MHz ultrasound is not optimal for utilizing the effect of ARF on nanoparticle transport in ECM. The most relevant frequency in clinical and pre-clinical trials relating to drug-delivery with the combined usage of ultrasound, microbubbles and nanoparticles currently is 1 MHz [9, 10, 14–18]. However, if multi-frequency transducers were available, the low frequencies in the kHz to a few MHz range can be used for microbubble excitation, while higher frequencies can be used for imaging and potentially improving the nanoparticle transport in ECM through ARF.

Chapter 6

Conclusion

A 5 mg/mL collagen gel with 1 mg/mL hyaluronic acid and 10% evaporated milk was chosen as an extracellular matrix phantom. The phantom was used for measuring the diffusion of two different Poly(Ethylbutyl Cyanoacrylate) nanoparticles under ultrasound treatment, in a custom built setup. The evaporated milk was included to increase the gel's acoustic attenuation, which is an important property for achieving a high acoustic radiation force which could improve the transport of nanoparticles.

Before any transport measurements could be done, a setup for measuring acoustic attenuation needed to be established, and the gels needed to be characterized. An acoustic attenuation measurement setup which had previously given inconsistent results when measuring samples with low attenuation was optimized. After the optimizations, a sufficiently high sensitivity was achieved, and the measured attenuation of gels increased with frequency as would be expected. The optimizations were performed on agarose gels due to late deliveries of collagen from the manufacturer.

To find a suitable additive for increasing attenuation, agarose gels were made with different concentrations of bovine serum albumin and evaporated milk. Both additives gave similar results, but evaporated milk was chosen as the additive moving forward. It has a slightly higher acoustic attenuation, and it is slightly easier to work with. The collagen gel with evaporated milk still had a very low attenuation, likely due to the samples being inhomogeneous. This was a general concern, and better methods for mixing the gel constituents are needed.

A custom built setup for measuring the effect of ultrasound treatment on the diffusion of nanoparticles was designed. Before being used, the setup was first characterized in a water tank where the beam profile and achieved acoustic pressures were investigated. This made the applied acoustic pressure to the sample predictable. An oversight in the design placed the sample slightly in the far-field of the transducer. This was compensated by applying a higher pressure.

Measurements with the setup on nanoparticle transport in the collagen gels were performed. The measurements revealed a positive correlation between diffusion coefficient, and ultrasound duty cycle and pressure. However, this is likely due to instabilities in the setup. There was a leak which contributed to vibrations and a gradual focal shift. Additionally, there were artifacts in the data when the ultrasound was applied. The setup thus needs some improvements before it gives reliable results.

Unlike in another study, it was not possible to separate the diffusion of the nanoparticles into two fractions. That study separated the particles into a mobile fraction with a diffusion coefficient similar to free diffusion in water, and a hindered fraction with a severely decreased diffusion coefficient. Only the latter fraction was observed. This is likely due to different

monomer in the polymeric nanoparticle, different concentration of particles, different collagen concentration or different PEGylation.

Bibliography

- [1] P. G. Corrie, 'Cytotoxic chemotherapy: Clinical aspects', *Medicine*, vol. 39, no. 12, pp. 717–722, Dec. 2011. DOI: 10.1016/j.mpmed.2011.09.012.
- [2] V. P. Chauhan and R. K. Jain, 'Strategies for advancing cancer nanomedicine', *Nature Materials*, vol. 12, no. 11, pp. 958–962, Oct. 2013. DOI: 10.1038/nmat3792.
- [3] *Stadig færre dør av kreft og hjerte- og karsykdom*, Dec. 2019.
- [4] R. K. Jain, 'Transport of molecules in the tumor interstitium: A review', *Cancer research*, vol. 47, no. 12, pp. 3039–3051, 1987.
- [5] F. Danhier, 'To exploit the tumor microenvironment: Since the EPR effect fails in the clinic, what is the future of nanomedicine?', *Journal of Controlled Release*, vol. 244, pp. 108–121, Dec. 2016. DOI: 10.1016/j.jconrel.2016.11.015.
- [6] Y. Nakamura, A. Mochida, P. L. Choyke and H. Kobayashi, 'Nanodrug delivery: Is the enhanced permeability and retention effect sufficient for curing cancer?', *Bioconjugate chemistry*, vol. 27, no. 10, pp. 2225–2238, 2016.
- [7] A. van Wamel, P. C. Sontum, A. Healey, S. Kvåle, N. Bush, J. Bamber and C. de Lange Davies, 'Acoustic cluster therapy (ACT) enhances the therapeutic efficacy of paclitaxel and abraxane® for treatment of human prostate adenocarcinoma in mice', *Journal of Controlled Release*, vol. 236, pp. 15–21, Aug. 2016. DOI: 10.1016/j.jconrel.2016.06.018.
- [8] S. Snipstad, S. Berg, Ý. Mørch, A. Bjørkøy, E. Sulheim, R. Hansen, I. Grimstad, A. van Wamel, A. F. Maaland, S. H. Torp and C. de Lange Davies, 'Ultrasound improves the delivery and therapeutic effect of nanoparticle-stabilized microbubbles in breast cancer xenografts', *Ultrasound in Medicine & Biology*, vol. 43, no. 11, pp. 2651–2669, Nov. 2017. DOI: 10.1016/j.ultrasmedbio.2017.06.029.
- [9] G. Dimcevski, S. Kotopoulos, T. Bjånes, D. Hoem, J. Schjøtt, B. T. Gjertsen, M. Biermann, A. Molven, H. Sorbye, E. McCormack *et al.*, 'A human clinical trial using ultrasound and microbubbles to enhance gemcitabine treatment of inoperable pancreatic cancer', *Journal of Controlled Release*, vol. 243, pp. 172–181, 2016.
- [10] Y. Wang, Y. Li, K. Yan, L. Shen, W. Yang, J. Gong and K. Ding, 'Clinical study of ultrasound and microbubbles for enhancing chemotherapeutic sensitivity of malignant tumors in digestive system', *Chinese Journal of Cancer Research*, vol. 30, no. 5, p. 553, 2018.
- [11] H. Chen, W. Kreider, A. A. Brayman, M. R. Bailey and T. J. Matula, 'Blood vessel deformations on microsecond time scales by ultrasonic cavitation', *Physical review letters*, vol. 106, no. 3, p. 034301, 2011.

- [12] H. Chen, A. A. Brayman and T. J. Matula, 'Characteristic microvessel relaxation timescales associated with ultrasound-activated microbubbles', *Applied physics letters*, vol. 101, no. 16, p. 163 704, 2012.
- [13] C. de Lange Davies, 'Ultrasound-mediated transport of nanoparticles in tissue: Creating a predictive model combining theory, simulations and experiments.', internal, project description, 2020.
- [14] S. Kotopoulis, A. Delalande, M. Popa, V. Mamaeva, G. Dimcevski, O. H. Gilja, M. Postema, B. T. Gjertsen and E. McCormack, 'Sonoporation-enhanced chemotherapy significantly reduces primary tumour burden in an orthotopic pancreatic cancer xenograft', *Molecular imaging and biology*, vol. 16, no. 1, pp. 53–62, 2014.
- [15] S. Eggen, M. Afadzi, E. A. Nilssen, S. B. Haugstad, B. Angelsen and C. d. L. Davies, 'Ultrasound improves the uptake and distribution of liposomal doxorubicin in prostate cancer xenografts', *Ultrasound in medicine & biology*, vol. 39, no. 7, pp. 1255–1266, 2013.
- [16] S.-P. Li, G. Zhao and H.-Y. Chen, 'The relationship between steady shear viscosity and complex viscosity', *Journal of Dispersion Science and Technology*, vol. 26, no. 4, pp. 415–419, Jul. 2005. DOI: 10.1081/dis-200054555.
- [17] D. Bressand, A. Novell, A. Girault, W. Raoul, G. Fromont-Hankard, J.-M. Escoffre, T. Lecomte and A. Bouakaz, 'Enhancing nab-paclitaxel delivery using microbubble-assisted ultrasound in a pancreatic cancer model', *Molecular pharmaceutics*, vol. 16, no. 9, pp. 3814–3822, 2019.
- [18] C. W. Schultz, G. Ruiz de Garibay, A. Langer, J.-B. Liu, T. Dhir, C. Leitch, C. E. Wessner, M. Mayoral, B. Zhang, M. Popa *et al.*, 'Selecting the optimal parameters for sonoporation of pancreatic cancer in a pre-clinical model', *Cancer Biology & Therapy*, vol. 22, no. 3, pp. 204–215, 2021.
- [19] S. K. Hobbs, W. L. Monsky, F. Yuan, W. G. Roberts, L. Griffith, V. P. Torchilin and R. K. Jain, 'Regulation of transport pathways in tumor vessels: Role of tumor type and microenvironment', *Proceedings of the National Academy of Sciences*, vol. 95, no. 8, pp. 4607–4612, Apr. 1998. DOI: 10.1073/pnas.95.8.4607.
- [20] S. Sindhvani, A. M. Syed, J. Ngai, B. R. Kingston, L. Maiorino, J. Rothschild, P. MacMillan, Y. Zhang, N. U. Rajesh, T. Hoang, J. L. Y. Wu, S. Wilhelm, A. Zilman, S. Gadde, A. Sulaiman, B. Ouyang, Z. Lin, L. Wang, M. Egeblad and W. C. W. Chan, 'The entry of nanoparticles into solid tumours', *Nature Materials*, vol. 19, no. 5, pp. 566–575, Jan. 2020. DOI: 10.1038/s41563-019-0566-2.
- [21] S. Pandit, D. Dutta and S. Nie, 'Active transcytosis and new opportunities for cancer nanomedicine', *Nature Materials*, vol. 19, no. 5, pp. 478–480, Apr. 2020. DOI: 10.1038/s41563-020-0672-1.
- [22] R. K. Jain and T. Stylianopoulos, 'Delivering nanomedicine to solid tumors', *Nature reviews Clinical oncology*, vol. 7, no. 11, p. 653, 2010.
- [23] T. Lammers, F. Kiessling, W. E. Hennink and G. Storm, 'Drug targeting to tumors: Principles, pitfalls and (pre-) clinical progress', *Journal of Controlled Release*, vol. 161, no. 2, pp. 175–187, Jul. 2012. DOI: 10.1016/j.jconrel.2011.09.063.
- [24] S. Parveen, R. Misra and S. K. Sahoo, 'Nanoparticles: A boon to drug delivery, therapeutics, diagnostics and imaging', *Nanomedicine: Nanotechnology, Biology and Medicine*, vol. 8, no. 2, pp. 147–166, Feb. 2012. DOI: 10.1016/j.nano.2011.05.016.

- [25] S. Salatin, S. M. Dizaj and A. Y. Khosroushahi, 'Effect of the surface modification, size, and shape on cellular uptake of nanoparticles', *Cell Biology International*, vol. 39, no. 8, pp. 881–890, Apr. 2015. DOI: 10.1002/cbin.10459.
- [26] Y. (Barenholz, 'Doxil® — the first FDA-approved nano-drug: Lessons learned', *Journal of Controlled Release*, vol. 160, no. 2, pp. 117–134, Jun. 2012. DOI: 10.1016/j.jconrel.2012.03.020.
- [27] K. Knop, R. Hoogenboom, D. Fischer and U. S. Schubert, 'Poly (ethylene glycol) in drug delivery: Pros and cons as well as potential alternatives', *Angewandte chemie international edition*, vol. 49, no. 36, pp. 6288–6308, 2010.
- [28] J. J. Verhoef and T. J. Anchordoquy, 'Questioning the use of pegylation for drug delivery', *Drug delivery and translational research*, vol. 3, no. 6, pp. 499–503, 2013.
- [29] C. Frantz, K. M. Stewart and V. M. Weaver, 'The extracellular matrix at a glance', *Journal of Cell Science*, vol. 123, no. 24, pp. 4195–4200, Dec. 2010. DOI: 10.1242/jcs.023820.
- [30] A. B. Engin, D. Nikitovic, M. Neagu, P. Henrich-Noack, A. O. Docea, M. I. Shtilman, K. Golokhvast and A. M. Tsatsakis, 'Mechanistic understanding of nanoparticles' interactions with extracellular matrix: The cell and immune system', *Particle and Fibre Toxicology*, vol. 14, no. 1, Jun. 2017. DOI: 10.1186/s12989-017-0199-z.
- [31] J. R. E. Fraser, T. C. Laurent and U. B. G. Laurent, 'Hyaluronan: Its nature, distribution, functions and turnover', *Journal of Internal Medicine*, vol. 242, no. 1, pp. 27–33, Jul. 1997. DOI: 10.1046/j.1365-2796.1997.00170.x.
- [32] E. A. Swabb, J. Wei and P. M. Gullino, 'Diffusion and convection in normal and neoplastic tissues', *Cancer research*, vol. 34, no. 10, pp. 2814–2822, 1974.
- [33] J. Levick, 'Flow through interstitium and other fibrous matrices', *Quarterly Journal of Experimental Physiology: Translation and Integration*, vol. 72, no. 4, pp. 409–437, 1987.
- [34] C.-H. Heldin, K. Rubin, K. Pietras and A. Östman, 'High interstitial fluid pressure — an obstacle in cancer therapy', *Nature Reviews Cancer*, vol. 4, no. 10, pp. 806–813, Oct. 2004. DOI: 10.1038/nrc1456.
- [35] Y. Boucher, L. T. Baxter and R. K. Jain, 'Interstitial pressure gradients in tissue-isolated and subcutaneous tumors: Implications for therapy', *Cancer research*, vol. 50, no. 15, pp. 4478–4484, 1990.
- [36] P. A. Netti, D. A. Berk, M. A. Swartz, A. J. Grodzinsky and R. K. Jain, 'Role of extracellular matrix assembly in interstitial transport in solid tumors', *Cancer research*, vol. 60, no. 9, pp. 2497–2503, 2000.
- [37] K. Ropponen, M. Tammi, J. Parkkinen, M. Eskelinen, R. Tammi, P. Lipponen, U. Ågren, E. Alhava and V.-M. Kosma, 'Tumor cell-associated hyaluronan as an unfavorable prognostic factor in colorectal cancer', *Cancer research*, vol. 58, no. 2, pp. 342–347, 1998.
- [38] R. H. Tammi, A. Kultti, V.-M. Kosma, R. Pirinen, P. Auvinen and M. I. Tammi, 'Hyaluronan in human tumors: Pathobiological and prognostic messages from cell-associated and stromal hyaluronan', *Seminars in Cancer Biology*, vol. 18, no. 4, pp. 288–295, Aug. 2008. DOI: 10.1016/j.semcancer.2008.03.005.

- [39] S. Ramanujan, A. Pluen, T. D. McKee, E. B. Brown, Y. Boucher and R. K. Jain, 'Diffusion and convection in collagen gels: Implications for transport in the tumor interstitium', *Biophysical Journal*, vol. 83, no. 3, pp. 1650–1660, Sep. 2002. DOI: 10.1016/s0006-3495(02)73933-7.
- [40] M. E. Katt, A. L. Placone, A. D. Wong, Z. S. Xu and P. C. Searson, 'In vitro tumor models: Advantages, disadvantages, variables, and selecting the right platform', *Frontiers in Bioengineering and Biotechnology*, vol. 4, Feb. 2016. DOI: 10.3389/fbioe.2016.00012.
- [41] S. Nath and G. R. Devi, 'Three-dimensional culture systems in cancer research: Focus on tumor spheroid model', *Pharmacology & Therapeutics*, vol. 163, pp. 94–108, Jul. 2016. DOI: 10.1016/j.pharmthera.2016.03.013.
- [42] A. E. Forte, S. Galvan, F. Manieri, F. R. y Baena and D. Dini, 'A composite hydrogel for brain tissue phantoms', *Materials & Design*, vol. 112, pp. 227–238, 2016.
- [43] M.-K. Sun, J. Shieh, C.-W. Lo, C.-S. Chen, B.-T. Chen, C.-W. Huang and W.-S. Chen, 'Reusable tissue-mimicking hydrogel phantoms for focused ultrasound ablation', *Ultrasonics sonochemistry*, vol. 23, pp. 399–405, 2015.
- [44] C. Demitri, A. Sannino, F. Conversano, S. Casciaro, A. Distante and A. Maffezzoli, 'Hydrogel based tissue mimicking phantom for in-vitro ultrasound contrast agents studies', *Journal of Biomedical Materials Research Part B: Applied Biomaterials: An Official Journal of The Society for Biomaterials, The Japanese Society for Biomaterials, and The Australian Society for Biomaterials and the Korean Society for Biomaterials*, vol. 87, no. 2, pp. 338–345, 2008.
- [45] E. M. Ahmed, 'Hydrogel: Preparation, characterization, and applications: A review', *Journal of Advanced Research*, vol. 6, no. 2, pp. 105–121, Mar. 2015. DOI: 10.1016/j.jare.2013.07.006.
- [46] G. Forgacs, S. A. Newman, B. Hinner, C. W. Maier and E. Sackmann, 'Assembly of collagen matrices as a phase transition revealed by structural and rheologic studies', *Biophysical Journal*, vol. 84, no. 2, pp. 1272–1280, Feb. 2003. DOI: 10.1016/s0006-3495(03)74942-x.
- [47] G. Wood and M. K. Keech, 'The formation of fibrils from collagen solutions 1. the effect of experimental conditions: Kinetic and electron-microscope studies', *Biochemical Journal*, vol. 75, no. 3, pp. 588–598, 1960.
- [48] W. Comper and A. Veis, 'The mechanism of nucleation for in vitro collagen fibril formation', *Biopolymers: Original Research on Biomolecules*, vol. 16, no. 10, pp. 2113–2131, 1977.
- [49] W. Comper and A. Veis, 'Characterization of nuclei in in vitro collagen fibril formation', *Biopolymers: Original Research on Biomolecules*, vol. 16, no. 10, pp. 2133–2142, 1977.
- [50] X. Xin, A. Borzacchiello, P. Netti, L. Ambrosio and L. Nicolais, 'Hyaluronic-acid-based semi-interpenetrating materials', *Journal of Biomaterials Science, Polymer Edition*, vol. 15, no. 9, pp. 1223–1236, 2004.
- [51] S.-W. Tsai, R.-L. Liu, F.-Y. Hsu and C.-C. Chen, 'A study of the influence of polysaccharides on collagen self-assembly: Nanostructure and kinetics', *Biopolymers: Original Research on Biomolecules*, vol. 83, no. 4, pp. 381–388, 2006.

- [52] Y.-l. Yang and L. J. Kaufman, 'Rheology and confocal reflectance microscopy as probes of mechanical properties and structure during collagen and collagen/hyaluronan self-assembly', *Biophysical Journal*, vol. 96, no. 4, pp. 1566–1585, Feb. 2009. DOI: 10.1016/j.bpj.2008.10.063.
- [53] B. Johansson, 'Agarose gel electrophoresis', *Scandinavian Journal of Clinical and Laboratory Investigation*, vol. 29, no. sup124, pp. 7–19, 1972.
- [54] P. Zarrintaj, S. Manouchehri, Z. Ahmadi, M. R. Saeb, A. M. Urbanska, D. L. Kaplan and M. Mozafari, 'Agarose-based biomaterials for tissue engineering', *Carbohydrate polymers*, vol. 187, pp. 66–84, 2018.
- [55] A. D. Maxwell, T.-Y. Wang, L. Yuan, A. P. Duryea, Z. Xu and C. A. Cain, 'A tissue phantom for visualization and measurement of ultrasound-induced cavitation damage', *Ultrasound in medicine & biology*, vol. 36, no. 12, pp. 2132–2143, 2010.
- [56] S. Lopez-Haro, I. Bazan-Trujillo, L. Leija-Salas and A. Vera-Hernandez, 'Ultrasound propagation speed measurement of mimicking soft tissue phantoms based on agarose in the range of 25° c to 50° c', in *2008 5th International Conference on Electrical Engineering, Computing Science and Automatic Control*, IEEE, 2008, pp. 192–195.
- [57] C. C. Miller, 'The stokes-einstein law for diffusion in solution', *Proceedings of the Royal Society of London. Series A, Containing Papers of a Mathematical and Physical Character*, vol. 106, no. 740, pp. 724–749, 1924.
- [58] J. Kestin, M. Sokolov and W. A. Wakeham, 'Viscosity of liquid water in the range -8° c to 150° c', *Journal of Physical and Chemical Reference Data*, vol. 7, no. 3, pp. 941–948, Jul. 1978. DOI: 10.1063/1.555581.
- [59] P. N. Wells, 'Ultrasound imaging', *Physics in Medicine & Biology*, vol. 51, no. 13, R83, 2006.
- [60] V. Chan and A. Perlas, 'Basics of ultrasound imaging', in *Atlas of ultrasound-guided procedures in interventional pain management*, Springer, 2011, pp. 13–19.
- [61] B. B. Goldberg, J.-B. Liu and F. Forsberg, 'Ultrasound contrast agents: A review', *Ultrasound in Medicine & Biology*, vol. 20, no. 4, pp. 319–333, Jan. 1994. DOI: 10.1016/0301-5629(94)90001-9.
- [62] J. C. Dai, M. R. Bailey, M. D. Sorensen and J. D. Harper, 'Innovations in ultrasound technology in the management of kidney stones', *Urologic Clinics*, vol. 46, no. 2, pp. 273–285, 2019.
- [63] L. Claes and B. Willie, 'The enhancement of bone regeneration by ultrasound', *Progress in biophysics and molecular biology*, vol. 93, no. 1-3, pp. 384–398, 2007.
- [64] K. Ferrara, R. Pollard and M. Borden, 'Ultrasound microbubble contrast agents: Fundamentals and application to gene and drug delivery', *Annu. Rev. Biomed. Eng.*, vol. 9, pp. 415–447, 2007.
- [65] V. Frenkel, 'Ultrasound mediated delivery of drugs and genes to solid tumors', *Advanced drug delivery reviews*, vol. 60, no. 10, pp. 1193–1208, 2008.
- [66] J. Wu and W. L. Nyborg, 'Ultrasound, cavitation bubbles and their interaction with cells', *Advanced drug delivery reviews*, vol. 60, no. 10, pp. 1103–1116, 2008.
- [67] R. E. Apfel and C. K. Holland, 'Gauging the likelihood of cavitation from short-pulse, low-duty cycle diagnostic ultrasound', *Ultrasound in Medicine and Biology*, vol. 17, no. 2, pp. 179–185, 1991.

- [68] P. C. Lyon, L. F. Griffiths, J. Lee, D. Chung, R. Carlisle, F. Wu, M. R. Middleton, F. V. Gleeson and C. C. Coussios, 'Clinical trial protocol for tardox: A phase i study to investigate the feasibility of targeted release of lyso-thermosensitive liposomal doxorubicin (thermodox®) using focused ultrasound in patients with liver tumours', *Journal of therapeutic ultrasound*, vol. 5, no. 1, pp. 1–8, 2017.
- [69] P. C. Lyon, M. D. Gray, C. Mannaris, L. K. Folkes, M. Stratford, L. Campo, D. Y. Chung, S. Scott, M. Anderson, R. Goldin *et al.*, 'Safety and feasibility of ultrasound-triggered targeted drug delivery of doxorubicin from thermosensitive liposomes in liver tumours (tardox): A single-centre, open-label, phase 1 trial', *The Lancet Oncology*, vol. 19, no. 8, pp. 1027–1039, 2018.
- [70] S. A. Elder, 'Cavitation microstreaming', *The Journal of the Acoustical Society of America*, vol. 31, no. 1, pp. 54–64, 1959.
- [71] N. McDannold, N. Vykhodtseva and K. Hynynen, 'Targeted disruption of the blood-brain barrier with focused ultrasound: Association with cavitation activity', *Physics in Medicine & Biology*, vol. 51, no. 4, p. 793, 2006.
- [72] R. Apfel, 'Acoustic cavitation: A possible consequence of biomedical uses of ultrasound.', *The British journal of cancer. Supplement*, vol. 5, p. 140, 1982.
- [73] P. D. Edmonds and K. M. Sancier, 'Evidence for free radical production by ultrasonic cavitation in biological media', *Ultrasound in medicine & biology*, vol. 9, no. 6, pp. 635–639, 1983.
- [74] C. C. Coussios and R. A. Roy, 'Applications of acoustics and cavitation to noninvasive therapy and drug delivery', *Annu. Rev. Fluid Mech.*, vol. 40, pp. 395–420, 2008.
- [75] W. L. Nyborg, 'MECHANISMS FOR BIOEFFECTS OF ULTRASOUND RELEVANT TO THERAPEUTIC APPLICATIONS', in *Emerging Therapeutic Ultrasound*, WORLD SCIENTIFIC, Aug. 2006. DOI: 10.1142/9789812774125_0002.
- [76] F. L. Lizzi, R. Muratore, C. X. Deng, J. A. Ketterling, S. K. Alam, S. Mikaelian and A. Kalisz, 'Radiation-force technique to monitor lesions during ultrasonic therapy', *Ultrasound in medicine & biology*, vol. 29, no. 11, pp. 1593–1605, 2003.
- [77] S. O. Dymling, H. W. Persson, T. G. Hertz and K. Lindström, 'A new ultrasonic method for fluid property measurements', *Ultrasound in medicine & biology*, vol. 17, no. 5, pp. 497–500, 1991.
- [78] J. J. Rychak, A. L. Klibanov and J. A. Hossack, 'Acoustic radiation force enhances targeted delivery of ultrasound contrast microbubbles: In vitro verification', *IEEE transactions on ultrasonics, ferroelectrics, and frequency control*, vol. 52, no. 3, pp. 421–433, 2005.
- [79] M. K. Lovmo, P. T. Yemane, A. Bjorkoy, R. Hansen, R. Cleveland, B. Angelsen and C. de Lange Davies, 'Effect of acoustic radiation force on displacement of nanoparticles in collagen gels', *IEEE Transactions on Ultrasonics, Ferroelectrics, and Frequency Control*, pp. 1–1, 2020. DOI: 10.1109/tuffc.2020.3006762.
- [80] M. O. Culjat, D. Goldenberg, P. Tewari and R. S. Singh, 'A review of tissue substitutes for ultrasound imaging', *Ultrasound in Medicine & Biology*, vol. 36, no. 6, pp. 861–873, Jun. 2010. DOI: 10.1016/j.ultrasmedbio.2010.02.012.

- [81] A. Cafarelli, A. Verbeni, A. Poliziani, P. Dario, A. Menciasci and L. Ricotti, 'Tuning acoustic and mechanical properties of materials for ultrasound phantoms and smart substrates for cell cultures', *Acta Biomaterialia*, vol. 49, pp. 368–378, Feb. 2017. DOI: 10.1016/j.actbio.2016.11.049.
- [82] K. P. Mercado, M. Helguera, D. C. Hocking and D. Dalecki, 'Noninvasive quantitative imaging of collagen microstructure in three-dimensional hydrogels using high-frequency ultrasound', *Tissue Engineering Part C: Methods*, vol. 21, no. 7, pp. 671–682, 2015.
- [83] A. I. Farrer, H. Odéen, J. de Bever, B. Coats, D. L. Parker, A. Payne and D. A. Christensen, 'Characterization and evaluation of tissue-mimicking gelatin phantoms for use with mrgfus', *Journal of therapeutic ultrasound*, vol. 3, no. 1, p. 9, 2015.
- [84] E. L. Madsen, G. R. Frank and F. Dong, 'Liquid or solid ultrasonically tissue-mimicking materials with very low scatter', *Ultrasound in medicine & biology*, vol. 24, no. 4, pp. 535–542, 1998.
- [85] C. Lafon, V. Zderic, M. L. Noble, J. C. Yuen, P. J. Kaczkowski, O. A. Sapozhnikov, F. Chavrier, L. A. Crum and S. Vaezy, 'Gel phantom for use in high-intensity focused ultrasound dosimetry', *Ultrasound in medicine & biology*, vol. 31, no. 10, pp. 1383–1389, 2005.
- [86] L. M. Jawerth, S. Münster, D. A. Vader, B. Fabry and D. A. Weitz, 'A blind spot in confocal reflection microscopy: The dependence of fiber brightness on fiber orientation in imaging biopolymer networks', *Biophysical Journal*, vol. 98, no. 3, pp. L1–L3, Feb. 2010. DOI: 10.1016/j.bpj.2009.09.065.
- [87] N. Lang, S. Münster, C. Metzner, P. Krauss, S. Schürmann, J. Lange, K. Aifantis, O. Friedrich and B. Fabry, 'Estimating the 3d pore size distribution of biopolymer networks from directionally biased data', *Biophysical Journal*, vol. 105, no. 9, pp. 1967–1975, Nov. 2013. DOI: 10.1016/j.bpj.2013.09.038.
- [88] X. Chen, O. Nadiarynk, S. Plotnikov and P. J. Campagnola, 'Second harmonic generation microscopy for quantitative analysis of collagen fibrillar structure', *Nature protocols*, vol. 7, no. 4, pp. 654–669, 2012.
- [89] I. Freund and M. Deutsch, 'Second-harmonic microscopy of biological tissue', *Optics Letters*, vol. 11, no. 2, p. 94, Feb. 1986. DOI: 10.1364/ol.11.000094.
- [90] C. Metzner, P. Krauss and B. Fabry, 'Poresizes in random line networks', *arXiv preprint arXiv:1110.1803*, 2011.
- [91] P. Krauss, C. Metzner, J. Lange, N. Lang and B. Fabry, 'Parameter-free binarization and skeletonization of fiber networks from confocal image stacks', *PLoS ONE*, vol. 7, no. 5, F. J. Esteban, Ed., e36575, May 2012. DOI: 10.1371/journal.pone.0036575.
- [92] A. Finnøy, 'Acoustic and mechanical properties of microbubbles stabilized by polymeric nanoparticles', Master's thesis, Norwegian University of Science and Technology, 2013.
- [93] MATLAB, *version 9.9.0 (R2020b)*. Natick, Massachusetts: The MathWorks Inc., 2020.
- [94] G. Van Rossum and F. L. Drake, *Python 3 Reference Manual*. Scotts Valley, CA: CreateSpace, 2009, ISBN: 1441412697.
- [95] J. D. Hunter, 'Matplotlib: A 2d graphics environment', *Computing in Science & Engineering*, vol. 9, no. 3, pp. 90–95, 2007. DOI: 10.1109/MCSE.2007.55.

- [96] J.-Y. Tinevez, N. Perry, J. Schindelin, G. M. Hoopes, G. D. Reynolds, E. Laplantine, S. Y. Bednarek, S. L. Shorte and K. W. Eliceiri, 'TrackMate: An open and extensible platform for single-particle tracking', *Methods*, vol. 115, pp. 80–90, Feb. 2017. DOI: 10.1016/j.ymeth.2016.09.016.
- [97] C. C. Lee, M. Lahham and B. Martin, 'Experimental verification of the kramers-kronig relationship for acoustic waves', *IEEE transactions on ultrasonics, ferroelectrics, and frequency control*, vol. 37, no. 4, pp. 286–294, 1990.
- [98] A. C. Kak and K. A. Dines, 'Signal processing of broadband pulsed ultrasound: Measurement of attenuation of soft biological tissues', *IEEE transactions on biomedical engineering*, no. 4, pp. 321–344, 1978.
- [99] W. Sachse and Y.-H. Pao, 'On the determination of phase and group velocities of dispersive waves in solids', *Journal of applied Physics*, vol. 49, no. 8, pp. 4320–4327, 1978.
- [100] A. Dukhin, P. Goetz and B. Travers, 'Use of ultrasound for characterizing dairy products', *Journal of dairy science*, vol. 88, no. 4, pp. 1320–1334, 2005.
- [101] T. L. Harman, J. Dabney and N. J. Richert, *Advanced engineering mathematics with MATLAB*, 2nd ed. Brooks/Cole Pub., 2000.
- [102] A. Nuttall, 'Some windows with very good sidelobe behavior', *IEEE Transactions on Acoustics, Speech, and Signal Processing*, vol. 29, no. 1, pp. 84–91, 1981.
- [103] J. C. Bamber and C. Hill, 'Ultrasonic attenuation and propagation speed in mammalian tissues as a function of temperature', *Ultrasound in medicine & biology*, vol. 5, no. 2, pp. 149–157, 1979.
- [104] A. Erikson, H. N. Andersen, S. N. Naess, P. Sikorski and C. d. L. Davies, 'Physical and chemical modifications of collagen gels: Impact on diffusion', *Biopolymers: Original Research on Biomolecules*, vol. 89, no. 2, pp. 135–143, 2008.
- [105] T. Stylianopoulos, M.-Z. Poh, N. Insin, M. G. Bawendi, D. Fukumura, L. L. Munn and R. K. Jain, 'Diffusion of particles in the extracellular matrix: The effect of repulsive electrostatic interactions', *Biophysical journal*, vol. 99, no. 5, pp. 1342–1349, 2010.
- [106] O. Lieleg, R. M. Baumgärtel and A. R. Bausch, 'Selective filtering of particles by the extracellular matrix: An electrostatic bandpass', *Biophysical journal*, vol. 97, no. 6, pp. 1569–1577, 2009.
- [107] C. B. Raub, V. Suresh, T. Krasieva, J. Lyubovitsky, J. D. Mih, A. J. Putnam, B. J. Tromberg and S. C. George, 'Noninvasive assessment of collagen gel microstructure and mechanics using multiphoton microscopy', *Biophysical journal*, vol. 92, no. 6, pp. 2212–2222, 2007.
- [108] *Cell-bioink mixing: Syringe coupler method*, May 2020.
- [109] A. K. Åslund, E. Sulheim, S. Snipstad, E. von Haartman, H. Baghirova, N. Starr, M. Kvåle Løvmo, S. Lelú, D. Scurr, C. d. L. Davies *et al.*, 'Quantification and qualitative effects of different pegylations on poly (butyl cyanoacrylate) nanoparticles', *Molecular pharmaceutics*, vol. 14, no. 8, pp. 2560–2569, 2017.
- [110] S. Lee, H. Han, H. Koo, J. H. Na, H. Y. Yoon, K. E. Lee, H. Lee, H. Kim, I. C. Kwon and K. Kim, 'Extracellular matrix remodeling in vivo for enhancing tumor-targeting efficiency of nanoparticle drug carriers using the pulsed high intensity focused ultrasound', *Journal of Controlled Release*, vol. 263, pp. 68–78, 2017.

- [111] S. Wang, I. S. Shin, H. Hancock, B.-s. Jang, H.-s. Kim, S. M. Lee, V. Zderic, V. Frenkel, I. Pastan, C. H. Paik *et al.*, 'Pulsed high intensity focused ultrasound increases penetration and therapeutic efficacy of monoclonal antibodies in murine xenograft tumors', *Journal of controlled release*, vol. 162, no. 1, pp. 218–224, 2012.
- [112] A. Khaibullina, B.-S. Jang, H. Sun, N. Le, S. Yu, V. Frenkel, J. A. Carrasquillo, I. Pastan, K. C. Li and C. H. Paik, 'Pulsed high-intensity focused ultrasound enhances uptake of radiolabeled monoclonal antibody to human epidermoid tumor in nude mice', *Journal of Nuclear Medicine*, vol. 49, no. 2, pp. 295–302, 2008.
- [113] L. Tomasetti, R. Liebl, D. S. Wastl and M. Breunig, 'Influence of pegylation on nanoparticle mobility in different models of the extracellular matrix', *European Journal of Pharmaceutics and Biopharmaceutics*, vol. 108, pp. 145–155, 2016.

Appendix A

CORNING[®] COLLAGEN I High Concentration (HC), Rat Tail - Certificate of analysis

Used batches:

- LOT 0090001
- LOT 9161007

Certificate of Analysis

CORNING® COLLAGEN I High Concentration (HC), RAT TAIL

Collagen I is found in most tissues and organs, but is most plentiful in dermis, tendon and bones. Type I molecule is a heterotrimer [$\alpha_1(I)_2 \alpha_2(I)$] of 300 nm length being composed of two $\alpha_1(I)$ chains and one $\alpha_2(I)$ chain.¹ Collagen binding integrin receptors are $\alpha_1 \text{Beta}_1$, $\alpha_2 \text{Beta}_1$, and $\alpha_3 \text{Beta}_1$.² When used as a gel, collagen facilitates successful adaptation *in vitro* culture and enhances expression of cell-specific morphology and function. The Collagen HC is used in applications where a sturdy gel provides maximal support to maintain the three dimensional structure.³⁻⁵

CATALOG NUMBER: 354249 LOT NUMBER: 0090001

SOURCE: Rat tail tendon

QUANTITY: 100 milligrams protein (measured by Pyrochemiluminescence)

CONCENTRATION: 9.10 mg/mL

FORMULATION: 0.02 N Acetic Acid

USE: Corning Collagen I HC, rat tail, is used as a three dimensional gel. Please see reverse for gelling procedures. Use these as guidelines only - we recommend that each investigator empirically determine the optimal conditions for their unique applications.

QUALITY CONTROL: ≥ 90 % by SDS PAGE.

This product has been tested for its ability to promote the attachment and spreading of HT-1080 Human Fibrosarcoma cells.

Corning Collagen I HC, rat tail, is a membrane-filtered (0.2 micron) preparation. Tested and found negative for the presence of bacteria, fungi and mycoplasma.

STORAGE: Stable when stored at 2-8°C. **DO NOT FREEZE.**

On release this product has been successfully gelled over a wide range of dilutions and will form a gel up to a concentration of 0.3 mg/mL. Further dilution may decrease the rigidity of the gel as will the time from manufacture.

EXPIRATION DATE: June 23, 2022

REFERENCES:

1. Linsenmayer, T.F., Collagen, in Cell Biology of Extracellular Matrix (ed., E.D. Hay) pp 5-37, Plenum Press, NY (1991).
2. Chan, B.M., and Hemler, M.E., *J. Cell Biol.*, **120**:537 (1993).
3. Gautreau, A., et.al., *PNAS*, **96**:7300 (1999).
4. Abir, R., et.al., *Hum. Reprod.*, **14**:1299 (1999).
5. Abir, R., et.al., *Fertil. Steril.*, **75**:141 (2001).

SAFETY RECOMMENDATION: Handle in accordance with good industrial hygiene and laboratory safety practices.

Suggested Coating Procedures

Gelling Procedure- Corning Collagen I HC, rat tail, will gel when its pH is brought to alkalinity using the procedure below. Please use this as a guideline for determining the optimum concentration for your application.

- 1) Prepare ammonia vapor chamber by taping a sterile 2 inch gauze sponge to the inside lid of a 150 mm petri dish. Saturate the gauze with ammonium hydroxide. Place lid on 150 mm dish and set aside.
- 2) Place an even coating of Corning® Collagen I HC, rat tail, on surface to be coated. Thickness may be varied as desired. 50-100 µl of Corning Collagen I HC, rat tail, is sufficient to coat a 22 mm coverslip. For dishes of 100 mm diameter, add approximately 6.0 mL per dish; for 60 mm dishes add approximately 2.3 mL and for 35 mm dishes add approximately 1.0 mL.
- 3) Transfer coated coverslips or dishes with lids off to ammonia vapor chamber and expose for three minutes.
- 4) Soak coated coverslip or dishes in sterile dH₂O for 30 minutes (5 mL for 35 mm dishes, 10 mL for 60 mm dishes, etc.). Aspirate and replace with 0.5-1.0 mL of sterile dH₂O and let sit overnight lidded in a laminar flow hood.
- 5) Aspirate the dH₂O and replace with serum supplemented balanced salt solution and store at 2-8°C.

Alternate Gelation Procedure for Corning Collagen I HC, Rat tail

- 1.0 Place on ice the following:
 - 1.1 Corning Collagen I HC, rat tail
 - 1.2 Sterile 10X phosphate buffered saline (10X PBS)
 - 1.3 Sterile dH₂O
 - 1.4 Sterile 1 N NaOH
- 2.0 Determine the final volume of Corning Collagen I HC, rat tail, solution to be used and the desired final collagen concentration.
- 3.0 Place on ice a sterile tube of sufficient capacity to contain the final volume of Corning Collagen I HC, rat tail.
- 4.0 Perform the following steps using aseptic technique in a Class 100 Hood.
 - 4.1 Add to the tube the following volume of 10X PBS:

$$\frac{\text{Final Volume}}{10} = \text{mL 10X PBS}$$
 - 4.2 Calculate the volume of Corning Collagen I HC, rat tail, to be used (do not add to the tube until step 4.6):

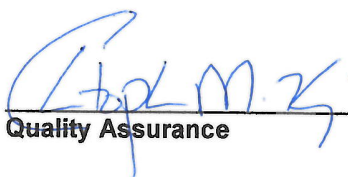
$$\frac{\text{Final volume} \times \text{Final collagen concentration in mg/mL}}{\text{Concentration in bottle (see lot specific spec. sheet)}} = \text{volume collagen to be added}$$
 - 4.3 Add to the 10X PBS the following volume of sterile ice cold 1 N NaOH:

$$(\text{volume collagen to be added}) \times 0.023 \text{ mL} = \text{volume 1 N NaOH}$$

- 4.4 Add to the 10X PBS/1 N NaOH the following volume of sterile ice-cold dH₂O:
 $(\text{Final volume}) - (\text{Volume collagen}) - (\text{Volume 10X PBS}) - (\text{Volume 1 N NaOH}) = \text{Volume dH}_2\text{O to add}$
- 4.5 Mix the contents of tube and hold in ice.
- 4.6 Add the calculated volume of Corning® Collagen I HC, rat tail, and mix. Leave on ice until ready for use.

- 5.0 The Corning Collagen I HC, rat tail, solution can be used immediately or held on ice for 2-3 hours.
- 6.0 When ready to use, aseptically deliver the solution into the cell culture device and allow to gel at 37°C for 30 minutes.

NOTE: For more details on Corning Collagen products and technical resources please visit support page at www.corning.com/lifesciences



Quality Assurance

June 04, 2020
Date

Appendix B

Precision Acoustics PA504 Test certificate

PRECISION ACOUSTICS LTD

Hampton Farm Business Park
Dorchester, DT2 8QH
UNITED KINGDOM

TRANSDUCER TEST CERTIFICATE

This certificate provides traceability of measurement to recognised national standards and to units of measurement realised at the National Physical Laboratory or other recognised national standards laboratories. Precision Acoustics Ltd is certified to the ISO 9001 standard.

Device Identification



Transducer S/N	PA504
Transducer Type	PZT - Curved Ceramic
Transducer Diameter	60.0 mm
Nominal Centre Frequency	1.00 MHz

Calibration Conditions

Calibration date	20/12/2016
Water temperature	22.0 °C
Water treatment	De-gassed, De-ionised, filtered
Acoustic path length	73 mm
Source signal type	Sine wave Toneburst
Peak to peak source signal amplitude	60 V
Electrical impedance	50 Ohms
Cable type, length	RG58, 1.5 m
Measurement type	Hydrophone measurement

Test Equipment used

Signal Generator	Keysight Technologies 33519B
Signal Amplifier	E&I A150
DAQ Device / Analyser	Agilent Technologies DSO-X 3024A

Calibrated by;	Checked by;
	
-----	-----

Thomas Kelley

Andrew Hurrell

TRANSDUCER TEST PROCEDURE

A full characterisation of an ultrasonic transducer requires an extensive set of measurements, involving a large number of parameters and a correspondingly large amount of time. For most applications, a more limited set of data will suffice. This is described below, for which there are three principal measurements of interest:

- * Variation of signal amplitude with frequency (all transducers)
- * Time domain response of transducer to short pulse (all transducers)
- * Lateral and axial dimensions of the focal spot (focussed transducers only)

A thorough description of the process for evaluating this range of parameters is provided in ASTM E1065-99 (2003), as well as a brief description of some of the problems that may be encountered. Of particular significance is the use of transient generators (pulser/receivers) when used to drive the transducer during a calibration. The output impedance of pulser/receivers tends to be relatively low for the duration of the drive signal, increasing to a much higher value when the transducer is used in receive mode. This leads to variable impedance loading at the terminals of the transducers, and can yield unpredictable results. Since the pulse width is often variable (or under user control), the same transducer can provide a significantly different frequency response simply by varying pulse width.

A calibration process must record the performance of the transducer ONLY and be independent of the equipment or the drive parameters used in conducting the measurement. For this reason, all Precision Acoustics Ltd transducer calibrations are based upon the "sinusoidal burst technique" as described in ASTM E1065-99 (2003). In summary, the transducer is driven by a sinusoidal tone burst such that it produces a corresponding ultrasonic signal in water. This signal is detected by a hydrophone and a voltage proportional to the acoustic signal is produced. This process is performed at a series of locations resulting in the generation of a profile of the acoustic beam. Additionally the ratio of applied electrical signal to the received electrical signal is calculated and this provides the sensitivity of the transducer at the frequency of the toneburst. This process is repeated for a range of tonebursts of different frequencies in order to obtain the full frequency response of the device under test. All equipment and cables used in this measurement have an impedance of 50 Ohms, thereby ensuring constant and reproducible transducer loading conditions.

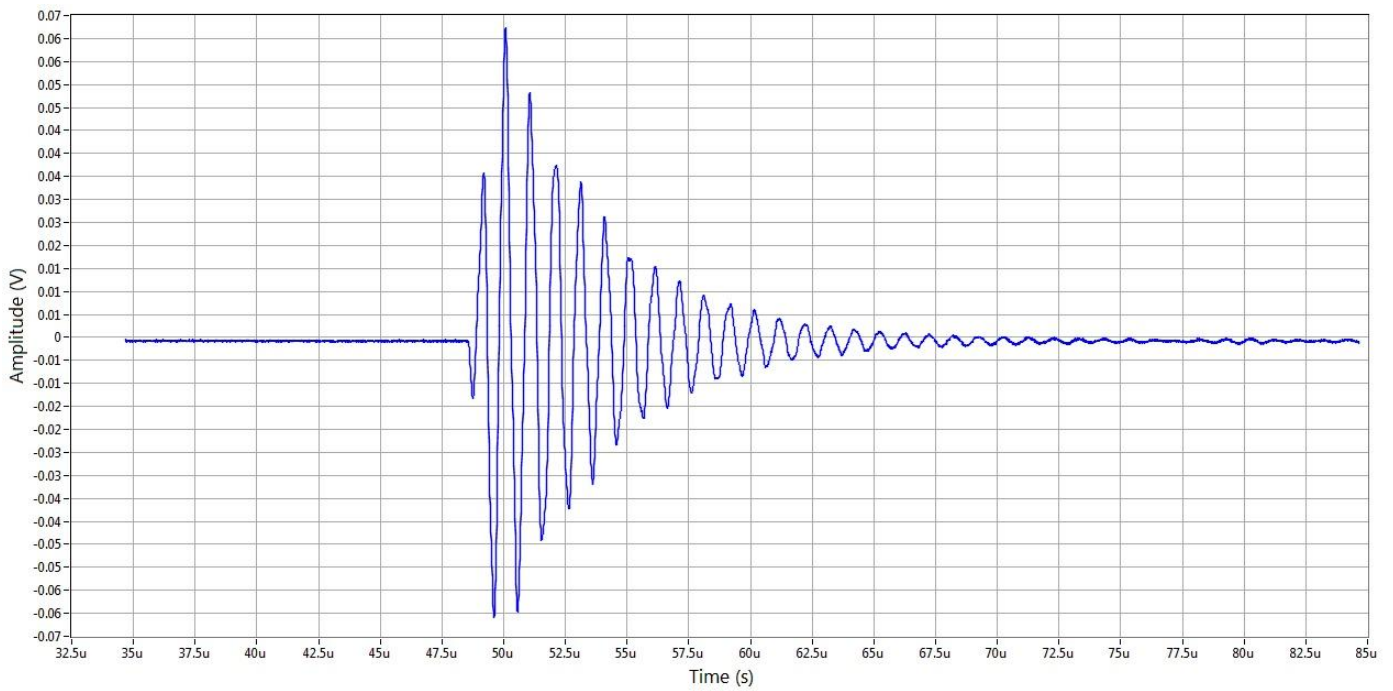
The position of the global maximum of the frequency response curve is identified and defined as the peak frequency. An amplitude limit is set (e.g. 6dB below the peak amplitude) and the frequencies at which the response curve crosses this amplitude threshold are determined. These are called the upper and lower frequency limits (f_u and f_l) respectively, from which the following parameters are calculated:

$$f_c = \frac{f_u + f_l}{2} , \quad BW = f_u - f_l , \quad Q = \frac{f_c}{BW} , \quad \%BW = 100 \frac{BW}{f_c}$$

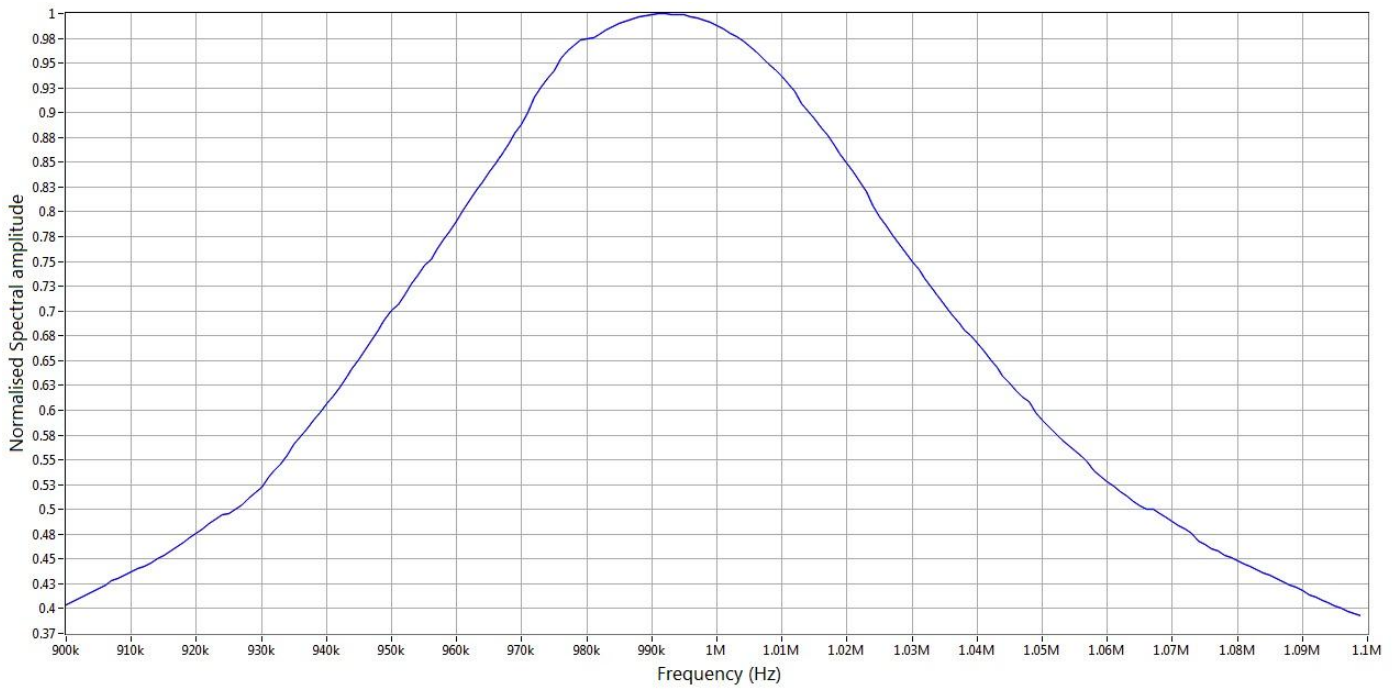
[f_c = Centre frequency, BW = Bandwidth, Q = Mechanical Q-factor, %BW = Percentage bandwidth]

The transient response of the transducer (i.e. time domain response to a short pulse) is measured by using a single cycle of a sine wave at its nominal frequency. It is important to note that this is not the shortest pulse that the transducer can produce, since transducers driven by a pulser often produce much shorter signals. However for the reasons discussed above it is repeatable and independent of measurement apparatus.

ASTM E1065-99 (2003) Standard Guide for Evaluating Characteristics of Ultrasonic Search Units, ASTM, West Conshohocken, PA 19428-2959 US

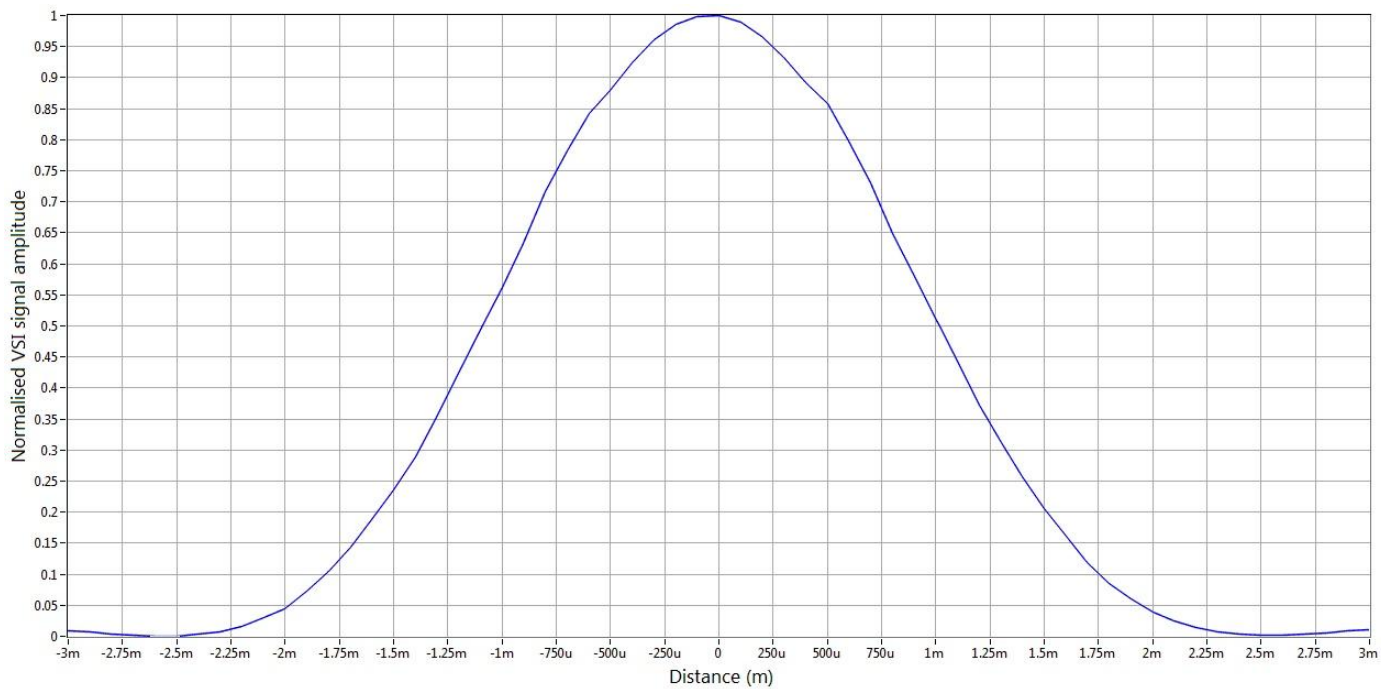


Time domain response to a single cycle sine wave at transducer's nominal centre frequency, PA504

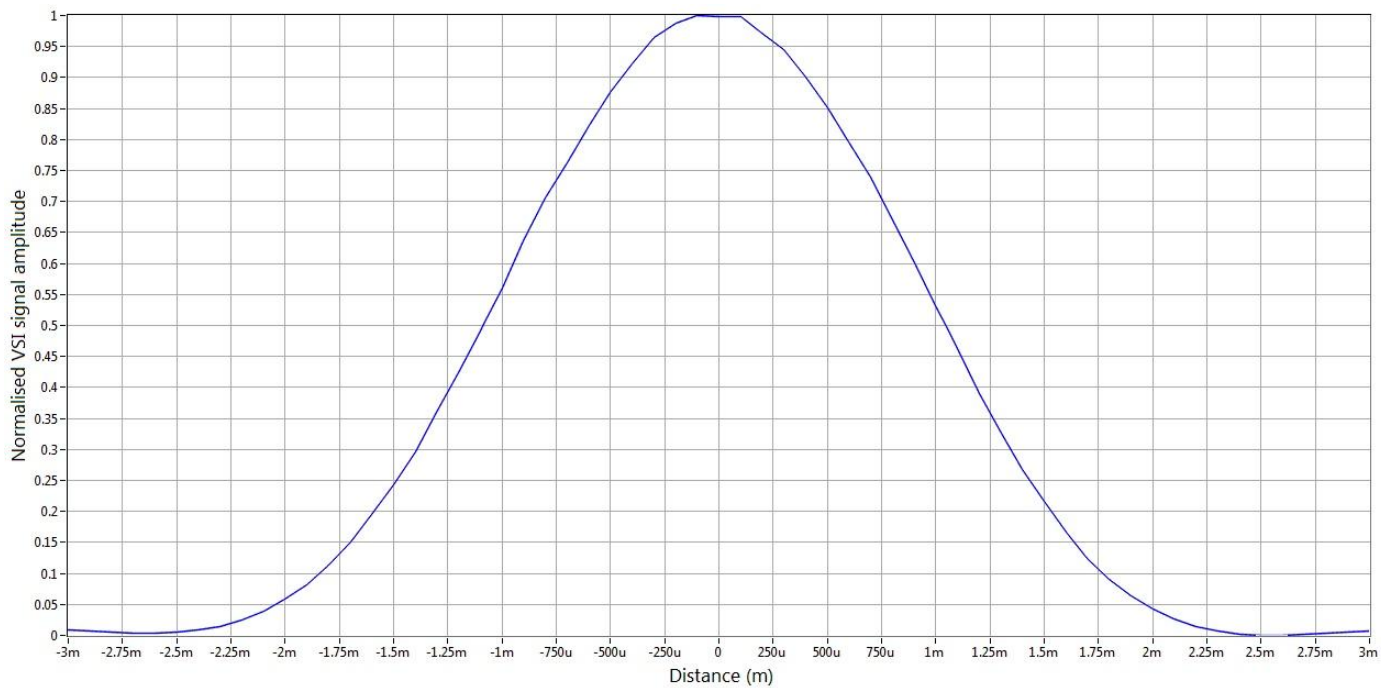


Swept frequency profile for transducer PA504

Peak Frequency (MHz): 0.99	-3.0 dB	-6.0 dB	-12.0 dB	-20.0 dB
Lower limit (MHz)	0.95	0.93	NaN	NaN
Centre frequency (MHz)	0.99	1.00	NaN	NaN
Upper limit (MHz)	1.03	1.07	NaN	NaN
Bandwidth (MHz)	0.08	0.14	NaN	NaN
Bandwidth (%)	8.44	14.14	NaN	NaN

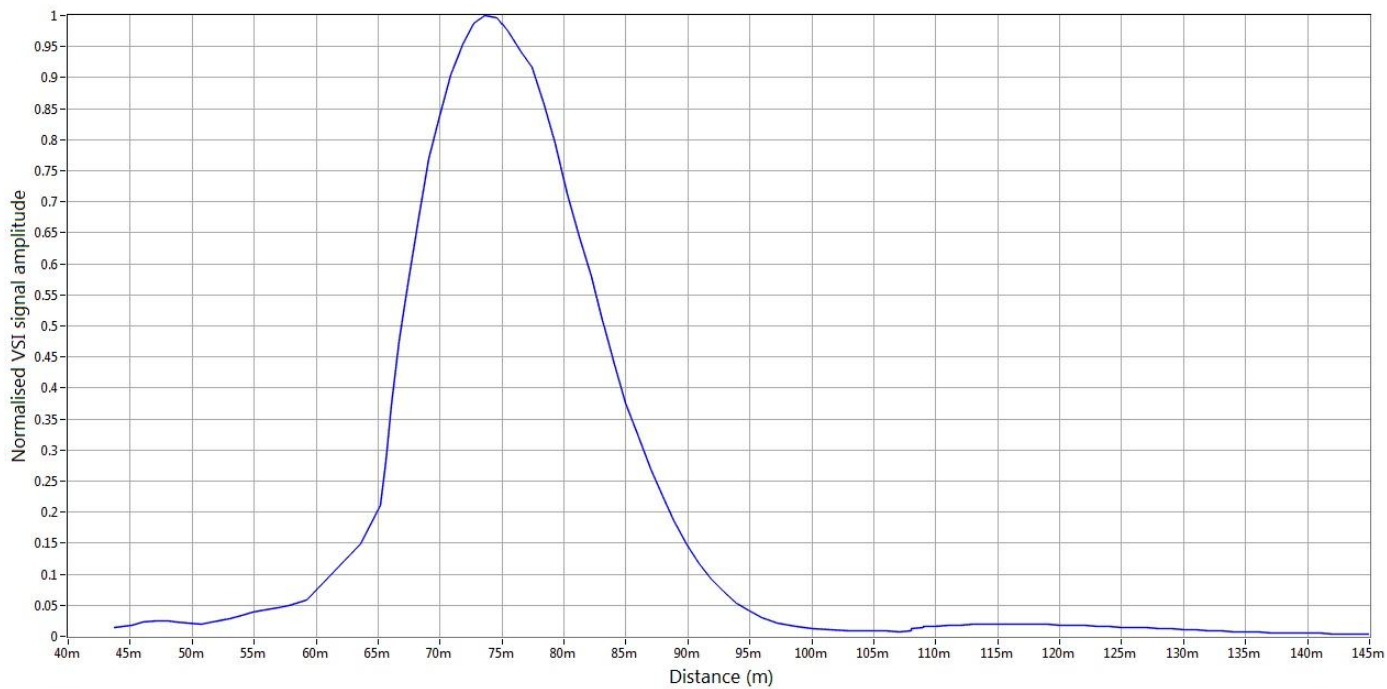


Transverse X Profile for PA504



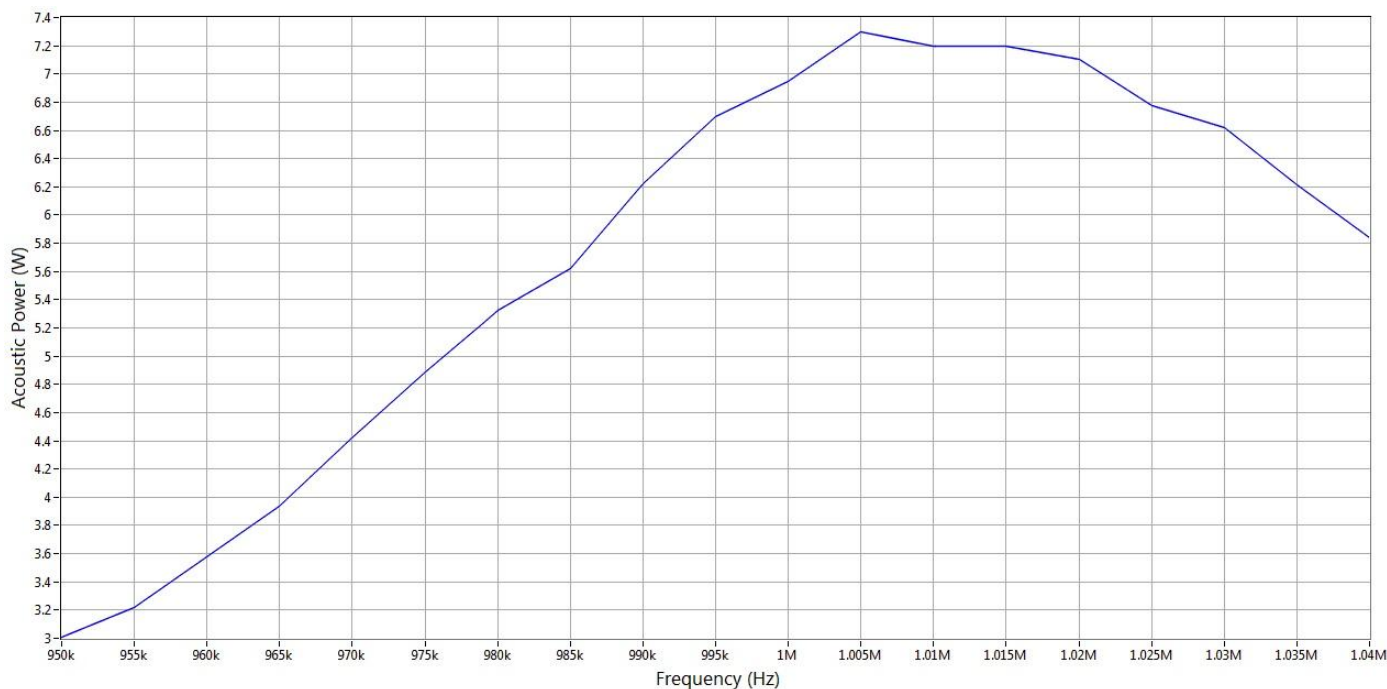
Transverse Y Profile for PA504

	-3.0 dB	-6.0 dB	-12.0 dB	-20.0 dB
X-profile beamwidth (mm)	2.11	2.89	3.83	4.53
Y-profile beamwidth (mm)	2.13	2.92	3.89	4.63

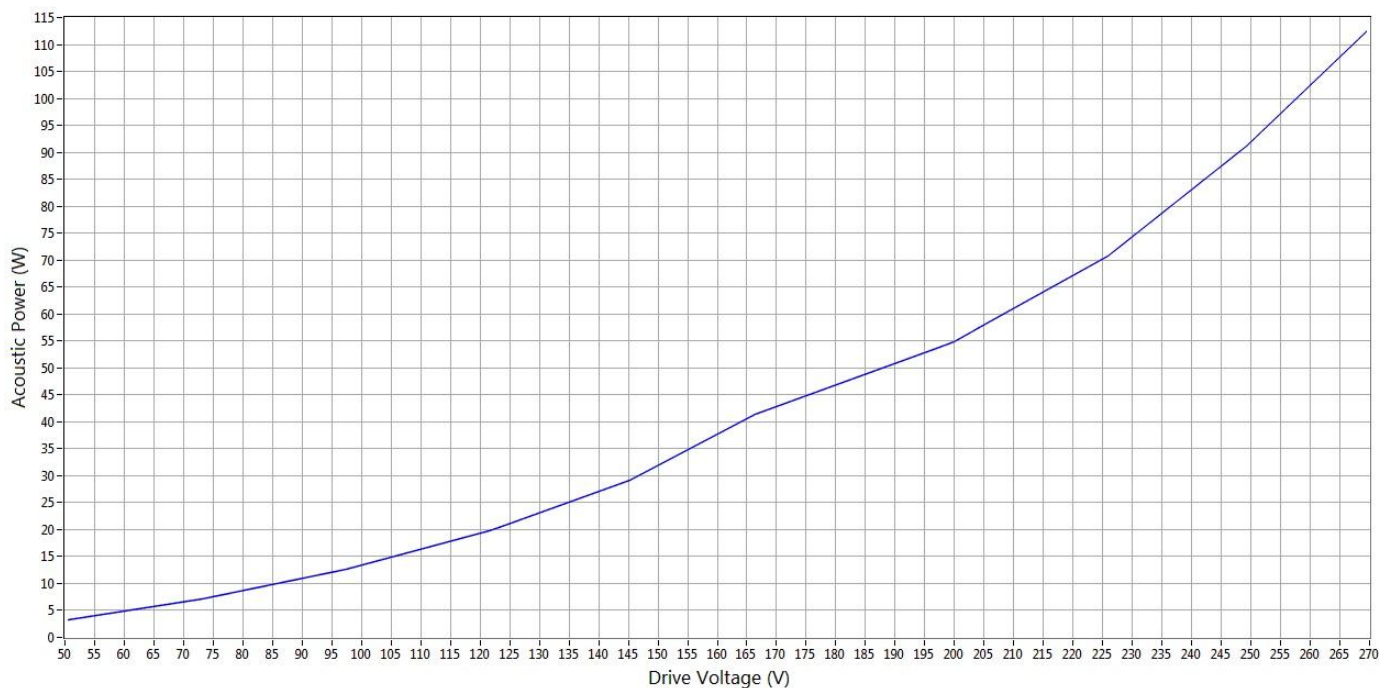


Axial Z Profile for PA504

Focal Peak (mm): 73.62	-3.0 dB	-6.0 dB	-12.0 dB	-20.0 dB
Axial profile beamwidth (mm)	16.27	21.88	32.16	NaN



Acoustic Power vs Frequency for PA504



Acoustic Power vs Drive Voltage for PA504

From the beam profiles obtained for this transducer the -6dB focal diameter is 2.91 mm. Assuming circular symmetry yields a focal area of 0.07 cm². Combining the acoustic power measurements with the focal spot size measurements results in a focal intensity of 1697 W/cm²

Due to internal heating, the transducer surface temperature can increase considerably when used with a drive level in excess of 100V. This is particularly true if the duration of the on-time bursts exceeds 15 seconds. The transducer has been tested for on-time bursts up to 30 seconds and gives constant output, but requires approximately 5 minutes to cool down before it should be used again. Beyond 270 V pk-pk input voltage the transducer starts to saturate and damage to the transducer may result. Therefore the transducer should not be driven with an input signal above this level.

